BIODISTRIBUTION AND CELL-TYPE AFFINITY OF MYOTROPIC EXTRACELLULAR VESICLE CANDIDATES

by

Kyle Shuler

A dissertation submitted to the Faculty of the University of Delaware in partial fulfillment of the requirements for the degree of Doctor of Philosophy in Applied Physiology

Winter 2023

BIODISTRIBUTION AND CELL-TYPE AFFINITY OF MYOTROPIC EXTRACELLULAR VESICLE CANDIDATES

by

Kyle Shuler

Approved: _____

John J. Jeka, Ph.D.
Chair of the Department of Kinesiology and Applied Physiology

Approved: _____

William B. Farquhar, Ph.D.
Dean of the College of Health Sciences

Approved: _____

Louis F. Rossi, Ph.D.
Vice Provost for Graduate and Professional Education and
Dean of the Graduate College

I certify that I have read this dissertation and that in my opinion it meets the academic and professional standard required by the University as a dissertation for the degree of Doctor of Philosophy.

Signed: _____

Shannon L. Lennon, Ph.D.
Professor in charge of dissertation

I certify that I have read this dissertation and that in my opinion it meets the academic and professional standard required by the University as a dissertation for the degree of Doctor of Philosophy.

Signed: _____

Melissa A.H. Witman, Ph.D.
Member of dissertation committee

I certify that I have read this dissertation and that in my opinion it meets the academic and professional standard required by the University as a dissertation for the degree of Doctor of Philosophy.

Signed: _____

Christopher R. Martens, Ph.D.
Member of dissertation committee

I certify that I have read this dissertation and that in my opinion it meets the academic and professional standard required by the University as a dissertation for the degree of Doctor of Philosophy.

Signed: _____

Emily S. Day, Ph.D.
Member of dissertation committee

ACKNOWLEDGMENTS

"If I have seen further it is by standing on the shoulders of giants" ~ Isaac Newton

I first heard this quote back in 2017, my first year working in the Molecular Physiology Lab at the University of Delaware. It instantly became my favorite quote of all time as it signifies how today's scientific breakthroughs are only possible due to the previous work of others. It also reminds me of all the individuals in my support network that have helped me to pursue my dreams.

Growing up, my parents, Ken and Michelle Shuler, worked very hard to provide an environment in which my brother, Ryan, and I could explore our imaginations and passions. One of my fondest early memories in science is when my Mom helped me build a monarch caterpillar habitat so it could undergo transformation into a butterfly. I will also never forget trips with my Aunt, Angela Shuler, to the Whittaker Center in Harrisburg, PA to visit the Kids Science Museum and see IMAX documentaries on insects, the human body, etc. These early childhood experiences undoubtedly fueled my love for biology that I still carry with me today. Thank you all, and the rest of our extended family, for your endless love and support over the years. I love you all very much. I was also lucky to have a very close friend group growing up that I always look forward to catching up and reminiscing with when the life permits. Colton, Brendan, Harry, thanks for being such great friends throughout the years and putting up with my scientific rants when we get together.

My passion for science had somewhat faded over the years, until I took a course in Exercise Physiology taught by Dr. Michael Holmstrup at Slippery Rock University of Pennsylvania. He and Dr. Brock Jensen delivered some of the most memorable lectures from my undergraduate career and inspired me to pursue scientific research. Dr. Holmstrup encouraged me to take additional Biology courses, such as Genetics, which provided me with my first wet lab experience. It was also with Drs. Holmstrup and Jeremy Dicus that I published my first peer-reviewed scientific paper. Thank you all for being such influential figures and reigniting my scientific curiosity. I would also like to thank my good friends, Matt and Brad, whom I met during my SRU years, for always being there and showing interest in my work over the years.

After graduating from SRU, Dr. Holmstrup reached out and recommended I speak with a professor by the name of Dr. Matthew Hudson, at the annual American College of Sports Medicine Mid-Atlantic Chapter meeting. I followed this advice and two years later, Dr. Hudson became my Ph.D. advisor in the Department of Kinesiology and Applied Physiology at the University of Delaware. Dr. Hudson gave me the opportunity to pursue research at the graduate level and provided an environment in which I could explore my ideas endlessly. During my 5th year of the Ph.D. program, Dr. Shannon Lennon took over as my primary advisor. Her unwavering commitment to helping me finish out the Ph.D. program ultimately brought this project to fruition. Thank you both as well as my other dissertation committee members, Drs. Melissa Witman, Christopher Martens and Emily Day, for your invaluable support and expertise over the past few years. Additionally, I would like to thank my friends, lab mates and collaborators, both current and previous, Eric, Andrew, John, Catherine, Gabe and Brittany, as well as all the other friends I made in

the KAAP department for all their support and guidance. Eric and Andrew, I wouldn't have made it this far without you guys there to help me maintain my sanity when times were tough. Thanks for being great lab mates and even better friends. John and Catherine, thank you for always being willing to help me through any problem I was experiencing in the lab, always being there to vent and to even jumpstart my car when I left the lights on all day. I am glad we met and became friends. Gabe, thanks for all your hard work helping me to keep the lab operating smoothly. It was a pleasure mentoring you and I know you will go on to do great things.

Last but not least, I would like to thank my wife, Em, our daughter, Adeline, whom was born just eight months ago, and our two dogs, Mini and Daisy. This is for you. Our growing family is the most important thing in my life and is my inspiration to continue on even when the road ahead seems impossible. Em, it's hard to believe we first met all the way back in high school when I had no idea what to do with my life and perhaps that would still be the case if we had never met. I know this has not been an easy past five years for you either, so thank you for all of your love, support and motivation along the way. Thank you for playing such a critical role in my transformation as a person and scientist. Thank you for being my partner through some of the most difficult and lowest years of my life. Moreover, thank you for always believing in me when I didn't believe in myself and for helping me reach my full potential. I will love you always. Addy, you are the most amazing daughter I could ever have hoped for. My favorite part of everyday is when Mommy brings you home from daycare and I get to see that big smile light up on your face. I cannot wait to watch you continue to grow and develop your own passions to pursue one day. Whatever you choose, I will love and support you always. Mini and Daisy, thanks for

always being so excited to see me after the long days in lab. No matter how bad the day was, your cuddles and kisses always put a smile on my face. Ultimately, I hope that all of this hard work and sacrifice will provide a better life for all of us in the long-run. I love you all so much and couldn't have done this without you. Additionally, I would like to thank all of my in-laws for welcoming into their family and always showing so much love for me and interest in my research. I love you all.

These are the "giants" that I had the privilege to stand on the shoulders of over the years so I could see further than I ever would have alone. I owe all my accomplishments, past, present and future, to them. They have all shaped me, not only as a scientist, but as a person. It is not often that we as scientists can say things with much certainty; however, I can say for certain that I would not be where I am today without these individuals. So thank you all once more for your support and guidance throughout this journey. It means more to me than words can say.

TABLE OF CONTENTS

LIST OF FIGURES

ABSTRACT

Muscular pathologies represent a class of diseases and disorders comprising both inherited genetic disorders (i.e. muscular dystrophies) and secondary conditions (i.e. cachexia). The most promising therapeutics for these conditions are adeno-associated virus (AAV)-mediated gene therapies. This strategy has shown promise in clinical trials; however, immunogenicity and lack of specificity of the AAV are major hurdles for clinical approval. Extracellular vesicles (EVs), or cell-derived nanoparticles, have been proposed as alternative delivery vectors. By engineering targeting moieties on the surface of EVs, researchers have enhanced EV tropism to specific cell-types. There are a number of native proteins involved in myogenic fusion and adherence in skeletal muscle development, such as MyoMaker (MYMK), MyoMixer (MYMX) and M-Cadherin (M-Cad), as well as the synthetic myotropic peptides, ASSLNIA (MP1) and RRQPPRSISSHP (MP2), that could be displayed on the surface of EVs; however, no successful myotropic EV formulation has been generated to date. **OBJECTIVES:** 1) Examine the myotropic properties of EVs displaying the native myotropic protein candidate, MYMK, in vivo. 2) Determine the myotropic properties of EVs displaying chimeric myotropic protein candidates in vitro. **HYPOTHESES:** 1) MYMK-EVs will show greater affinity for skeletal muscle relative to non-engineered Human Embryonic Kidney (HEK293) cell-derived EVs in both C57/BL6 (**1a**) and mdx (**1b**) mouse models. 2) EVs displaying chimeric myotropic proteins will demonstrate selective delivery of cargo to muscle cells over non-muscle cell types. **METHODS:** HEK293 cells were transfected with lentivirus containing a MYMK transgene followed by selection using fluorescence-assisted cell sorting (FACS) to generate a stable MYMK-EV producer cell line. 6-11 week old male C57 and mdx mice received MYMK or

control HEK293-EVs stained with either a lipophilic or amine-reactive dye. Select organs from the mice were harvested and analyzed via whole-organ fluorescence imaging, fluorescence microscopy and a fluorescent plate reader. For the in vitro experiments, plasmids encoding either MP-1 or MP-2 fused to the extracellular domain of prostaglandin F2 receptor inhibitor (PTGFRN) were transfected into HEK293 cells followed by antibiotic selection and FACS. EVs were labeled with an amine-reactive dye and incubated with muscle and non-muscle cell-types in vitro. The recipient cells were analyzed via fluorescence microscopy. **RESULTS:** There was no significant difference between the biodistribution of the MYMK-EVs and HEK293-EVs ($p < 0.05$) other than a significant decrease in the liver of mdx mice that received the MYMK-EVs as compared to the HEK293-EVs ($p = 0.04$). For both the MYMK ($p = 0.004$) and HEK293-EVs ($p < 0.0001$), a significant decline in signal was observed in the spleen of the mdx mice relative to the C57 mice. No signal above background was able to be measured in the tissues of mice that received EVs labeled with the amine-reactive dye. In vitro, the PTGFRN-EVs showed the highest affinity for the muscle cell-types as well as for HEK293 cells relative to non-engineered HEK293 EVs ($p < 0.0001$). The MP1-EVs also showed significant increases in delivery to these cell-types (HEK293: $p < 0.0001$, C2C12: $p = 0.002$, CM: $p < 0.0001$). The MP2-EVs showed enhanced delivery to the Kupffer cells ($p = 0.003$), but not to the muscle cell-types or HEK293 cells. **CONCLUSION:** MYMK did not significantly alter the biodistribution of EVs in vivo. PTGFRN-EV and MP1-EVs may represent promising myotropic EV candidates for future in vivo biodistribution experiments.

Chapter 1

REVIEW OF LITERATURE

1.1 Neuromuscular Pathologies Overview

Muscular pathologies comprise a wide range of diseases and disorders affecting the musculoskeletal system. This family of pathologies can be further subdivided as those primarily affecting the skeletal and/or cardiac musculature, typically though a genetic mutation, or secondary pathologies where skeletal and/or cardiac muscle dysfunction is a comorbidity associated with another pathology, such as cancer.[1,2]

Primary congenital muscular pathologies, such as the muscular dystrophies, occur at a rate of 1-10 per 100,000 people in the population. In Duchenne Muscular Dystrophy (DMD), the most severe of these diseases, there is a median life expectancy of ~ 29.9 years with ventilatory support.[3] This disease is attributed by mutations in the dystrophin gene, resulting in a shift in the reading frame and subsequently no production of the dystrophin protein. Dystrophin functions as a scaffolding protein for the dystrophin associated glycoprotein complex (DAGC), and connects it to the extracellular matrix, and cytoskeletal proteins, such as actin.[4] Numerous signaling molecules, such neuronal nitric oxide synthase, also bind to the DAGC, thus lack of dystrophin expression leads to the dissociation of the DAGC and disrupts not only the structural integrity of muscle fibers, but also initiates pathological signaling events or the inhibition of beneficial signaling pathways.[4] This leads to ischemia,[5] oxidative

stress,[6] impaired calcium homeostasis associated with the sarcoplasmic reticulum and mitochondrial dysfunction,[7] reduced regeneration by muscle stem cells (MuSCs),[8] and chronic inflammation.[9] In addition, although this is a degenerative disorder, the muscle fibers actually undergo compensatory hypertrophy due to chronic activation of the Akt signaling pathway.[10] This process inhibits autophagic pathways in the muscle fibers, leading to the accumulation of dysfunctional proteins that are largely responsible for the compensatory hypertrophy. Ultimately, these pathogenic events result in the progressive degeneration of the functional muscle fibers that are gradually replaced by adipose and fibrotic tissues.[11] As dystrophin is also critical for proper function of cardiac muscle, this disease eventually leads to the development of dilated cardiomyopathy which is most often the cause of death in DMD patients.[12] Other mutations, such as those involved in Becker Muscular Dystrophy, result in the production of a truncated form of the dystrophin protein and thus have a less severe phenotype and improved life expectancy.[13] Overall, there exists a wide variety of genetic mutations that can occur in dystrophin and other muscle-enriched proteins with a range of severity and clinical manifestations.[14]

Muscular pathologies may also present as secondary or acquired conditions as a comorbidity of some of the most prevalent diseases facing modern society, such as cancer, acquired immunodeficiency syndrome, rheumatoid arthritis, chronic obstructive pulmonary disease, as well as heart and renal failure.[2] Muscle degeneration is also associated with other conditions, such as aging (sarcopenia) and anorexia.[15] The processes underlying muscle degeneration in these conditions commonly involve chronic inflammatory signaling and metabolic resistance to anabolic signaling promoting a chronic catabolic state in the musculature.[16,17] Common inflammatory

modulators in these conditions include tumor necrosis factor-α (TNF-α), and interleukins-1, -6 and -8.[18,19] Immune cells and in the case of cancer-related cachexia, tumor cells, produce these proinflammatory cytokines, which then activate signaling pathways such as nuclear factor-kappa B (NF-κB) activating muscle degeneration thought the ubiquitin proteasomal pathway and Janus kinase (JAK), which suppresses anabolic signaling.[18,20] Ultimately, these secondary pathologies greatly worsen patient quality of life and disease prognosis.[2]

Overall, muscular pathologies represent an expansive category of diseases and disorders greatly impacting the lives of many. They range from inherited disorders arising from genetic mutations in genes encoding proteins that are critical to muscle function to acquired secondary pathologies as comorbidities of other conditions. Regardless of the cause, these are devastating conditions requiring advanced therapeutic interventions.

1.2 Current Treatment Modalities for Muscular Pathologies

A number of treatment modalities exist for the treatment of muscular pathologies, including glucocorticoids and various gene and cell therapies.[21-23] However, the only therapeutic currently approved by the United States Food and Drug Association (FDA) is glucocorticoid treatment while cell and gene therapies are still largely being studied in clinical trials and preclinical investigations. Moreover, although these treatment strategies have proven effective, they are non-specific to the musculature and thus suffer from off-target effects.[21,24,25]

1.2.1 Corticosteroids

The current standard of care for many congenital muscular diseases, such as DMD, is the use of glucocorticoids, prednisone, prednisolone and deflazacort.[26] These compounds diffuse through the membrane of cells and bind to cytosolic glucocorticoid receptors which then translocate to the nucleus (Figure 1.1).[26] Once inside the nucleus, the receptor-ligand complex suppresses the NF-κB signaling pathway, which is chronically activated in a number of muscular pathologies, including DMD.[9,26] This mechanism of action ameliorates the chronic degenerative inflammatory state associated with the disease.[26] Glucocorticoids have been successful in ameliorating disease outcomes and preventing delays in ambulatory milestones associated with muscular pathology.[27,28] However, long-term treatment suffers from a number of adverse effects largely caused by off-target *cis*-repression of genes such as corticotropin releasing hormone, osteocalcin and proopiomelanocortin.[24] Side effects to glucocorticoid treatment include delayed growth, osteoporosis, excessive weight gain, as well as behavioral and skin disorders.[24,26] Although glucocorticoids have been successful in alleviating disease symptoms, they cause severe adverse side effects and are ultimately non-curative.[24,26]

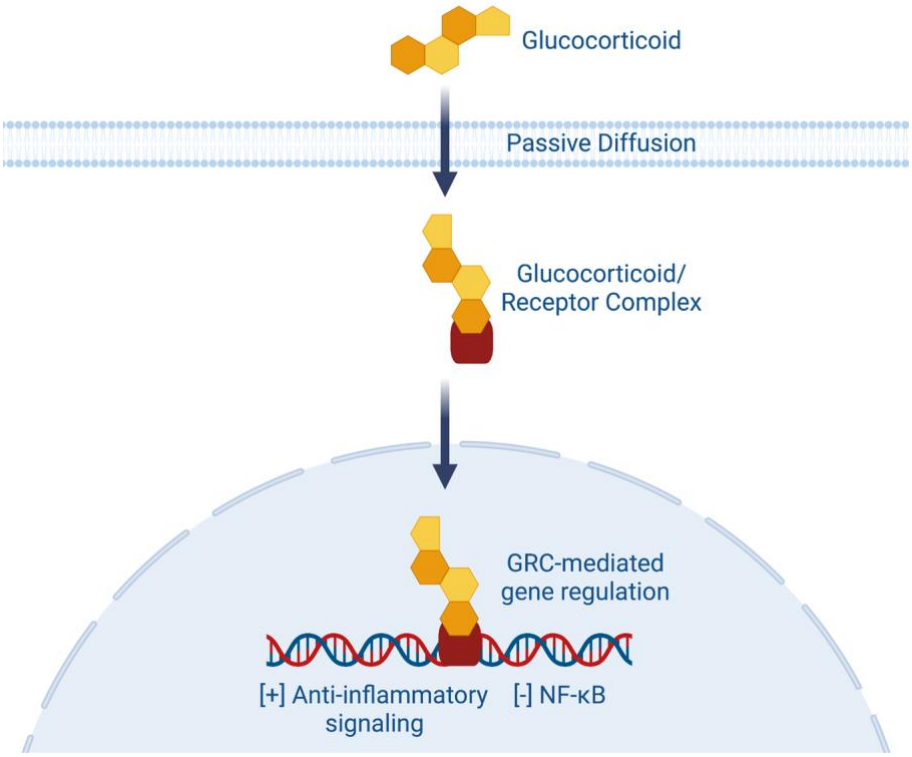

Figure 1.1 Mechanism of action of glucocorticoids. A glucocorticoid molecule traverses the plasma membrane via passive diffusion, forming a glucocorticoid-receptor complex (GRC) in the cytosol, which translocates into the nucleus to modulate gene expression. The GRC binds with the glucocorticoid response elements to upregulate genes promoting anti-inflammation and represses expression of Nuclear Factor kappa B (NF-κB). Adapted from Kourakis et al.[23]

1.2.2 Gene Therapies/Editing

The definition of gene therapies established by the FDA is "the administration of genetic material to modify or manipulate the expression of a gene product or to alter the biological properties of living cells for therapeutic use."[29] Thus, gene therapies can be characterized into the categories of gene replacement, gene suppression, and gene-editing.[22] Gene replacement therapy aims to provide a wildtype copy of a gene that is mutated in a patient in order to ameliorate disease progression.[22,30] Gene suppression

therapies, such as antisense oligonucleotides, correct the open reading frame of a gene by binding with the mutated sequence within an exon, causing RNA Polymerase to skip over the sequence during transcription.[22,31] The restoration of the open reading frame typically results in the production of a truncated yet functional protein that ameliorates the disease phenotype.[22,30] The most recent form of gene therapy is gene editing, which typically employs a nuclease, such as zinc finger nuclease, transcription activator-like effector nuclease, or clustered regularly intersperse short palindromic repeats-associated nuclease along with guiding RNA molecules to locate and modify mutated DNA sequences in the genome.[32]

The most commonly used delivery vehicle for gene therapies is the adeno-associated viral (AAV) vector.[30,33] AAVs are non-enveloped, proteinaceous viral particles belonging to the parvovirus family.[30,33] They enter cells via membrane protein receptor-mediated uptake and then translocate to the nucleus where the transgene is largely expressed extra-chromosomally as an episome.[30,33] There have been reports of AAV transgene integration which may provide long-term expression, although this raises the risk of mutagenesis.[34] Thus, the duration of therapeutic benefit following gene therapy is poorly understood and may be dependent on the cell division rate of the target organ.[34] A major limitation that persists with the utilization of AAV as a gene therapy vector is cellular and humoral immunogenicity to the viral capsid.[25,35,36] AAVs closely mimic their parent adenovirus which naturally infects infants in the first years of life, resulting in upwards of 40% of people having pre-existing cellular and humoral immunity capable of destroying/neutralizing AAV vectors.[37] Even if a patient does not already have pre-existing immunity to AAV, once the AAV is administered, they will develop immunity to the vector, diminishing its

safety and efficacy.[36] This reduces the ability to perform repeat dosing if the therapeutic effect of the gene therapy wanes over time either due to degradation of the episome or dilution of the episome in highly proliferative cell types.[36] In light of this, efforts have been made to engineer both the capsid proteins and the DNA plasmids with organ/tissue-tropic properties to enhance transgene expression in the disease target, while avoiding off-target delivery to non-muscle tissues.[38-40] For example, various AAV serotypes have been investigated for their tropism to various organs/tissues, with AAV serotypes 6, 8 and 9 as having enhanced tropism to muscle.[38,41,42] In addition to the natural tropism of AAV serotypes, researchers have investigated the incorporation of synthetically-designed myotropic peptides, such as ASSLNIA, into the capsid of AAV2 at position 587 and 588, with the 587 modification showing enhanced myotropism in mice.[39] Furthermore, another myotropic peptide candidate has been used to effectively direct a peptide-morpholino ASO construct to dystrophic muscle in mice, effectively restoring dystrophin expression.[43] Muscle-specific promoters, such as skeletal muscle α-actin, muscle creatine kinase and desmin, are largely employed to diminish off-target transgene expression.[44] While these strategies have led to improvements in the immunogenic profile of AAVs in laboratory studies, 40% of individuals already possess immunity to the vector and this strategy will likely not fully ameliorate the immune response to the viral capsid proteins.[37] Thus, a less immunogenic vector is likely needed for further advancement in the delivery of gene therapies.

1.2.3 Cell Therapies

Cell therapy refers to living cell products that are administered to a patient to ameliorate or cure a disease.[45] Cell therapies can either be autologous, coming from the same patient that will be receiving them, or allogeneic, coming from a donor.[46] Prominent cell therapies under investigation for the treatment of muscular diseases include induced pluripotent stem cells (iPSCs),[47] mesenchymal stem cells,[48] as well as muscle-specific stem cells, such as satellite cells or myogenic progenitor cells.[49]

Induced pluripotent stem cells (iPSCs) are pluripotent stem cells derived from somatic cells by using retroviruses to over-express the Yamanaka transcription factors Octamer 3/4 (Oct3/4), SRY-box containing gene 2 (Sox2), and Krüppel-like factor 4 (Klf4).[50,51] iPSC therapies often need to be autologous due to host rejection of the donor cells.[47] Once the iPSCs have achieved pluripotent colonies, they may be reprogrammed to differentiate into various cell types or implanted back into the patient's body to treat various conditions.[47] For example, Hallett et al.,[52] demonstrated that iPSCs derived from skin fibroblasts in non-human primates could effectively be transformed into midbrain-like dopaminergic neurons and transplanted into the midbrain. Following transplantation, the authors noted long term restoration of motor function was similar to baseline levels.[52] Although iPSCs are limited in that they must be used as an autologous therapy, they are advantageous in the sense that they can divide indefinitely while maintaining pluripotency.[50] In addition to Yamanaka transcription factors, iPSCs may also be transfected or edited to express proteins of interest or correct genetic mutations.[53] In the case of muscular pathologies, such as DMD, iPSCs may be generated from other somatic cell-types, transfected or edited to overcome the underlying mutation, and then injected into the skeletal muscle tissue of

the patient from which they came, now harboring a wildtype or less severe genotype.[54] The hope is, once in the intramuscular niche, the iPSCs will differentiate into skeletal muscle fibers with the genetic mutation largely corrected. Exposing the iPSCs to myogenic regulatory factors, such as paired-box transcription factor 7 or MyoD, may help to promote a myoblast-like phenotype and thus enhance the ability of the cells to engraft into the recipient muscle tissue.[54]

MSCs are an innately multipotent stem cell lineage derived from bone marrow, adipose tissue, umbilical cord blood or the placenta.[55-57] Given their mesenchymal origin, these cells have the ability to undergo osteo-, adipo-, chondro- and myogenic differentiation, allowing these cells to be harvested, expanded and then administered into the primary location of the pathology, such as joints, muscle, heart, etc to support regeneration.[58] Further, myocardial infusion of MSCs maintained ex vivo with a cardiogenic cocktail were shown to improve contractile function following myocardial infarction in rodents and humans.[59,60] MSCs therapeutic applications pertain to tissue regeneration and modulation of inflammation and immune responses.[58] Given their ability to differentiate into a number of cell types, MSCs were originally thought to act via engraftment into the diseased tissue to facilitate regeneration.[58] However, recent investigations have demonstrated that the therapeutic properties of MSCs are largely due to a plethora of secreted paracrine factors, such as various growth factors and cytokines, released by the cells.[61,62] MSCs have been heavily investigated and have shown therapeutic potential in preclinical studies for the treatment of muscular diseases.[48] For example, bone marrow-derived MSCs in which a micro-dystrophin gene was constitutively expressed were administered to mdx mice, resulting in a restoration of dystrophin expression in 6-11% of observed muscle fibers.[63] Although

this is a relatively low number of affected muscle fibers, this work demonstrates that MSCs may extravasate from the circulation into skeletal muscle where they could mediate other degenerative and inflammatory pathways involved in muscle diseases. Using systemic delivery of human adipose-derived MSCs, Vieira et al.,[64] noted human dystrophin expression in ~50% of the muscle fibers in a model of limb girdle muscular dystrophy. Furthermore, in a small clinical investigation of nine DMD patients that received systemically-delivered umbilical cord blood-derived MSCs, improvements in pulmonary and skeletal muscle function were achieved.[23]

Muscle stem cells (MuSCs), comprising satellite cells (SCs) and their progeny myoblasts, have been investigated for the treatment of muscular disorders, such as DMD.[49] In vivo, MuSCs are involved in the development of the fetal muscular system as well as regeneration of damaged muscle fibers in adult musculature.[65] The quiescent SCs use various proteins, such as M-Cadherin (M-Cad), to adhere to the skeletal muscle cell membrane.[66] Upon activation via damage to the adjacent muscle fiber or via stimulation by growth factors during development, the SCs express myogenic regulatory factors, such as MyoD and myogenin, that enable the transition of SCs into myoblasts.[65] The resultant myoblasts express the proteins MyoMaker (MYMK) and MyoMixer (MYMX), which mediate membrane fusion and cytosolic exchange, respectively.[67,68] These processes allow the MuSCs to selectively fuse with the adjacent muscle fiber to mediate regeneration.[67,68] Given this physiological role in muscle regeneration, numerous groups have investigated the use of autologous and allogeneic muscle stem cells as therapeutic agents for the treatment of muscle diseases.[49,69] Human Pax7+ SCs transplanted into mice resulted in the generation of new human-derived muscle fibers as well as replenishment of Pax7+ SCs.[70] Despite

this, numerous clinical trials have demonstrated poor engraftment and clinical outcomes from SC and MB transplantation which has been largely attributed to host rejection of allogeneic cell types as well as phenotypic alterations in the cells caused by ex vivo expansion.[69] However, studies have been conducted in large animal models over recent years to optimize various parameters of muscle stem cell transplantation with improved success rates in dystrophin restoration and muscle regeneration.[71] Ongoing clinical trials are investigating the long-term implications of myoblast infusion on muscle function in DMD patients.[72]

Related to the mechanism of action and mode of delivery, key limitations to administering iPSCs, MSCs and MuSCs for the treatment of muscular diseases persist. These include the extremely large number of cells needed to treat the entire muscular system via systemic injection, complications with the host immune response to allogeneic cell therapies and poor engraftment of the administered cells into the diseased muscle.[63] Given these complications, as well as the data demonstrating that various stem cell populations release an abundance of regenerative and anti-inflammatory factors, it is feasible that these cell types may be cultured ex vivo and these therapeutic factors may be purified from the culture media for subsequent therapeutic applications. This form of "cell-free" cell therapy may overcome the many limitations experienced by current cell therapies.

1.3 Extracellular Vesicle-Based Therapeutic Applications

1.3.1 Overview/Biogenesis

According to the Minimal Information for Studies of Extracellular Vesicles 2018 (MISEV 2018), EV is a generic umbrella term referring to a lipid membrane

bound particle released by cells.[73] EVs can be categorized by both their pathway of biogenesis or by their size.[73] As EVs are highly heterogeneous and many of their characteristics overlap with other biomolecules that are very prevalent in cell-conditioned culture media (CM) and human serum, it is very difficult to accurately identify the EV pathway of biogenesis.[73-75] Thus, EVs are typically characterized by their size as either small EVs (sEVs, < 200 nm) or medium/large EVs (m/l EVs >200 nm). EVs can also be subcategorized by their densities or by biochemical analyses identifying protein markers such as the cluster of differentiation (CD) proteins (CD9, CD63, CD81, etc.), syntenin-1, annexin A-5, ALIX, etc.[73] The term exosome refers to EVs, typically 50-200 nm in diameter, produced via the endocytosis of a portion of the plasma membrane which is then incorporated into multivesicular endosomes (MVE), selectively packaged with molecular cargoes and then released to the extracellular environment upon fusion of the MVE with the plasma membrane.[74] The ESCRT, Syntenin-Alix, and sphingomyelinase sorting pathways, as well as the tetraspanins previously mentioned are all involved in the biogenesis and packaging of molecular cargoes into exosomes.[74] (Figure 1.2) Ectosomes refer to EVs that bud straight off of the cell membrane, encapsulating a portion of the cytosol and its contents in the process. These EVs can range from 100-1,000 nm in size.[76] (Figure 1.2) Apoptotic bodies are another class of EVs but are distinct from exosomes and ectosomes as they are released by dying cells and hold little therapeutic relevance.[74]

Once released into the extracellular milieu, EVs deliver their cargo into recipient cells via numerous mechanisms, including direct membrane fusion, macro- and micro-pinocytosis, or endocytosis mediated by membrane receptors, membrane rafts, clathrin and caveolin.[75,77] Transmembrane proteins on EVs act as ligands to

protein receptors on recipient cell types, thus increasing the chance of an EV being taken up by the recipient cell via one of the previously mentioned mechanisms.[75,77] Through these mechanisms, the molecular cargo of EVs is transferred into the recipient cells where it can directly engage in signaling pathways (proteins and mRNA) or modulate gene expression (non-coding RNA species).[75,77,78]

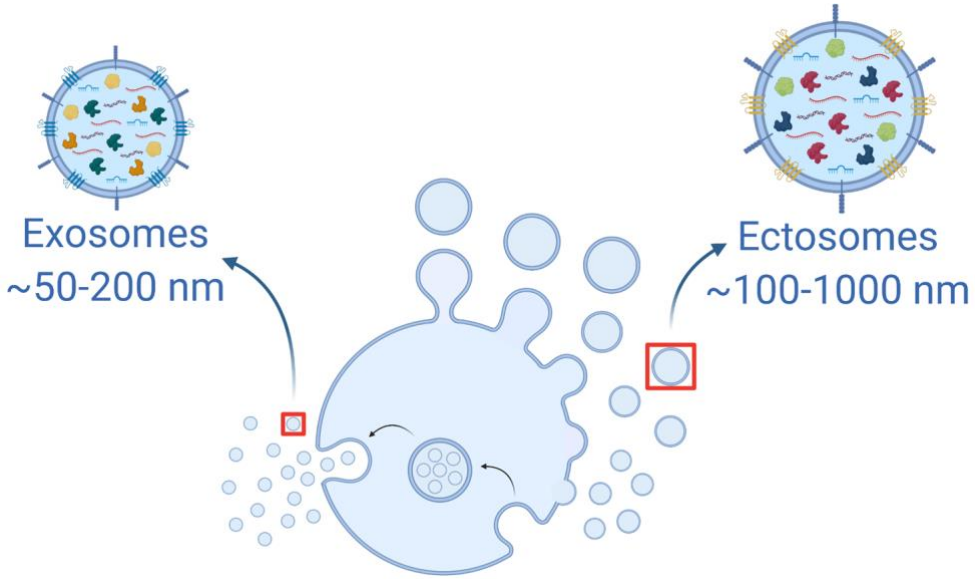

Figure 1.2 EV biogenesis and general size distribution depicting the generation of exosomes released by the exocytosis of multivesicular endosomes and ectosomes which bleb directly from the plasma membrane as described by Vader et al.[75]

1.3.2 Native EV-Based Therapeutics

Depending on the cell-type of origin and the pathological indication of interest, EVs have great potential as a next-generation "cell-free" cell-based therapeutic.[79] Numerous cell-types have been investigated for the therapeutic properties of the native EVs produced in cell culture with MSCs,[80] MuSCs,[81] and cardiosphere-derived cells (CDCs)[82] showing the most promise related to the treatment of muscular pathologies.

Each of these cell types were once thought to act primarily via engraftment into the host tissue; however, more recent work began to reveal that these cells primarily operate via the release of paracrine factors, such as vascular endothelial-derived growth factor, angiopoietin-1, fibroblast growth factor 2, insulin-like growth factor-1, transforming growth factor-β, hepatocyte growth factor, interleukin 6, monocyte chemoattractant protein-1, or stromal cell-derived factor 1α.[83,84] Thus, as research into the therapeutic role of EVs has accelerated, various research groups have begun investigating the EV species released from these well-studied therapeutic cell-lines.

MSCs are the most commonly studied stem cell type in regard to therapeutic EV production. These cells can be harvested from adipose tissue, bone marrow, blood, or umbilical cord blood.[85] Numerous studies suggest that EVs released by MSCs are responsible for transferring much of the paracrine factors previously mentioned, giving them the potential to treat various conditions including neurological disorders, cardiovascular diseases, musculoskeletal conditions and different cancers.[86-88] The angiogenic, anabolic and anti-inflammatory properties of the factors suggested to be released within MSC-EVs hold great potential for the treatment of these conditions. These factors are attributed to MSC-EVs ability to promote vascular remodeling via upregulation of angiogenesis, cellular proliferation and extracellular matrix digestion.[89] A notable attribute of these EVs that is quite relevant to the treatment of muscle disease is their immunomodulatory properties.[90] As muscle diseases, such as DMD, are highly associated with chronic inflammation, the proposed anti-inflammatory properties of MSC-EVs may provide valuable therapeutic potential.[91] In the presence of an activated immune system, MSC-EVs are suggested to dampen the immune response by mitigating the activation of dendritic cells, natural killer cells,

CD4+ and CD8+ T Cells, and the conversion of macrophages from a proinflammatory M1 phenotype to an anti-inflammatory M2 phenotype.[92,93] Specific to the treatment of muscular disease/degeneration, MSC-EVs were found to enhance myogenesis in the C2C12 cell line in vitro.[87] This research group also noted benefits in the tibialis anterior muscle of C57/BL6 mice treated with cardiotoxin, including increased cross-sectional area, decreased fibrosis and improved capillary density.[87] The myogenic miRNAs 1,133, 206, and 494 have been found to be associated with MSC-EVs, potentially explaining the MSC-EV myogenic properties.[87,88] The regenerative properties of MSC-EVs in the treatment of muscular damage following cardiotoxin injury are largely attributed to their miRNA content as well as their ability to modulate nuclear factor kappa-B signaling, a prominent signaling pathway involved in muscle degeneration.[87] In the mdx mouse model of DMD, systemic injection of bone marrow-derived MSC-EVs ameliorated disease symptoms, decreasing serum creatine kinase and muscular fibrosis and inflammation, attributed to the restoration of the dystrophin-associated glycoprotein complex.[94] However, it should be noted that MSCs release regenerative biomolecules both in EVs as well as freely into the culture media and discerning the two can be very difficult.[95] Whittaker et al.,[96] highlighted this issue when they implemented size exclusion chromatography to separate EVs from the remainder of the MSC secretome and demonstrated that EV fractions did not induce angiogenesis in the tube-formation assays as previously thought.[96] Thus, more standardized and rigorous protocols for the preparation of MSC-EVs are needed to fully elucidate their therapeutic potential.

As many of the therapeutic outcomes associated with MSCs are attributed to their secretome, some groups have ventured to study the therapeutic properties of the

MuSC secretome. Recent work from our research group demonstrated that the EV-containing secretome from MuSCs is effectively taken up by muscle cells in vitro, and confers cargo that improves mitochondrial function following oxidative stress.[81] However, the methods used in this study concentrated the entire secretome of the MuSCs, thus although EVs were present within the secretome, we cannot say for certain they were the cause of the restorative effects on mitochondrial respiration. It has been shown that MuSCs co-cultured with smooth muscle cells enhanced smooth muscle cell proliferation and when implanted in the hindlimb musculature of mice following ischemic injury, alginate-encapsulated MuSCs improved the recovery by increasing perfusion to the ischemic muscle.[83] Others have suggested that MuSC-derived IGF-II drives macrophages towards an M2 anti-inflammatory phenotype.[97] Further, Fry et al.,[98] noted that in response to hypertrophic stimuli, muscle progenitor cells, a MuSC sub-type, secrete exosomes containing miR-206 which downregulates Rrbp1 in fibrogenic cells, preventing excessive extracellular matrix deposition and allowing for hypertrophic processes to function appropriately. In addition, Murach et al.,[99] demonstrated in vivo communication between satellite cells and muscle fibers during hypertrophy. They go on to elucidate that the EVs transfer miRNAs known to modulate the expression of ECM-related proteins such as matrix metalloproteinase 9. Cumulatively, these studies suggest that MuSCs, similar to MSCs, release various factors, some of which may be contained within EVs, and that they play a large role in their function in vivo. Furthermore, little research has been conducted outside of our own research lab investigating the potential of harvesting MuSC-EVs ex vivo for their use as a therapeutic modality for muscular diseases. Similar to MuSC therapies based

transplantation of the cells, a key limitation remains harvesting enough cells to produce the quantity of EVs needed for in vivo administration.

In recent years, cardiosphere-derived cells (CDCs) and the EVs they produce have gained recognition as valuable therapeutic agents for a number of diseases.[100] CDCs are regarded as a cardiac progenitor cell with the ability to differentiate into the three main cell-types found in the heart: endothelial, smooth muscle, and myocardial cells.[101] When these cells were injected directly into the heart, they were found to prevent age-related fibrosis and declines in cardiac function.[102] However, similar to the other stem cell types discussed, it has since been revealed that these cells predominantly act via the release of paracrine factors that modulate regeneration and inhibit fibrogenesis and immune cell activation in recipient cardiac tissue.[100] Ibrahim et al., [100] identified exosomes released by the CDCs as key mediators of these therapeutic effects, noting enhanced proliferation and angiogenesis in vitro as well as improved cardiac function as a result of increased viable mass following myocardial infarction in vivo. The authors suggest that miRNA-146a is a key mediator in this response, as it is a known regulator of signaling mediators of the NF-kB pathway. Additionally, research has implicated CDC-EVs in switching macrophages from the pro-inflammatory M1 phenotype to an anti-inflammatory M2 phenotype in an arginase-1-dependent and VEGF independent manner.[103] In addition to these findings, CDC-EVs are also implicated in modulating the IL-6/IL-6-R axis via miR-125b which downregulates the expression of the IL-6 receptor.[100] Overall, this work demonstrates clear implications for CDC-EVs in immunomodulation and myocardial regeneration following cardiac infarction. The ability for a therapeutic to regenerate cardiac muscle is essential for the treatment of muscular diseases, such as DMD, as progressive

cardiomyopathy is the most common cause of death in these conditions.[12] Importantly, Aminzadeh et al.,[82] demonstrated that CDC-EVs recapitulate the benefits of CDCs on cardiac function, ambulation, and overall mortality in mdx mice. Additionally, they show improvements in calcium cycling, oxygen consumption as well as full-length dystrophin protein restoration in primary cardiomyocytes derived from iPSCs generated from a DMD patient. These findings, if recapitulated in human patients in vivo, would hold very promising implications for the treatment of DMD and muscular diseases as a whole.

Overall, EVs display great potential as biocompatible vectors of therapeutic biomolecules. Various cell-types are currently under investigation for production of therapeutic EVs, such as MSCs, iPSCs and CDCs. The data largely show that the EVs produced by these cell types confer much of the therapeutic effects of these cells. Although these therapeutic EV formulations are very promising, their therapeutic contents are limited to what these cell-types innately produce. Thus, if a higher concentration of a particular molecule is needed to adequately treat a specific disease, further engineering of the EV constructs is needed.

1.3.3 Engineering EVs with Exogenous Payloads

As discussed in the previous section, depending on the cellular source, many native EV species may have naturally-occurring therapeutic properties. However, solely focusing on EVs endogenous payloads and targeting moieties may limit the number of diseases that can be treated. Thus, a means of overcoming this limitation is to engineer the EVs to express cargoes and surface molecules of interest, effectively

expanding the theoretical number of disease indications that EVs may be used to treat.[104]

In order to engineer the EVs with therapeutic compounds, a number of strategies have been demonstrated to be effective. Modifications can be made to the producer cells by transducing the cells with a gene encoding a protein of interest which is then incorporated into the EVs the cells produce.[104] Additionally, a protein or molecule of interest may simply be incubated with the producer cells which the cells uptake via endocytosis, package into an exosome or ectosome based on the mechanism of biogenesis and then re-release the molecule into the culture media packaged inside the indicated EV population.[104] Alternatively, EVs may be loaded with various therapeutic constructs post-isolation via a number of strategies including transfection with a cationic reagent, electroporation, sonication, or repeated freeze-thaw cycles.

Genetic modification of cells is often used in the production of cell, gene, and protein therapies.[105] The engineered producer cells essentially function as factories in which therapeutic constructs may be generated following genetic modifications. This strategy has been extended to the production of recombinant EV-based therapeutics in which a molecule of interest is over-expressed in the producer cells and subsequently incorporated into the EVs produced.[106] A common method of genetically modifying the EV-producer cells is to transfect the cells with a DNA plasmid encoding a gene of interest downstream of a high-expressing promoter such as the cytomegalovirus promoter.[106] Cationic reagents, such as polyethylenimine or calcium-phosphate, are often used to enhance the uptake of the DNA-plasmid into the producer cells, where the plasmid is then translocated to the nucleus and largely expressed as an episome.[105]

Antibiotic resistance genes are often incorporated into the plasmid which can be used to select for cells that were successfully transfected.[105] This approach may be used to increase the production of RNA and subsequently protein in the producer cells and subsequently increase the incorporation of these molecules into the EVs produced.[106] Specifically, this approach has been used to produce EVs expressing chimeric proteins incorporating an RNA-binding protein on an intracellular domain of CD9, an EV-enriched tetraspanin protein.[107] This allowed for increased incorporation of miR-199 into the EVs and subsequent delivery to target cells. Cheng et al.,[108] used this platform to over-express T-cell-specific CD3 and tumor-enriched epidermal growth factor receptors in EVs, suggesting the cumulative response of the two expressed proteins resulted in homing of T-cells to breast cancer cells.

In a landmark study of engineered EV therapeutics, Dooley et al.,[109] used plasmid transfection of highly-enriched EV transmembrane proteins discovered via mass spectrometry to over-express these proteins at the EV surface. In the prostaglandin F2 receptor inhibitor (PTGFRN) over-expressing EV formulation they effectively conjugated various functional molecules, such as IL-7, IL-12, CD-40, alpha-CD3 to the extracellular domain of PTGFRN to display the molecules at the surfaces of the EVs. They then used these EVs for immune-modulation and demonstrated significantly enhanced potency of these compounds on regulating immune cell activity in vitro when displayed on the PTGFRN-EV construct versus the compounds alone.[109] For enhanced intraluminal cargo loading, the group identified MARCKS and BASP1 as highly-enriched scaffolding proteins with hydrophobic regions embedded in the plasma membrane and a cytosolic domain to which functional molecules could be conjugated.[109] Using these scaffolds, they then

proceeded to load proteins of various sizes into the EV lumen, including the RNA-binding MS2 bacteriophage major coat protein, chicken ovalbumin, and Cas9, of which the ovalbumin formulation was used in vivo to successfully mount immune responses against the ovalbumin antigen.[109] Branching off of this work, the company has launched its ExoSTING platform, in which PTGFRN-expressing EVs are loaded with cyclic dinucleotide agonists of the STimulator of InterferoN Genes (STING) pathway.[110] When injected intratumorally in mice, this EV formulation resulted in a targeted anti-tumor immune response due to induction of interferon signaling which subsequently lead to activation of Th1 and CD8+ T-cells.[110] This technology is currently undergoing a first in-human phase 1/2 clinical trial to evaluate its safety/efficacy at treating advanced solid tumors.[111] More recently, the company has deployed yet another engineered EV therapeutic construct, termed exoASO-STAT6, which delivers an ASO targeted toward the genetic sequence encoding signal transducer and activator of transcription 6 (STAT6) displayed on the surface of EVs.[112] In mice, intratumoral administration of this EV formulation resulted in a M2 to M1 transition in macrophage phenotype mediated by the knock down of STAT6 and expression of nitric oxide synthase 2. [112] This resulted in a proinflammatory response in the tumor microenvironment and up to 90% growth inhibition of the tumor cells and 50-80% total remission in the mice.[112]

Substantial progress in engineered EV therapeutics has also been achieved by Evox Therapeutics out of Oxford, United Kingdom. In 2012, this group demonstrated the ability to use engineered EVs displaying the neuron-targeted rabies virus glycoprotein fused to Lamp2b to selectively deliver siRNA to various cell-types within the mouse brain.[113] This EV formulation showed little off-target effects and

successfully knocked down RNA and protein expression of the BACE1 gene, which is of interest in the treatment of Alzheimer's disease.[113] Recently, researchers from this group developed an engineered EV formulation displaying decoy receptors for various cytokines, tumor necrosis factor alpha (TNF-α) and IL-6.[114] Specifically, by displaying tumor necrosis factor-1 and IL-6 signal transducers at the EV surface, the engineered EVs were able to act as decoys, binding to both TNF-α and IL-6 and ameliorating disease progression in mouse models of systemic, neural, and digestive inflammation.[114]

Another strategy is to load therapeutic payloads onto EVs via membrane conjugation rather than into the EV lumen.[104] The EV membrane is composed of a phospholipid bilayer with a hydrophobic center, thus amphiphilic molecules composed of a therapeutic construct with the addition of a hydrophobic domain, such as a cholesterol or palmitoyl group, may be inserted into the EV membrane and presented at its surface. Cholesterol groups associated with Y-like RNA molecules have been used to functionalize the EV surface.[115] Specifically, aptamer technology was then used to associate a targeting ligand to the RNA molecules and the EVs were used to deliver miRNAs and siRNAs to various cancer types. Additionally, cholesterol-conjugated ASOs were used in the generation of the exoSTING and exoASO-STAT6 formulations by Codiak BioScience as previously mentioned.[110,112]

Another common approach to introducing therapeutic payloads into EVs is via electroporation.[104] This method introduces an electric field to generate transient pores in the EV membrane, allowing easier access of therapeutic constructs, such as non-coding RNAs or ASOs, into the EV lumen and then removing the electric field to restore EV integrity with the biomolecules now encapsulated.[116] The efficiency of this

method has been shown to be far superior to passive incubation with miRNA cel-39; however, its efficiency with larger molecules such as mRNA and proteins may be less.[117] Further, the true efficiency of these loading protocols is unclear as free miRNA is often removed via ultracentrifugation, which does not fully remove free miRNA from EV preparations.[118]

These studies established a number of methods for generating EV formulations containing or displaying exogenous therapeutic payloads. Although these strategies allow for efficient loading of therapeutics onto or into EVs, they largely still do not address EV biodistribution. Thus, the EVs may not be delivered to the target tissue/cell-type efficiently. This would presumably result in the need for larger doses and potentially even adverse off-target effects as discussed with other delivery vectors, such as AAV. Thus, in order to achieve the full efficacy of EV-based drug delivery in diseases present in hard-to-reach organs/tissues, such as skeletal and cardiac muscle, specific engineering of the EV surface moieties is likely necessary.

1.4 Biodistribution of Native and Engineered EVs

1.4.1 Biodistribution and Tropism of Native EVs

Native EVs innately display tropism to particular cell- and tissue-types depending on the cell-type they are released from, showing strongest tropism for their parental cell type.[119] However, EVs are also suggested to act via paracrine and endocrine mechanisms, delivering molecular cargoes to various cell-types.[120]

Much of the work conducted investigating intercellular and even interspecies tropism has been conducted with EVs derived from various cancer cell lines. The EVs derived from tumor cell-types, such as breast, colorectal, and pancreatic cancer cells

display tissue-tropic properties in the progression of cancer metastasis depending on the integrin protein profile in the EV membrane.[121] For instance, it is suggested that EVs released by colorectal cancer cells are enriched in integrin beta-1, enhancing the tropism of the EVs to fibroblasts which subsequently become activated and facilitate the generation of the proinflammatory metastatic niche.[122] EV-associated integrin proteins were also found to play a critical role in cancer EV biodistribution in another study where EVs derived from MDA-MB231 breast cancer cells localized to the lungs via an integrin α6β4 and α6β1-dependent mechanism.[121]

Although the cell and tissue-tropic properties of EVs are well characterized in terms of pathogenesis, these properties may potentially be exploited for enhanced delivery of therapeutics in the treatment of various pathologies. Recombinant EVs can be generated by cells in vitro, purified and then administered in vivo as a delivery vector endogenously produced or exogenously loaded therapeutic. A crucial factor in the efficacy of EVs as a therapeutic delivery system is their ability to deliver the therapeutic payload to the diseased cell/tissue-type. Overall, EVs administered in various animal models have largely been found to localize to the liver, kidneys, lungs and spleen.[123] Wiklander et al.,[124] noted that EV tissue-tropism is largely dependent on the cell-type of origin as well as the route of administration. When non-modified HEK293 EVs were administered intravenously in mice, they found that the EVs largely localized to the liver followed by the spleen, gastrointestinal tract and lungs. The authors also examined the biodistribution of EVs derived from C2C12 myotubes, B16F10 melanoma cells, mouse bone marrow-derived dendritic cells, rat oligodendrocytes, and human-derived HEK293 and MSCs. Surprisingly, C2C12 myotube-derived EVs showed the greatest accumulation in the liver, whereas the

melanoma cell-derived EVs showed preferential distribution to the GI tract and DC-EVs primarily accumulated in the spleen. The MSC-EVs showed the highest accumulation in the liver, similar to C2C12 EVs.[124]

As discussed previously, MSC-EVs are of great interest as a therapeutic for a number of disease indications; however, given that upwards of 71% of the EVs are taken up by the liver, this may reduce their therapeutic potential for ameliorating diseases located elsewhere in the body, such as skeletal and cardiac muscle.[125] Another group corroborated these findings by showing that intravenously administered MSC-EVs predominantly accumulate in the liver and spleen but to a lesser extent in the skeletal system where many of the pathologies exist that these EVs are aimed at treating. Driedonks et al.,[126] recently investigated the biodistribution of EVs from Expi293F cells, a suspension-adapted HEK cell line, engineered to express palmitoylated EGFP-Nanoluciferase that were additionally stained with MemGlow 700 nm dye via intravenous and intranasal injection in mice and macaques. In the macaques, Expi293F EVs administered intranasally failed to show any signal in the plasma. It is hypothesized that the EVs may have gotten caught in the nasal cavity, mucosa, or the lungs. However, the intravenously administered EVs were detectable with an average half-life between 20 to 40 minutes which is considered typical. The authors also detected fluorescently-tagged EVs in the cerebrospinal fluid, potentially allowing delivery of EV molecular contents to the central nervous system. An interesting component not typically examined in the previous studies was the uptake of the Expi293F EVs by peripheral blood mononuclear cells (PBMCs). They noted uptake of the EVs by granulocytes, monocytes, CD3+ lymphocytes as well as CD20+ B cells. Upon examination of the tissue biodistribution following intravenous

administration in mice, the authors observed the greatest accumulation of EV-derived fluorescence in the liver followed by the kidney, spleen, heart and lungs. In the macaque model, a strong signal was observed in the liver and lungs, with limited signal found in the kidney, heart, colon and brain. The only native EVs to date that appear to show innate tropism to a muscle cell-type (e.g. cardiac muscle) are CDC-EVs.[127] This was demonstrated by tracking a CDC-EV-enriched Y-RNA-derived small RNA species dubbed NT4 using quantitative PCR to detect this RNA in various tissues. Using this method, they observed the greatest delivery of NT4 in the cardiac musculature when examined on a per gram of tissue basis. Beyond the cardiac tissue, the liver, kidney, spleen and lungs showed the greatest uptake, with minimal delivery to the brain as well. However, when the data are viewed as a percentage of total signal, the liver still showed the greatest uptake of NT4, with the heart displaying the second highest signal.

Another critical consideration for EV biodistribution is the disease status of the recipient. For example, in a model of acute kidney disease, MSC EVs were found to localize to the kidney due to the pro-inflammatory environment, which was not observed in the wild-type mouse model.[128] Intravenous administration of macrophage-derived EVs carrying the exogenously-loaded protein, tripeptidyl peptidase-1, in a mouse model of Neuronal Ceroid Lipo-fuscinoses 2 showed enhanced accumulation to the brain; however, the EVs still largely accumulated in the liver, lungs, spleen, and kidneys.[129] Additionally, the study by Ciullo et al.,[127] mentioned previously, noted that CDC-EVs administered to mice intravenously following cardiac injury showed enhanced delivery to the heart, liver and brain relative to the wildtype mice. Thus,

understanding how various diseases influence EV biodistribution will be critical for the progression of EVs as a therapeutic modality.

Overall, EVs appear to hold great potential as drug delivery vectors; however, as demonstrated by the studies summarized here, EVs largely accumulate in organs such as the liver, spleen, kidneys and lungs. Thus, in order to unlock their full potential as delivery vectors, EVs may require further engineering to better deliver therapeutic payloads to target tissues/cells while avoiding organs, such as the liver, which both reduce the efficacy of the treatment as well as pose safety concerns for patients.

1.4.2 Engineering EVs for Enhanced Tropism to Specific Cell-Types

In the various engineering strategies described earlier, it has been demonstrated that EVs can be modified to display specific proteins and other targeting moieties to impart tropism for a given tissue/cell-type by either genetically engineering the producer cells or chemically modifying the EVs post-release.[130] In combination with their inherent stability and biocompatibility, the ability to engineer EVs to display targeting moieties has the potential to overcome many of the limitations associated with current drug delivery vectors, such as AAV.

Using genetic engineering strategies, producer cells can be engineered to produce EVs displaying transmembrane proteins that are specific to known tissue/cell-enriched receptor proteins.[130] This process often involves the transfection of a plasmid encoding the desired targeting protein upstream of a known EV-enriched protein as a scaffold and downstream of a constitutively-active promoter sequence such as the cytomegalovirus (CMV) promoter.[130] LAMP-2b, a member of the lysosome-

associated membrane protein family, has commonly been used as a scaffold protein for extramembranous display of targeting motifs.[113,130] EVs displaying the rabies virus glycoprotein (RVG) peptide (TIWMPENPRPGTPCDIFTNSRGKRASNG) fused to the extramembranous N-terminus of LAMP-2b via genetic modification of donor cells has been demonstrated to mediate enhanced delivery of EV cargo to cells of the CNS.[113] The RVG targeting moiety has also been used to deliver miR-124 to neurons in a mouse model of ischemia.[131] It has been demonstrated that tumor-derived EVs target various cell and tissue-types during metastasis depending on the EV membrane integrin protein signature.[132] Conjugation of the αγ integrin-specific iRGD peptide (CRGDKGPDC) to LAMP-2b via genetic engineering of mouse immature dendritic cells was shown to result in the production of EVs with enhanced affinity for breast cancer cells.[133] The authors utilized this platform to shuttle the chemotherapeutic agent doxorubicin into the tumor cells. The same iRGD peptide was also utilized to target KRAS siRNA in a subcutaneous adenocarcinoma human alveolar basal epithelial cell mouse model.[134] tLyP-1 peptide (CGNKRTR), a non-small cell lung cancer (NSCLC)-homing peptide, was used to selectively target neuropilin-1 (NRP1) and neuropilin-2 (NRP2) receptors to deliver siRNA to lung cancer cells.[135] The LAMP-2b scaffolding model for EV surface engineering has also been applied to the treatment of osteoarthritis where the chondrocyte affinity peptide (DWRVIIPPRPSA) was utilized for targeted delivery of EVs containing miRNA-140 in rats.[136] A mesenchymal stem cell affinity peptide (E7) conjugated to LAMP-2b was used for targeted delivery of kartogenin-containing EVs into the knee joints of rats.[137] EVs displaying platelet-derived growth factor receptor fused to the GE11 peptide were used to target the miRNA let-7 to EGFR-expressing breast cancer cells.[138] Although LAMP2b has been

the most commonly utilized scaffolding protein to which targeting moieties are fused, the proteins PTGFRN or syntenin may present more highly enriched scaffolds to enhance EV-engineering efficiency.[109] The PTGFRN scaffolding platform was utilized to generate EVs displaying antibodies targeting CD3 (T-cells) and EGFR (breast cancer cells).[138] Genetic engineering presents a promising strategy for producing recombinant EVs displaying targeting moieties, although this may be highly dependent on the ability of the end protein product to be incorporated into the EVs. Careful selection of scaffolding proteins, such as PTGFRN and syntenin, may overcome this, allowing for reproducible generation of targeted EV formulations. Although this approach has led to the generation of a number of promising targeted EV formulations, no successful myotropic EV formulation has been reported to date. The closest attempt utilized the myotropic peptide ASSLNIA fused to the extramembranous domain of Lamp2b.[113] This formulation showed promising results in C2C12 myotubes in vitro but failed to recapitulate this myotropism in vivo. Given that this peptide and others have demonstrated successful muscle-targeted delivery with other constructs, such as AAVs and ASOs,[39,43] perhaps the improved scaffolding proteins, such as PTGFRN,[109] would unlock the myotropic potential of these muscle-targeted peptide-EV constructs. Further, a number of endogenous proteins, such as MYMK, MYMX, and M-Cad exist that have key roles in myogenic fusion and adherence in physiology.[66,67] These may present promising candidate proteins to express in EVs to generate novel myotropic EV formulations expressing naturally-occurring muscle-enriched proteins.

In addition to genetic engineering of producer cells in the “upstream” portion of the EV production process, EVs may also be engineered during “downstream”

processing via chemical modification of EV surface moieties.[130] This strategy expands the repertoire of targeting moieties that may be utilized, as genetic engineering is limited to protein-based targeting moieties that are able to be encoded by a plasmid, whereas chemical modification can use a range of compounds.

A common method of chemically adhering a targeting moiety to the surface of EVs is by generating an amphiphilic construct consisting of the targeting molecule fused to a lipophilic molecule that can be inserted into the EV phospholipid bilayer.[130] This method was used to adhere aminoethyl anisamide to the membrane of macrophage-derived EVs via fusion of this molecule to polyethylene glycol (PEG)-grafted 1,2-dioleoyl-sn-glycero-3-phosphoethanolamine (DSPE-PEG).[129] This surface-modified EV formulation allowed for targeted delivery of paclitaxel into lung cancer cells. DSPE-PEG-mediated surface modification in combination with folate was also successfully utilized to conjugate αγ-integrin-targeting peptide RGD (CRGDKGPDC) to the surface of EVs for targeted delivery of erastin to breast cancer cells.[115] Cholesterol presents another lipophilic molecule that may be adhered to targeting moieties for efficient insertion into the EV phospholipid bilayer.[139] For example, Pi et al.,[115] used cholesterol-containing RNA aptamers targeting prostate specific membrane antigen or epidermal growth factor receptors to functionalize the surface of EVs for targeted delivery of EVs to deliver survivin siRNA into prostate, breast and colorectal cancer xenografts. This method has also been utilized to adhere the aptamer, AS1411, to the surface of EVs, which facilitated the targeting of the EVs to nucleolin-expressed breast cancer tissues in vivo. This enabled the efficient delivery of the miRNA let-7, resulting in the inhibition of tumor growth.[140] Another chemical method utilizes a set of reactions referred to as “click chemistry” whereby copper-catalyzed azide-alkyne

cycloaddition reactions facilitate the attachment of azide-containing compounds to alkylated amine groups on EV surface proteins.[141] Jia et al.,[142] employed this method to conjugate the neuropilin-1-targeted RGE peptide (RGERPPR) to the surface of EVs. Using this modified EV formulation, the authors selectively delivered the anti-tumor compound curcumin to glioma cells both in vitro and in vivo. Click chemistry has also been utilized to attach the cyclo (Arg-Gly-Asp-D-Tyr-Lys) peptide, referred to as c(RGDyK), to the surface of MSC-EVs.[141] This protein displays high affinity for integrin αvβ3 in reactive cerebral vascular endothelial cells following ischemia. The authors demonstrated that displaying this protein at the EV surface allowed for the targeted delivery of curcumin to microglia, neurons and astrocytes, and resulted in suppression of the inflammatory response and cellular apoptosis following middle cerebral artery occlusion and reperfusion injury. Further, Koh et al.,[143] also utilized this method to generate an EV-mediated checkpoint therapeutic for cancer therapy. They disrupted the SIRPα-CD47 checkpoint cascade that cancer cells utilize to avoid detection by macrophages by adhering a SIRPα antibody to the surface of EVs in a syngeneic mouse model of cancer. This resulted in enhanced clearance of tumor cells by macrophages as well as T cells. The RVG peptide, mentioned previously, has also been successfully displayed at the surface of MSC-EVs via conjugation to the phospholipid dioleoylphosphatidylethanolamine.[144] When administered in a mouse model of Alzheimer's disease, these EVs targeted cells of the cortex and hippocampus and were reported to prevent memory deficits associated with this mouse model. Both genetic and chemical engineering present promising strategies for the generation of EVs displaying targeting moieties specific to various tissue/cell types. Genetic engineering offers a method of expressing targeting proteins via natural cell

transcription and translation mechanisms, although this poses limitations with the degree to which the protein of interest can be expressed and the degree to which it is incorporated into the EVs of the producer cells. These factors are somewhat controllable by utilizing constitutively active promoters to produce as much of the protein as possible and using targeting proteins fused to extracellular domains of EV-enriched transmembrane proteins to enhance the display of the proteins at the EV surface. Chemical engineering strategies present a potentially more tunable approach to modifying the surface of EVs as they often utilize highly efficient chemical reactions and lipophilic molecules to insert targeting moieties into the EV phospholipid bilayer. However, it should be noted that incorporation of synthetic constructs may forgo EVs biocompatible nature by enhancing recognition by immune cells. More work is needed to fully elucidate approaches that maximize efficiency and safety in developing targeted EV constructs for precision drug delivery.

1.5 Summary

Muscular pathologies comprise a family of degenerative muscle diseases and disorders spanning from primary genetic muscular diseases, such as DMD, to severe secondary muscle conditions, such as cancer cachexia. Although promising strides in the development of therapeutics for these conditions have been made, key limitations regarding toxicity and immunogenicity persist. EVs represent a highly biocompatible delivery vector, naturally used by cells in the body to transmit molecular cargoes via paracrine and endocrine mechanisms. By engineering EVs to display targeting moieties to particular tissue/cell types, they may be utilized as biocompatible, targeted drug delivery vehicles. Although this strategy has the potential to overcome many of

the limitations of current vectors for therapeutics used to treat muscular pathologies, such as AAV, very few studies have investigated the implementation of engineered EVs for the targeted delivery of therapeutics to skeletal and cardiac muscle. The only documented attempt ultimately ended in failure in vivo.[113] However advancements in EV-scaffolding proteins for enhanced engineering could be a promising strategy for generating improved myotropic EV formulations.[109] Additionally, a number of proteins expressed in muscle stem cells and myoblasts possess critical functions in myogenic fusion and adherence.[66,67] If expressed in the EV membrane, these proteins could feasibly impart these myotropic properties on the EVs. Thus, more work is needed to fully elucidate the potential of these novel myotropic EVs to deliver therapeutic cargoes in a targeted manner.

Chapter 2

GENERATION AND BIODISTRIBUTION OF EVS DISPLAYING RECOMBINANT TMEM8C (MYOMAKER) PROTEIN

2.1 Introduction

Muscular pathologies comprise a wide range of diseases and disorders affecting the musculoskeletal system, including genetic conditions, such as muscular dystrophies as well as secondary muscular pathologies, such as cancer cachexia.[1,2] Current treatment modalities, such as glucocorticoids and gene therapies have provided significant progress in the treatment of these disorders.[22,27] However, these therapeutics are non-specific to muscle and cause harmful off-target effects in patients.[24] Thus, a myotropic (muscle-targeted) delivery system is needed to enhance the efficacy and reduce the off-target effects of current therapeutics.

Extracellular vesicles (EVs) are a heterogeneous class of cell-derived nanoparticles varying in size (30-1000 nm) and mechanism of biogenesis.[74] Due to their biocompatibility and engineerability, EVs are suggested to be ideal vectors for biotherapeutics.[130] More specifically, EVs can be engineered to display various targeting moieties, altering the tropism of the EVs for targeted delivery of luminal cargo to specific cell/tissue types.[145] For example, Wood et al., engineered EVs expressing the neuron-targeted rabies virus glycoprotein (RVG) fused to the lysosome-associated membrane glycoprotein 2 isoform B (Lamp2b), an EV-enriched membrane protein, for targeted delivery of a silencing ribonucleic acid (siRNA) to neurons in mice.[113] More recently, researchers have engineered EV products utilizing the proteins PTGFRN[109] or syntenin/syndecan-1[114] as scaffolds to which targeting moieties can be conjugated, resulting in EV formulations with enhanced affinity for

the target cell-types. Although EVs have the potential to be highly engineerable and biocompatible drug delivery vectors, no successful myotropic EV formulation has been generated to date. A previous formulation utilizing the myotropic peptide, ASSLNIA, fused to Lamp2b showed promising results in vitro, but failed to demonstrate myotropic biodistribution in vivo.[113] Other studies have reported enhanced myotropism of adeno-associated Virus (AAV)[39] and Antisense oligonucleotide (ASO)[43] drugs conjugated to myotropic peptides in vivo. However, the pool of myotropic EV candidates remains sparse.

The strategies for muscle-targeted delivery of therapeutics attempted thus far have largely focused on engineering synthetic myotropic peptides (MPs), ASSLNIA and RRQPPRSISSHP, either directly to the therapeutic (ASO) or the vector used for delivery (AAV2 or EV). However, many native muscle-enriched membrane proteins exist. The proteins MyoMaker (MYMK) and MyoMixer (MYMX) are myogenic membrane-fusion proteins involved in the fusion of myoblasts into muscle fibers during embryonic development and repair of adult muscle.[67,68] It was found that when the genes encoding either of these proteins were deleted, complete fusion of myoblasts into myotubes was inhibited, emphasizing their roles in muscle-specific membrane fusion.[67] Further, when over-expressed via transfection in fibroblasts, MYMK enabled the fusion of the fibroblasts to myotubes in vitro.[67] In addition, M-Cadherin (M-Cad) is a membrane protein that adheres quiescent satellite cells to adjacent muscle fibers.[68] Given the physiologic roles of these proteins in membrane fusion/adherence to the muscle fiber membrane and the sparsity of myotropic EV candidates, we examined the myotropic properties of EVs expressing each of these native myotropic protein candidates. Preliminary experiments screening these myotropic EV candidates

identified the MYMK-EV formulation as showing the greatest myotropic potential in vitro. We assessed this by measuring the delivery of EV-derived protein cargo into C2C12 myotubes in vitro, a cell-type that is commonly used for these types of experiments.[113] In the current study, we examined the myotropic properties of EVs displaying the native myotropic protein candidate, MYMK, in vivo. We hypothesized that MYMK-EVs would show greater affinity for skeletal muscle relative to non-engineered Human Embryonic Kidney (HEK293) cell-derived EVs in both C57/BL6 and mdx (DMD, exon 23 nonsense point mutation) mouse models.

2.2 Materials/Methods

2.2.1 Animals

For the in vivo biodistribution experiments, 6-11 week old male C57/BL6 and mdx mice were used. For both sets of biodistribution experiments utilizing either a lipophilic or amine-reactive probe, C57 and mdx mice were randomly assigned to 3 experimental groups each: no injection control, HEK-EV injection, or MYMK-EV injection. Thus, a total of 36 mice were utilized for these experiments. Male mice were used exclusively as DMD is an X chromosome-linked genetic condition, thus it affects males at a rate of 1:3,500-6,000 live births and largely does not affect females (1:50,000,000 live births).[146] Mice were group housed on a 12-hour light cycle and had free access to food and water throughout the duration of the experiments. All mouse experiments conducted were approved by the University of Delaware IACUC under AUP 1387.

2.2.2 Transient Transfections

For experiments involving transient transfections, Human Embryonic Kidney 293 (HEK293) cells were transfected with plasmids encoding GFP-tagged MYMK, MYMX, or M-Cad downstream of a cytomegalovirus promoter using the JetOPTIMUS cationic lipid reagent at a 1:1 ratio for 4 h per the manufacturer's instructions. 24 h later, we proceeded to EV purification protocol. Transfection efficiency was confirmed using the 488 nm channel on the ImageExpress Pico (Molecular Devices, San Jose, CA) to obtain representative images of the endogenous GFP tag-derived signal for each transfection group.

2.2.3 Generation of Stable Cell Lines for MYMK-EV Production

To generate a (HEK293) cell line that stably over-expressed MYMK, HEK293 cells were transduced with lentiviral particles (LVP) containing the MYMK transgene cloned into a pLenti-C-mGFP-P2A-Puro plasmid at a multiplicity of infection (MOI) of 10 LVP/cell. This was based on preliminary experiments that found this MOI to be sufficient (Figure A.1). The cells were then expanded back to 90-95% confluency before subsequent passaging. The FACSAria Fusion (BD Biosciences, Woburn, MA) was used to select for stable clones displaying the highest MYMK expression as determined by the endogenous mGFP tag. The cells were subsequently expanded to 875cm² flasks (Falcon, Corning, NY) in growth medium (GM) containing high glucose DMEM, 5% FBS and 100U/mL of p/s. Once in the 875cm² flasks, the cells were expanded to 90-95% and the serum-containing GM was switched to serum-free OptiMEM for EV production. Two washes with 1X PBS + 10% OptiMEM or DMEM were used to remove residual serum-containing GM. The cells were incubated in the

OptiMEM for 48 h before the EV-conditioned media was collected. The cells were subsequently passaged using 0.25% trypsin-EDTA (ThermoFisher, Waltham, MA) followed by inoculation into new 875cm² flasks. Total viable cell density was routinely measured and only cells with a viability of ≥ 90% were used for EV production. Additionally, aliquots of 1.0e7 cells were collected at passages 19, 21 and 23 and stored in the liquid nitrogen vapor phase. To measure MYMK expression in the cells over the time of EV production, the aliquots were then thawed and spun at 500 x g for 5 min. The pellets were resuspended in 1 ml of 1X RIPA buffer with 1X protease and phosphatase inhibitor cocktail and vortexed at max speed for 3 x 10 sec. 100 ul of cell lysate was loaded into a 96-well plate in triplicate and analyzed using the 488 nm channel on a fluorescent plate reader.

2.2.4 EV Purification

For the HEK, MYMK, MYMX and M-Cad EVs produced following transient transfection for preliminary *in vitro* uptake experiments in C2C12, EVs were concentrated using the polyethylene glycol-based reagent, ExoQuick TC (Systems Biosciences, Palo Alto, CA), added at a 1:5 ratio with the conditioned media. The media-ExoQuick solutions were incubated at 4°C overnight and then spun at 1,500 x g for 30 min the following day. The EV-containing pellets were re-suspended in 100 ul of 1X PBS prior to downstream analysis.

For the HEK and MYMK-EVs produced for the biodistribution experiments, the harvested conditioned media was centrifuged at 500 x g for 10 min to remove dead cells and then at 2,000 x g for 20 min to remove larger cell debris. The EVs were then purified from the conditioned media via ultracentrifugation (UC) at 100,000-150,000 x

g for 60-90 min. In experiments in which the EVs were stained, the pellet was washed with 25 ml of 1X PBS following staining and the EVs were re-pelleted via UC following staining at 150,000 x g for 60 min. All centrifugation steps were performed at 4℃.

2.2.5 Nanoparticle Tracking Analysis (NTA)

A Nanosight NS300 (Malvern Panalytical, Malvern, PA), with a 532 nm green laser and NS300 FCTP Gasket (Malvern Panalytical, Malvern, PA), was used for NTA characterization of the number and size of the EVs in each sample. The EV samples were then analyzed using a camera level of 12 and a detection threshold of 10. Three 30 second videos were obtained for each sample. The EV samples were diluted to a working concentration of ~1e9/mL for analysis and were administered into the gasket using a sterile BD Plastipak syringe (Becton Dickinson S.A., Madrid, Spain).

2.2.6 Flow Cytometry

A FACS Aria Fusion was used to examine the efficiency with which each native myotropic protein candidate was incorporated into EV. To do so each EV sample was labeled using ExoGlow Red (Systems Biosciences, Palo Alto, CA) following the manufacturer's instructions. Briefly, dye stock was added to each sample at a 1:500 dilution and incubated at 37℃ for 20 min while shaking at 350 rpm. ExoQuick TC was then add to each sample at a 1:5 ratio and incubated at 4℃ overnight. The next day, the samples were re-pelleted at 1,500 x g for 30 min at 4℃. The supernatant was then carefully aspirated and the pellets were re-suspended in 100 ul of 1X PBS. For flow cytometry, the samples were further diluted 1:100 in 0.1um-

filtered 1X PBS and analyzed using a FACS Aria Fusion. Specifically, the GFP and PE-A laser lines were utilized to measure the signal from the GFP-tagged recombinant proteins (MYMK, MYMX, M-Cad) and the ExoGlow Red stain, respectively. Gating was established by first running unstained, non-engineered HEK293 EVs and modifying the gating parameters to exclude this signal. The labeled samples from each of the cell lines were then run through the instrument until 30,000 total events were captured. The data were analyzed using FCS Express to measure the percentage of events that were positive for both GFP and the ExoGlow Red stain to obtain an estimate of the percentage of EVs that were positive for the recombinant proteins following transient transfection.

2.2.7 Screening of Native Myotropic EV Candidates

For the preliminary screening of the native myotropic EV candidates, EVs were labeled with 40 uM carboxyfluorescein diacetate succinimidyl ester (CFDA-SE) for 2 hours at 37℃. To remove unbound dye, the EV samples were then incubated with ExoQuick-TC at a 1:5 sample:reagent ratio at 4℃ overnight. The samples were then centrifuged at 1,500 x g for 30 min re-pellet the labeled EVs. The labeled pellet was re-suspended in 100 ul 1X PBS prior to downstream experiments. C2C12 myoblasts were seeded in half surface area 96-well plates (Greiner Bio-One, Monroe, NC) at 10,000 cells/well in growth medium containing 10%, 1% p/s in DMEM. After 24 hours, the medium was switched to differentiation medium containing 2% horse serum rather than FBS. After six days in the DM, the C2C12 myoblasts had fully differentiated into myotubes at which time they were incubated with 5.0e8 of each EV formulation as determined by NTA. After 24 hours, the medium was changed to DM

containing Live-Cell NucBlue for 20 min at 37℃ to label the nuclei. The C2C12 myotubes were then imaged on an ImageExpress Pico and the images were analyzed to measure the CFSE-derived signal in the 488 nm channel relative to each nuclei.

2.2.8 BCA Protein Assay

The BCA protein assay was used to determine the protein concentration of EV samples following the manufacturer's instructions. EVs were lysed using 1X RIPA buffer and 1X protease and phosphatase inhibitor cocktail. Protein concentrations were determined using a BioTek Synergy 2 plate reader (Agilent, Santa Clara, CA). The derived protein concentration was compared to the particle count obtained from NTA to determine the protein/particle ratio as a measure of sample purity.[72]

2.2.9 Western Blotting

SDS-PAGE was performed with a Quadra Mini Vertical Blotting System (CBS Scientific, San Diego, CA). Samples were mixed with 4x lithium dodecyl sulfate (LDS) sample buffer along with 1.0% Triton X-100, and 15 mM dithiothreitol. The samples were then heated at 95°C for 10 min. Once denatured, the samples were then loaded into a RunBlue 4–12% TEO-Tricine Protein Gel and run at 130 V in RunBlue TEO-Tricine run buffer for 1.5 hr with a stir bar and ice pack. A Power Blotter system (Thermo Fisher Scientific, Waltham, MA) was used to transfer the proteins on the gel to a nitrocellulose membrane with 0.2 μm pore size for 10 min. The membranes were blocked using Omniblok™ overnight at 4°C with gentle rocking. After blocking, the membranes were incubated overnight at 4°C with primary antibody solution (1:1000 dilution for anti-Alix and anti-Tsg101, 1:2000 dilution for anti-GAPDH, and 1:5000

dilution for β-actin) with gentle rocking. After primary antibody incubation, the membranes were washed three times with tris buffered saline (TBS) containing 0.1% Tween-20 (TBS-T) for 5 min per wash. The membranes were then incubated with HRP-conjugated secondary antibodies (anti-mouse or anti-rabbit depending on primary antibody species) for 1 hr at RT (1:100000) with gentle rocking. Membranes were washed two times with TBS-T for 5 min per wash and two times with TBS for 5 min again. The blots were incubated with enhanced chemiluminescent (ECL) substrate to develop and then imaged on and Odyssey infrared imaging system for analysis.

2.2.10 Fluorescent Plate Reader Assays

Cell and EV lysates were generated as described previously. Equal amounts of cell and EV lysates were loaded into a 96-well plate and analyzed on the BioTek Synergy 2 plate reader using the 488 nm channel to measure the MYMK expression in both the cell and EV lysates throughout EV production.

2.2.11 Transmission Electron Microscopy (TEM)

The EV samples were concentrated to ~ 1.0e11-2.0e11 particles/mL. 400 mesh carbon-coated copper grids were floated onto each sample. The grids were washed with four drops of water and negatively stained with 2% uranyl acetate (aq). Prior to the addition of the sample, the grids were glow discharged with a Pelco easiGlow glow discharge unit (Ted Pella Inc, Redding, CA), making the carbon film hydrophilic. The samples were then imaged using a Zeiss Libra 120 transmission electron microscope (Oberkochen, Germany) operating at 120 kV. Images were obtained with a Gatan Ultrascan 1000 CCD camera (Warrendale, PA).

2.2.12 In Vivo Biodistribution of MYMK and HEK293 EVs

Biodistribution of MYMK and non-engineered HEK293 EVs were assessed using two sets of experiments. In the first set of experiments, EVs were labeled with 5 µM DiD for 20 min at 37℃. A preliminary experiment revealed that free DiD not bound to EVs floats to the to the surface of PBS under UC at 150,000 x g for 1 h (Figure A.2), thus we determined UC was a sufficient method to remove unbound dye from the sample and pellet the DiD-labeled EVs. Following labeling, NTA was utilized to measure the concentration of the EVs. 1.2e11 labeled EVs were administered to both C57/BL6 and mdx mice (N = 3 male mice/group, 6-11 weeks old) via tail vein injection. After 24 hours, the mice were anesthetized using 3% isoflurane gas. Once under anesthesia, the gastrocnemius, heart, diaphragm, brain, liver, spleen and kidneys were harvested from the mice and washed with 1X PBS. The organs were then kept in 1X PBS on ice as the others were harvested. Immediately following the dissection, the organs were imaged on an IVIS Lumina III (Perkin Elmer, Waltham, MA) using excitation 689 nm and emission 713 nm. Additionally, the whole organs or sections of the larger organs were homogenized in 1 ml of TPER or NPER (brain) using 1.4 mm ceramic beads (Omni International, Kennesaw, GA) in a Mini Bead Mill (VWR, Radnor, PA) and 100 ul of tissue homogenate was loaded into a 96-well plate and analyzed using a fluorescent plate reader to obtain quantitative fluorescence data, normalized to tissue weight (g).

The second set of experiments examined the intracellular delivery of EV-derived protein. EV luminal proteins were stained with 5 µM CT-R for 30 min at 37℃. The unbound dye was removed via elution through PD-10 desalting columns

following the manufacturer's instructions (Cytiva Life Sciences, Marlborough, MA). The stained EVs were then re-pelleted at 150,000 x g for 1 h and resuspended in 1X PBS. In the first set of biodistribution experiments, NTA-derived particle count was used to determine the EV dose. In the second set of experiments, a fluorescent plate reader was used to normalize the doses of EVs due to a discrepancy noted in experiment one between the NTA particle count and the fluorescent signal. Thus, the EVs were produced using the equivalent number of cells as in the first set of experiments and then the fluorescence intensity was used to determine the volume of sample injected. After 24 hours the same organs were harvested as in the first set of experiments; however, the organs were frozen in OCT freezing compound (Electron Microscopy Sciences, Hatfield, PA) using a copper block placed in liquid nitrogen. The samples were then cryo-sectioned prior to immunohistochemistry (IHC). The sections were fixed in 4% PFA followed by three 5 min washes with 1X PBS prior to blocking with 1% BSA for 30 min at RT. 25 ul of Phalloidin-488 was then added to 1% BSA in 1X PBS and 50 ul was add to each tissue section for 30 min at RT. This was removed with three 5 min washes with 1X PBS. After the final wash, all of the PBS was removed and one drop of Prolong Diamond Antifade Mountant with DAPI was added to each section prior to placement of the coverslip. The slides were allowed to cure overnight prior to imaging, per the instructions for the mountant. The slides were imaged on an Image Express Pico using a 20X objective lens and the following excitation/emission wavelengths were used: 577/602 nm for CT-R, 484/501 nm channel for Phalloidin-488, and 358/461nm for DAPI. For the in vitro experiment to verify ability of CT-R-labeled EVs to deliver labeled-protein into cells, HEK293 cells were seeded at 10,000 cells/well in a half surface area 96-well plate. 4 hours later the

growth medium was changed to growth medium containing CT-R-labeled EVs determined using a fluorescent plate reader. 24 h later the cells were stained with 5uM DiO for 15 min at 37°C followed by Live-Cell NucBlue at 37°C. Following staining, the cells were imaged on the ImageExpress Pico using the 358/461 nm for the Live Cell NucBlue, 484/501 nm for DiO, and 577/602 nm for CT-R. Additionally, we stained for dystrophin protein expression in the gastrocnemius muscle. Tissue sections were fixed using 4% PFA for 10 minutes at RT. This was washed off by 3 x 5 min washes with 1X PBS. The sections were then blocked using 1% BSA for 30 min at RT. This was dumped off without washing followed by incubation with Rabbit polyclonal Anti Dystrophin C-Terminus primary antibody at a 1:100 dilution in 1% BSA overnight at 4C. The next day, the primary antibody solution was washed with 3 x 5 min washes with 1X PBS. This was followed by incubation with Goat anti-rabbit AlexaFluor 647 IgG F(ab')2 frag at a 1:200 dilution in 1% BSA at RT for 1 hour. This was then washed off with 3 x 5 min washes in 1X PBS and mounted using Prolong Diamond Antifade with DAPI. The slides were allowed to cure overnight at RT prior to being imaged on the Image Express Pico the following day. The Cy5 channel was utilized to image dystrophin and the DAPI channel was utilized to image the nuclei.

2.2.13 Statistical Analysis

For initial in vitro experiments, a one-way ANOVA with a Tukey post hoc test for multiple comparisons was utilized to test for statistical significance. For the in vivo biodistribution experiments, a two-way ANOVA with a Tukey post hoc multiple comparisons was utilized to test for statistical significance. For all in vitro experiments, three independent experiments were conducted. The data are presented

as the average of the means +/- standard error (SE). For animal experiments, 3 mice were utilized per experimental group, equating to a total of 36 mice. Data for each experimental group are presented as the average of the means +/- SE. A p value < 0.05 was considered significant for all experiments. All statistical analyses were conducted in GraphPad Prism 9.4.1.

2.2.14 Key Resources

Animals

Reagent/Resource	Vendor	Catalog Number
C57BL/10ScSn Mice	The Jackson Laboratory	Strain #:000476
C57BL/10ScSn-Dmdmdx/J Mice	The Jackson Laboratory	Strain #:001801

Transfections

Reagent/Resource	Vendor	Catalog Number
Tmem8c (GFP-tagged) - Mouse RIKEN cDNA	OriGene	CAT#: MG202529
Gm7325 (GFP-tagged)	OriGene	CAT#: MG225058
Cdh15 (GFP-tagged)	OriGene	CAT#: MG222127
Lenti ORF particles, Tmem8c (GFP-tagged)	OriGene	CAT#: MR202529L4V

jetOPTIMUS DNA Transfection Reagent	Polyplus Transfection	Ref # 117-07

Molecular Staining/Imaging

Reagent/Resource	Vendor	Catalog Number
ExoGlow-Protein EV Labeling Kit (Red)	Systems Biosciences	EXOGP100A-1
Vybrant® CFDA SE Cell Tracer Kit	Invitrogen, ThermoFisher Scientific	V12883
NucBlue™ Live ReadyProbes™ Reagent (Hoechst 33342)	Invitrogen, ThermoFisher	R37605
Vybrant™ DiD Cell-Labeling Solution	Invitrogen, ThermoFisher Scientific	V22887
Vybrant™ DiO Cell-Labeling Solution	Invitrogen, ThermoFisher Scientific	V22886
CellTracker™ Red CMTPX dye	Invitrogen, ThermoFisher Scientific	C34552
Paraformaldahyde, 16% (PFA)	Electron Microscopy Sciences	15710-S
Blocker™ BSA (10X) in PBS	Thermo Scientific	37525
Oregon Green™ 488 Phalloidin	Invitrogen, ThermoFisher Scientific	O7466

ProLong™ Diamond Antifade Mountant with DAPI	Invitrogen, ThermoFisher Scientific	P36962
Anti-Dystrophin Antibody, Rabbit	Abcam	ab15277
Goat anti-Rabbit AlexaFluor 647 IgG F(ab')2 frag	Invitrogen, ThermoFisher Scientific	A21246

Cell Lines/Culture

Reagent/Resource	Vendor	Catalog Number
293 [HEK293]	American Type Culture Collective	CRL-1573
Tmem8c (MYMK) Producer Cells	Stably transfected HEK293 cells (above)	
C2C12 Myoblasts	American Type Culture Collective	CRL-1772
Dulbecco's Modified Eagle Medium (DMEM), High Glucose	Gibco, ThermoFisher Scientific	11965092
Opti-MEM, Reduced Serum Medium	Gibco, ThermoFisher Scientific	31985062
Fetal Bovine Serum, Premium Plus (FBS)	Gibco, ThermoFisher Scientific	A4766801
Horse Serum (HS)	Gibco, ThermoFisher Scientific	16050122

Penicillin/Streptomycin (10,000 U/mL)(p/s)	Gibco, ThermoFisher Scientific	15140122
Trypsin-EDTA (0.25%), phenol red	Gibco, ThermoFisher Scientific	25200056

Protein Assay and Western Blotting

Reagent/Resource	Vendor	Catalog Number
RIPA buffer (5X)	Thermo Scientific	J62524.AE
Halt™ Protease Inhibitor Cocktail, EDTA-Free (100X)	Thermo Scientific	87785
BCA Protein Assay Kit	Thermo Scientific	J63283.QA
4x Lithium Dodecyl Sulfate (LDS) Sample Buffer	Abcam	Ab119196
Triton X-100	Abcam	Ab286840
Dithiothreitol	Abcam	141390
RunBlue 4–12% TEO-Tricine Protein Gel	Abcam	ab139602
RunBlue TEO-Tricine run buffer	Abcam	ab119197
0.2 µm Pore Size Nitrocellulose Membrane	GE Healthcare	10600004
Omniblok™	AmericanBIO	AB10109
anti-Alix Antibody	Cell Signaling Technology	E4T7U

anti-Tsg101 Antibody	ProteinTech	14497-1-AP
anti-GAPDH	ProteinTech	60004-1-Ig
Anti-β-actin Antibody	Cell Signaling Technology	8H10D10
HRP-conjugated secondary antibody, Rabbit	LICOR	926-80011
HRP-conjugated secondary antibody, Mouse	LICOR	926-80010
SuperSignal™ West Femto Maximum Sensitivity Substrate	Thermo Scientific	34095

2.3 Results

2.3.1 Screening of Native Myotropic Protein Candidates

Following the initial transient transfection of the MYMK, MYMX and M-Cad plasmids, the cells displayed varying levels of recombinant protein expression, measured using confocal microscopy to analyze the signal from the GFP tag associated with each protein (Figure 2.1A & B). Following the transfections, NTA was used to examine the particle concentration and size distribution of the EVs produced. Cells receiving only the transfection reagent (TR) and the cells transfected with MYMK released significantly less EVs than the other groups ($p < 0.05$; Figure 2.1C); however, there were no differences in the modal size of the EVs produced in each group with an average modal size of 122.8 nm ($p = 0.1885$) which fell in the range typically associated with EVs (Figure 2.1C). Transmission electron microscopy

(TEM) was used to qualitatively assess the EVs produced in each group. The TEM results provide representative data suggesting that EVs make up a very small fraction of the total biomolecular constituents in the conditioned culture medium when using precipitation as the purification method, especially in the presence of FBS. This is evidenced by the abundance of serum-derived lipoproteins and protein aggregates observed in the TEM images, which tend to make up a large proportion of biomolecular constituents in each image (Figure 2.1D). Given these initial results in the screening experiments, serum-free OptiMEM medium was used as the HEK293 EV production medium for all subsequent experiments, which is consistent with others for this cell-type.[147] Additionally, using flow cytometry, the fluorescence intensity of the endogenous GFP-tag associated with the recombinant proteins of each M-EV formulation was measured. The ubiquitous EV luminal protein counterstain, ExoGlow-Red, was used to calculate the percentage of total EVs containing the myotropic proteins. Both MYMK and the MYMK + MYMX (M&M) groups showed a significant level of recombinant protein incorporation into the EVs relative to the EVs from non-transfected HEK293 cells (NT) (MYMK, $p = 0.002$; M&M, $p = 0.0124$; Figure 2.1E). However, the M&M group showed lower protein incorporation overall.

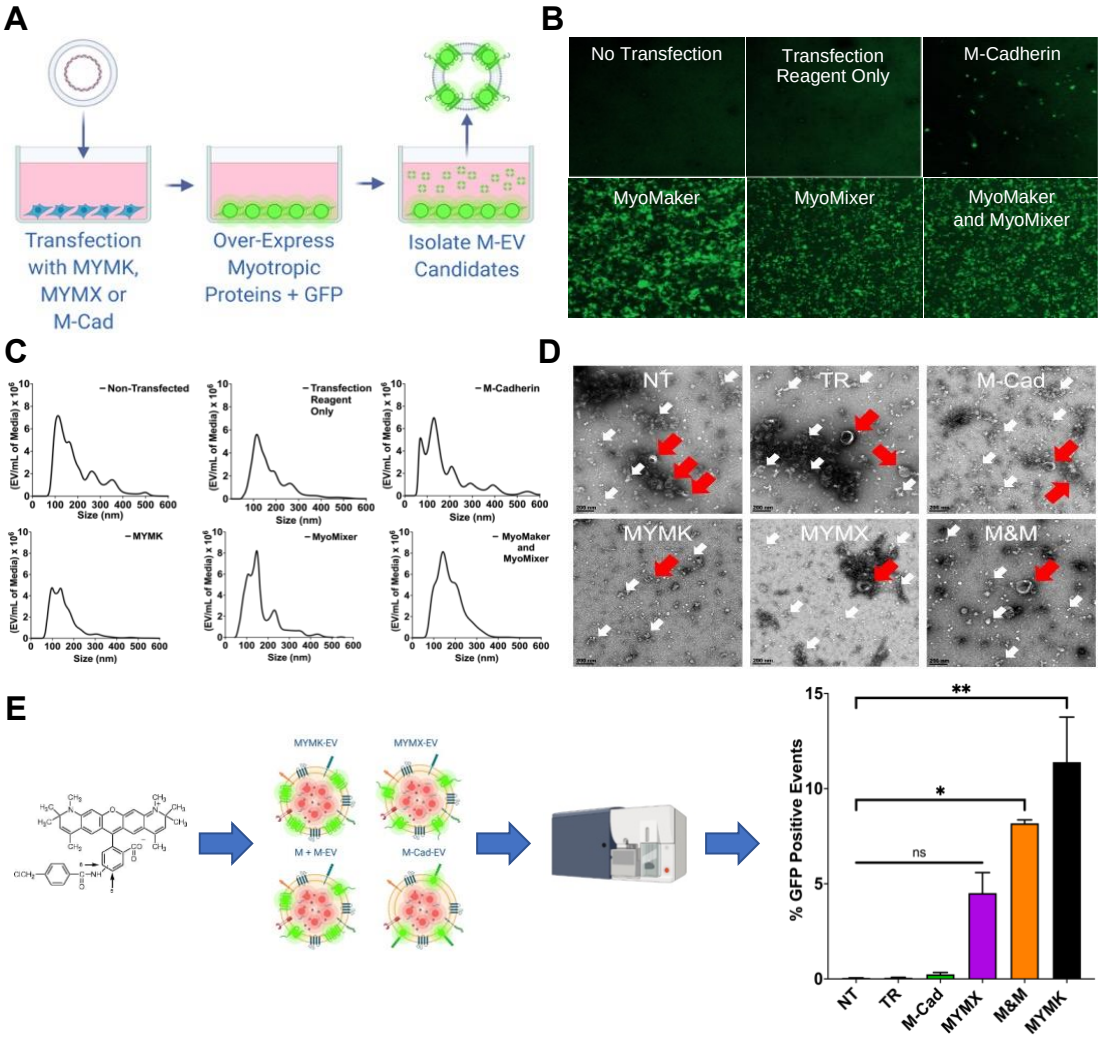

Figure 2.1 Characterization of native myotropic EV candidates and producer cells. **A)** Transfection workflow used for generation of myotropic EV candidates. **B)** Confirmation of successful transfection, noting variance in transfection efficiency. **C)** Nanoparticle tracking analysis data demonstrating concentration and size of particles in EV samples. **D)** Transmission electron microscopy images of each EV sample. **E)** Flow cytometry workflow and data measuring incorporation of each myotropic protein candidate into EVs indicating relative to NT-EVs. NT: EVs from HEK293 cells that were not transfected; TR: EVs from cells that received only the transfection reagent; MYMK: MyoMaker; MYMX: MyoMixer; M&M: MyoMaker and MyoMixer. * $p < 0.05$, ** $p < 0.01$, ns: not significant. N = 3 independent experiments.

To analyze the myotropic properties of the native M-EV candidates, the luminal protein cargo of each formulation was labeled with the amine-reactive probe, CFDA-SE, and incubated with C2C12 myotubes in vitro. The fluorescent signal from the labeled EV cargo delivered into the myotubes was measured using fluorescence microscopy. The MYMK-EVs were the only group to show a significant difference in delivered protein cargo with a 125% increase in the fluorescently-labeled protein cargo delivered into the myotubes compared to control EVs produced by non-transfected (NT) HEK293 cells (p = 0.0005; Figure 2.2).

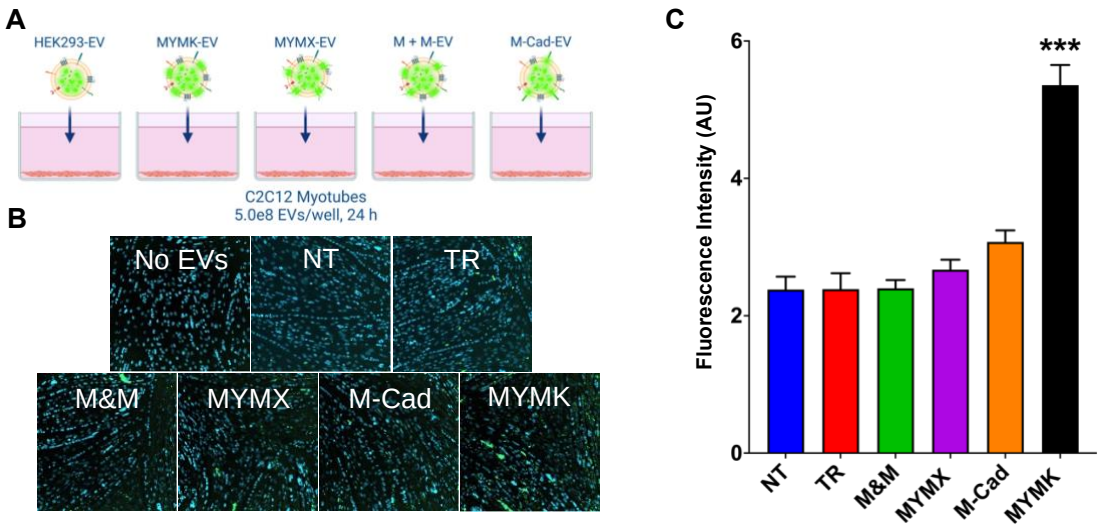

Figure 2.2 In vitro uptake assay to assess myotropic properties of each M-EV candidate. **A)** Experimental design displaying each M-EV formulation and control HEK293-EVs. Each formulation was incubated with fully differentiated C2C12 myotubes in vitro for 24 h prior to fluorescence imaging and analysis. **B)** Representative 10X fluorescence images depicting the labeled protein cargo (green) delivered into the myotubes, identified using a nuclear stain (blue). **C)** Quantification of the fluorescence intensity of the labeled protein delivered into the myotubes by each EV candidate relative to NT-EVs. NT: EVs from cells that were not transfected; TR: EVs from HEK293 cells that received only the transfection reagent; MYMK: MyoMaker; MYMX: MyoMixer; M&M: MyoMaker and MyoMixer. *** $p < 0.001$. N = 3 independent experiments.

2.3.2 Stable Producer Cell Line Generation

The in vitro experiments identified the MYMK-EV formulation as the most promising native M-EV construct. The next step was to analyze the myotropic properties of MYMK-EVs in vivo. This required much larger quantities of EVs than previously needed in the early in vitro experiments. It was estimated that a total of 2.9-3.8e12 EVs would be needed to dose the 3-4 mice per experimental group for the eight experimental groups. In order to produce this quantity of EVs, a stable cell line was needed to scale up into larger cell culture vessels to produce the needed quantities. The transfection efficiency of the cationic lipid reagent jetOPTIMUS was compared to lentiviral vectors containing a MYMK-encoding plasmid. Following selection of the GFP positive cells using fluorescence assisted cell sorting, cells transfected with either method were passaged ten times. Over the course of these passages, the cells transfected with the cationic lipid reagent displayed a dramatic 89% decrease in fluorescence signal (Figure 2.3A) while the cells transfected using the lentiviral vectors showed a more modest 19% decline in signal (Figure 2.3B). This coincides with the previous literature suggesting that cationic lipid-based reagents result in a much less efficient incorporation of the transgene into the recipient cells' genomes via homologous recombination as opposed to lentiviral transduction of the transgene. Thus, the MYMK-EV producer HEK293 line was generated using the lentiviral transduction method. The stably transfected cells were successfully seeded into a 6-well plate and then scaled to 875 cm^2 flasks for MYMK-EV production.

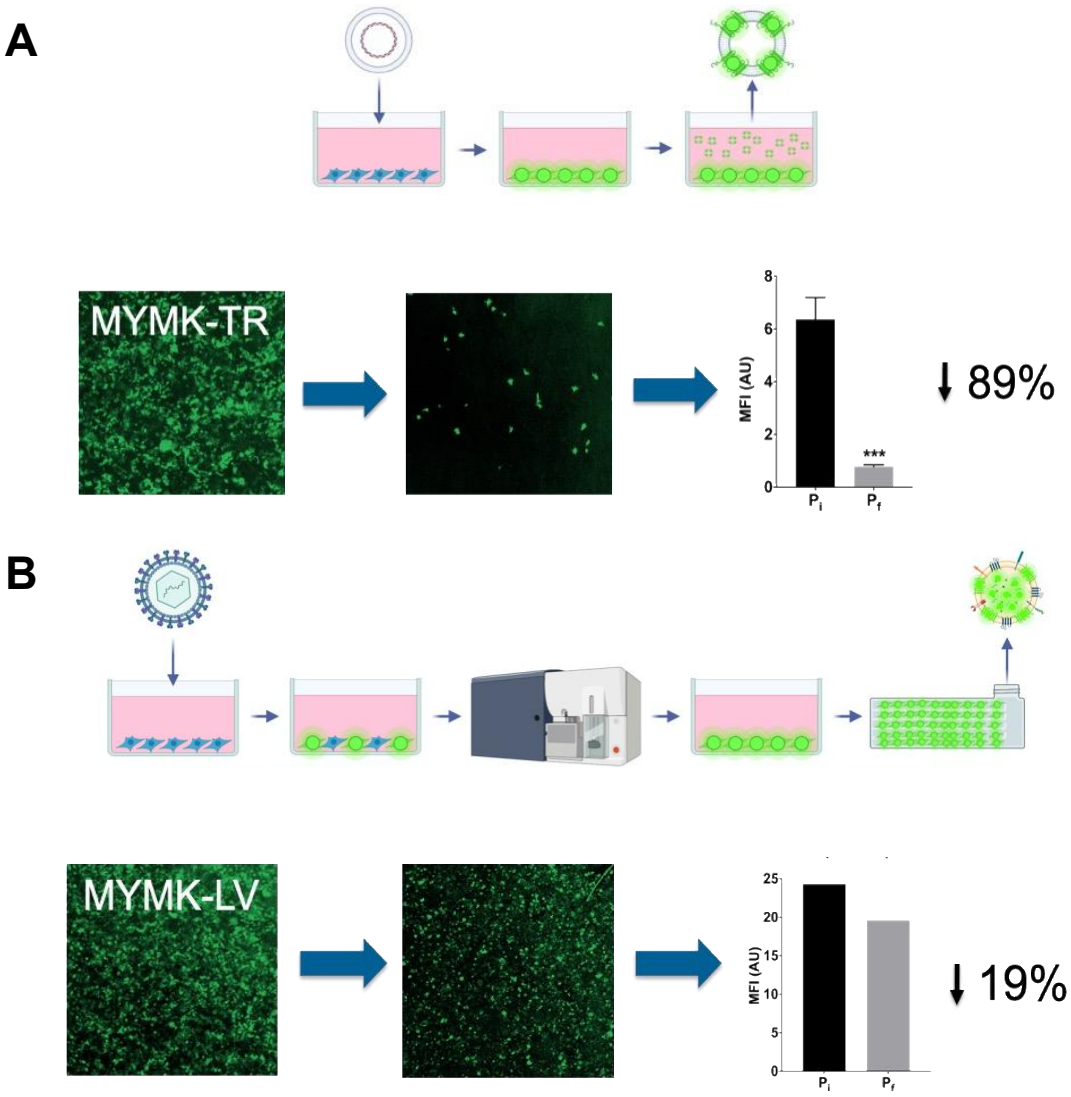

Figure 2.3 Comparison of cationic reagent and lentiviral transfection workflows for the generation of a stable MYMK-expressing cell line. **A)** Cationic lipid transfection workflow and data demonstrating an 89% decline in fluorescent signal over 10 passages following cationic lipid-based transfection. **B)** Lentiviral transfection workflow and data demonstrating a 19% decline in fluorescent signal over 10 passages following lentiviral transfection and selection using fluorescence-assisted cell sorting. Data presented as mean fluorescence intensity. MFI: mean fluorescence intensity. *** $p<0.001$. N = 3 independent experiments.

2.3.3 EV Characterization

Once a stable MYMK-EV producer cell line was established the EVs produced were analyzed using NTA, TEM and western blot as per the MISEV guidelines (Figure 2.4). The NTA revealed particles in the typical size range of EVs with a modal size of ~ 155.4 nm for EVs from non-transfected HEK293 cells and ~ 131.4 nm from the MYMK-EV producer cells (Figure 2.4A&B). The producer cells and EVs were also analyzed using a fluorescent plate reader to track MYMK expression/contents over 6 passages during EV production (Figure 2.4C). This revealed no significant change in the expression of MYMK in the cells over this timeframe; however, the EVs could not be detected using this method. TEM was used to analyze the morphology of the EVs produced by each of these cell lines. Both produced particles in a similar size range (~ 50-200 nm) as demonstrated by the NTA data with the typical EV cup-shaped morphology. However, in addition to the typical EV-like particles, TEM revealed additional debris that co-precipitated with the EVs during ultracentrifugation (Figure 2.4D). EV samples were probed for the canonical EV-enriched protein markers, ALIX and TSG101 as well as cellular markers, beta actin and GAPDH, that are not typically enriched in EVs. Western blot analysis confirmed the presence of the EV markers in the UC pellet sample; however, it also revealed the pellet to be positive for beta actin and GAPDH. This confirmed the previous suspicions that cellular debris made it through the clarification process and into the UC pellet sample. In addition, ALIX and TSG101 were also identified in the supernatant following UC, suggesting that these proteins may be secreted independent of EVs as well (Figure 2.4E).

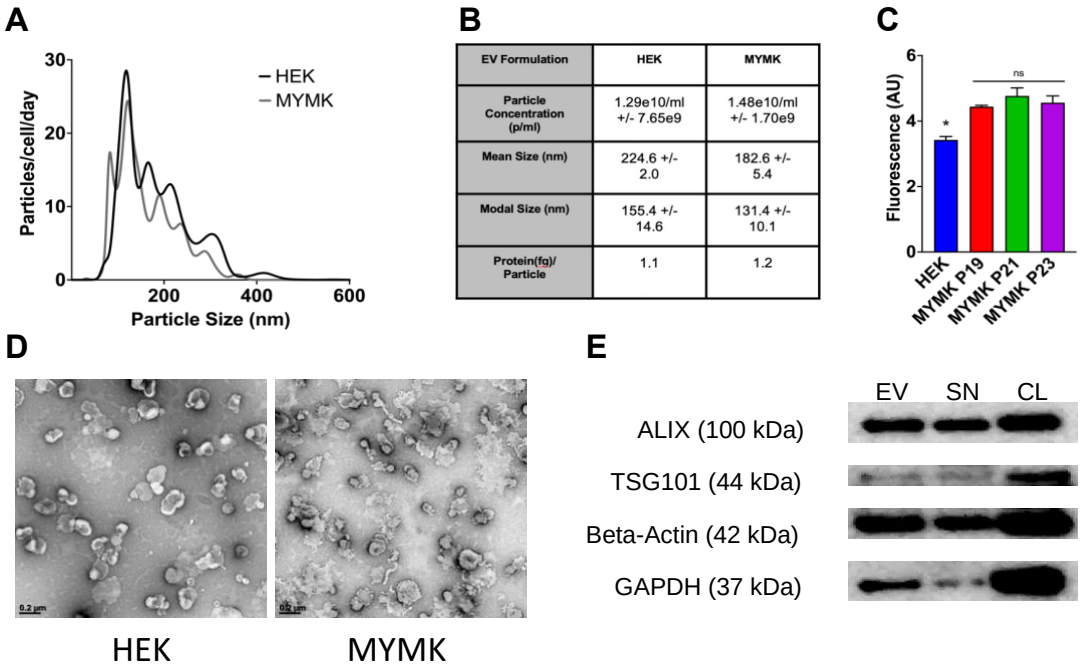

EV Formulation	HEK	MYMK
Particle Concentration (p/ml)	1.29e10/ml +/- 7.65e9	1.48e10/ml +/- 1.70e9
Mean Size (nm)	224.6 +/- 2.0	182.6 +/- 5.4
Modal Size (nm)	155.4 +/- 14.6	131.4 +/- 10.1
Protein(fg)/ Particle	1.1	1.2

Figure 2.4 Characterization data for EVs produced by stable MYMK-expressing cell line and HEK293 control cell line and producer cells. **A)** NTA histogram of MYMK and HEK EVs depicting concentration and size distribution. **B)** Table depicting concentration, size and protein content of HEK and MYMK-EVs. **C)** Fluorescence intensity of MYMK-producer cells over multiple passages (P19-23) during EV production as compared to HEK293 control cells **D)** Representative TEM images of HEK and MYMK-EV samples. **E)** Western blot analysis identifying the presence of EV and non-EV-enriched proteins in the EV samples as well as ultracentrifuge supernatant (SN) and producer cell lysate (CL). * $p < 0.05$. ns: not significant. N = 3 independent experiments.

2.3.4 Biodistribution of EVs Using a Lipophilic Dye

DiD-labeled HEK and MYMK-EVs were administered to C57 or mdx mice via tail vein injection (Figure 2.5A). The organs were harvested 24 h later and immediately imaged on an IVIS (Figure 2.5C), after which they were homogenized and the EV-derived fluorescent signal was analyzed using a fluorescent plate reader (Figure 2.5B). No significant differences were observed between the biodistribution of the MYMK-EVs and non-engineered HEK293-EVs in the C57 or mdx mice with the majority of signal derived from each formulation predominantly localizing to the

spleen and the liver. However, when comparing the biodistribution of the EVs in C57 to mdx mice, there was a significant decrease in fluorescence signal detected in the spleen for both EV types. Specifically, we observed a 64% ($p < 0.0001$) decrease in fluorescent signal in the spleens of mdx mice relative to C57 following administration of the HEK-EV formulation and a 41% decrease ($p = 0.004$) following administration of the MYMK-EV formulation. Interestingly, as the signal derived from the spleen decreased when comparing C57 to mdx mice, we also observed a nonsignificant increase in signal derived from many of the peripheral organs corresponding to the decreased signal in the spleen, potentially suggesting redistribution of the EVs in the mdx mice as compared to the C57 mice. Additionally, there was a 34% decrease ($p = 0.04$) in fluorescent signal in the liver of mdx mice that received the MYMK-EV formulation as compared to that in the liver of C57 mice that received the same EVs, but this was not observed in the mice that received the HEK293-EV formulation.

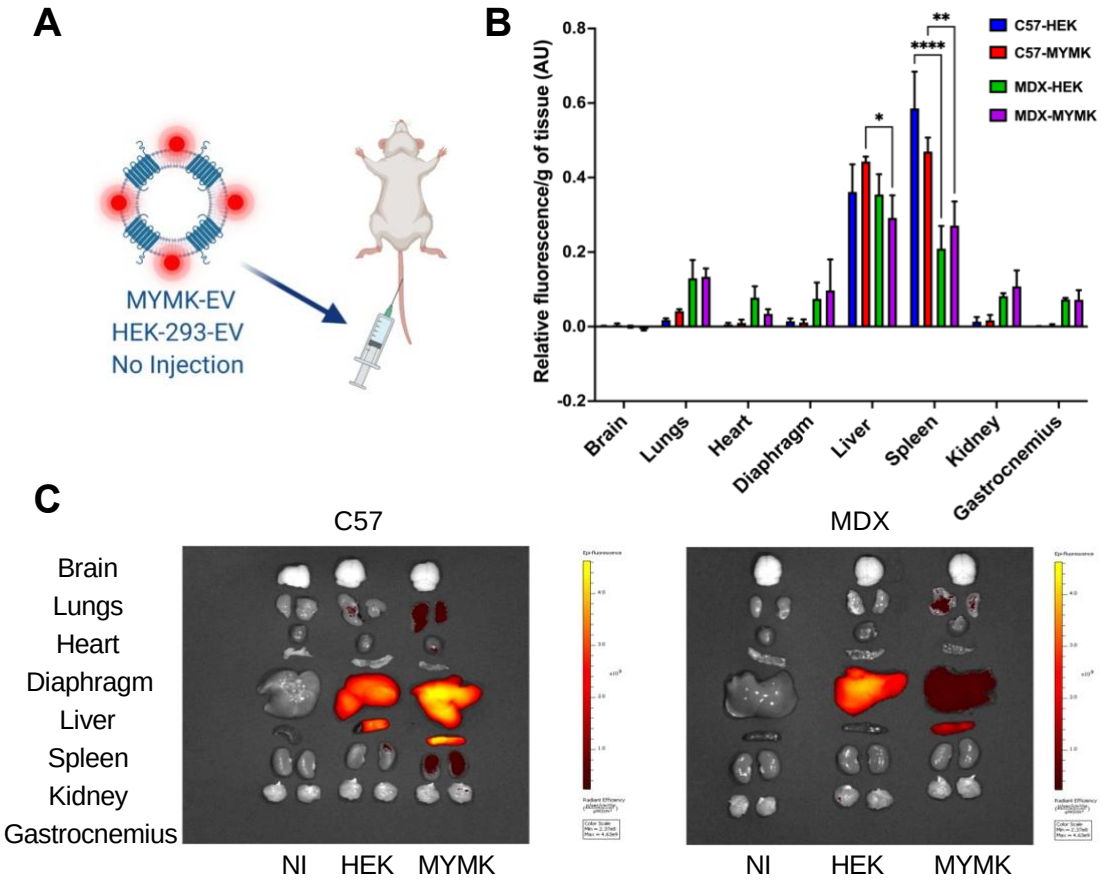

Figure 2.5 In vivo biodistribution of DiD-labeled MYMK and HEK-EVs. **A)** Experimental groups for injections into tail vein of C57 and mdx mice. **B)** Quantitative analysis of relative fluorescence intensity of homogenized tissue 24 h after injection, normalized by tissue weight (g) and non-injected tissue signal subtracted. **C)** Representative images of organs from C57 and mdx mice 24 h following injections taken on in vivo imaging system. N = 18 total mice, 3 mice per group. NI = No Injection. HEK = HEK293-EV Injection. MYMK = MYMK-EV injection. * $p < 0.05$, ** $p < 0.01$, **** $p < 0.0001$.

2.3.5 Biodistribution of EVs Using an Amine-Reactive Dye

Following the biodistribution experiments using the lipophilic probe, we next assessed the biodistribution of the MYMK-EVs labeled with CT-Red. The proposed mechanism by which this class of dye works is by permeating the phospholipid bilayer

of the EV followed by cleavage by intracellular esterases packaged within the EV. This transformation renders the dye impermeable to the phospholipid bilayer, allowing it to interact with any exposed amine groups within the EV. We chose the amine-reactive dye in addition to the lipophilic dye to enable us to track the intracellular delivery of EV-derived protein cargo into recipient tissues.

To dose the EVs for these experiments, a fluorescent plate reader was used rather than NTA. When analyzing batches of EVs derived from the same flasks of producer cells, it became evident that the measured particle count using NTA varied depending on which dye was used (Figure 2.6A). Specifically, the sample stained with CT-Red had a concentration of 2.44e11 particles/ml whereas the sample stained with DiD had a concentration of 8.21e11 particles/ml; however, there was no effect on particle size. To minimize this variability, the EV doses were selected based on the fluorescent signal derived from the labeled protein in each sample rather than particle count (Figure 2.6B).

HEK and MYMK-EVs were injected into both C57 and mdx mice at equivalent fluorescence intensities. Neither the fluorescent plate reader or IHC/imaging were able to reliably identify an EV-derived protein signal in any of the examined tissues above the autofluorescence of the tissue itself (Figure 2.6D). A follow-up analysis of the EVs ability to deliver cargo into HEK293 cells in vitro confirmed the successful labeling of the EVs (Figure 2.6C), indicating the EVs either contained inadequate protein cargo to be imaged in vivo at the given dose, or the labeled protein cargo may have been degraded within the 24 hour timespan following administration.

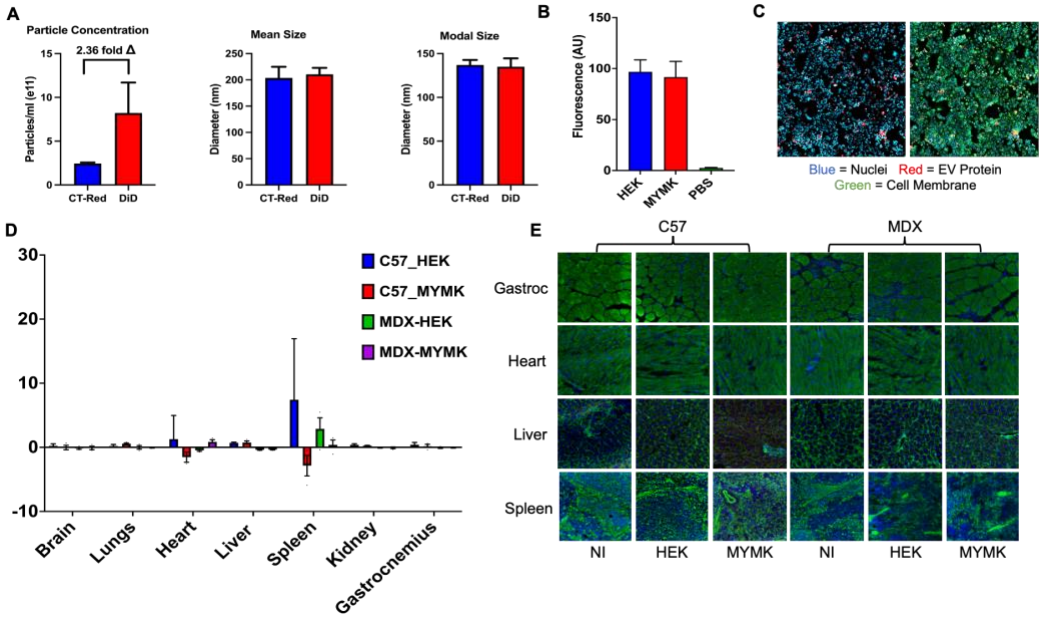

Figure 2.6 In vivo biodistribution of HEK and MYMK-EVs labeled with an amine-reactive probe. **A)** Particle concentration, mean and modal size of EVs labeled with CellTracker-Red or DiD (N = 2 independent experiments). **B)** Fluorescence signal of EVs labeled with amine-reactive probe. **C)** Uptake of amine-labeled EVs by HEK293 cells in vitro (10X). **D)** Quantitative analysis of relative fluorescence intensity of homogenized tissue 24 h after injection, normalized by tissue weight (g) and non-injected tissue signal subtracted. **E)** Representative 40X fluorescent images of tissues of interest (gastrocnemius and heart) and off-target tissues known to take up the majority of intravenously administered EVs (liver and spleen) labeled with phalloidin 488 conjugate (green) and DAPI (blue). For in vivo experiments, N = 18 total mice, 3 mice per group. For non-animal experiments, N=3 independent experiments unless otherwise indicated.

2.4 Discussion

In the current study, we examined a panel of native proteins with known myotropic properties in vivo for their ability to promote enhanced delivery of EV-derived cargoes into skeletal muscle. We chose the proteins MyoMaker (MYMK) and MyoMixer due their roles in promoting myoblast fusion to skeletal muscle fibers following injury as well as the protein M-Cadherin, due to its role in adhering

quiescent satellite cells to skeletal muscle fibers.[67,68] To generate EVs displaying these candidate proteins, we over-expressed each protein via cationic lipid transfection in HEK293 cells and harvested the EVs from the cell culture supernatant. Our early results from conducting uptake experiments in C2C12 myotubes in vitro identified the MYMK-EV formulation as the most promising candidate with a ~ 125% increase in protein delivery into C2C12.

Given these early findings, we generated a stable MYMK-expressing cell line and administered the MYMK-EVs to C57 and mdx mice in vivo with two different labeling methods. Overall using the lipophilic dye, DiD, we saw a typical biodistribution pattern for both EV formulations, with the majority of the fluorescent signal originating from the liver and spleen. The primary outcome we observed was a significant decrease in the fluorescent signal in the spleen in MDX relative to C57 mice, regardless of the EV formulation administered. Simultaneous with this decrease was a non-significant increase in each of the peripheral tissues, except for the brain. In addition, the only observed difference in the biodistribution of the HEK293 and MYMK-EVs was a significant decrease in the MYMK-EV signal in the liver of mdx mice relative to that of the HEK293-EVs.

Although the MYMK-EV formulation yielded promising results in vitro, we did not see any difference in the delivery of these EVs to the skeletal muscle in vivo relative to the non-engineered HEK293 EVs. This is a similar outcome to that of Wood et al.,[113] whom investigated the biodistribution of EVs displaying the myotropic peptide, ASSLNIA, fused to Lamp2b. Like the current study, they showed enhanced delivery of EV cargoes to C2C12 in vitro but no difference in vivo.[113] The in vivo intramuscular niche is a more complex environment than myotubes in vitro, as it

includes an endothelium and extracellular matrix that the EVs must first traverse before reaching the target muscle fibers.[148,149] The targeting strategy employed by our group and others utilized a targeting moiety at the EV membrane surface. The proposed mechanism is that when the EV comes in contact with the skeletal muscle, the targeting moiety will enhance the fusion of the EV with the skeletal muscle fiber membrane and promote delivery of the luminal cargoes. It is largely assumed that EVs pass efficiently through biological barriers, such as the endothelium.[77] However, skeletal muscle contains capillaries with a continuous endothelium with < 1 nm gaps between cells and a maximal reported endosomal diameter of 70-80 nm, thus making it more difficult for molecules to easily traverse.[148,149] Given that the modal size of EVs is typically ~ 100-200 nm and the EVs utilized in the current study were measured to have a modal size of ~ 151 nm (HEK-EV) and ~134 nm (MYMK-EV), it is possible that EVs were unable to traverse this endothelial barrier as efficiently as proposed. This may also apply to other similar biological barriers containing a continuous endothelium, such as the blood brain barrier (BBB). Although groups have reported successful targeting to the brain, the results of the current study as well as other recent reports conflict with these findings. For example, studies have reported that intranasal delivery of EVs enhances the efficiency of EV delivery to the brain;[150] however, a recent study by Driedonks et al.,[126] demonstrated that HEK293 EVs delivered intranasally largely did not make it past the nasal passage. Further, a recent study demonstrated that 30 but not 80 nm synthetic nanoparticles were able to traverse the BBB, suggesting there is likely a size limit to the particles/biomolecules that can be transcytosed across.[151] Tumor cells are another common target of engineered EVs and NPs. As drug targets, tumors benefit from the enhanced permeability and retention

(EPR) effect due to their dysfunctional "leaky" endothelium and reduced lymphatic drainage.[152] Thus it is thought that larger drug carriers, such as EVs, may pass through this endothelium and access the tumor cells more efficiently. Despite the EPR effect, a meta-analysis of over one hundred preclinical studies suggests that only ~ 0.7% of injected NPs actually reach the tumor.[153] Further, a biodistribution study of gold NPs that were 15, 50, 100 and 200 nm in diameter demonstrated that the larger sized NPs, in the modal size range of EVs, predominantly localized to the liver and spleen, whereas the smaller NPs had a longer circulation time and had improved distribution to the periphery.[154] These findings in combination with those of the current study suggest the size of drug carrier plays a large role in its biodistribution and EVs ~ 100-200 nm modal size may reduce the accessibility of EVs to tissues perfused by capillaries with a continuous endothelium.

In the current study, we calculated the proportion of EV-derived fluorescent signal retained in the tissue normalized by organ weight in both C57 and mdx mice. We found that ~ 0.3% of the MYMK-EVs and 0.04% of the HEK-EVs were retained in the skeletal muscle tissue (gastrocnemius) of the C57 mice. Although these data represent a 6.5-fold increase in the signal observed in the skeletal muscle, these results were not statistically significant as the majority of the EV-derived signal was localized to the spleen (MYMK: ~ 47%, HEK: ~ 58%) and liver (MYMK: ~ 44%, HEK: ~ 36%). Thus, with such a minimal effect on the overall biodistribution of the EVs, it is questionable whether or not this engineering strategy holds any clinical relevance. It should be noted that, in the case of DMD, even modest improvements in delivery may have a clinically relevant effect on dystrophin expression and muscle functionality.

However, the large percentage of EV cargo delivered to the liver and spleen still remains a major concern for patient safety.

Interestingly, in mdx mice the signal in the spleen showed a significant decline in EV-derived signal for both MYMK and HEK-EVs. Specifically, in the mdx mice the spleen accounted for ~ 27% and ~21% of the EV-derived fluorescent signal in the MYMK and HEK-EV groups respectively. The MYMK-EVs also showed a significant decrease in the liver of mdx mice relative to C57 mice, which was not observed for the HEK-EVs. Simultaneously, with the decrease in signal in the spleen, we observed a non-significant increase in EV-derived signal in all peripheral tissues except for the brain. The gastrocnemius showed the greatest increase relative to the C57 mice, accounting for 7.2% (23-fold) of the EV-derived signal in the MYMK-EV group and 7.3% (181.5-fold) of the signal in the HEK-EV group. Overall, these data show a redistribution of the injected EV cargo away from the spleen and liver toward the peripheral tissues, with the greatest increase noted in the skeletal muscle.

DMD is characterized by chronic and progressive inflammation caused by the absence of dystrophin protein expression.[9] DMD is largely a skeletal and cardiac muscle condition; however, dystrophin is expressed in the cells of numerous other organs throughout the body, including lungs, kidney, brain, etc.[155-157] When tissues undergo chronic inflammation, immune cells are known to migrate across the endothelium into the inflamed tissues via chemotaxis to facilitate repair.[158] Given the decreased signal in the spleen and increased signal in the skeletal muscle, and to a lesser extent the other peripheral tissues, of the mdx mice, it appears that the immune system could have a role in facilitating the redistribution of intravenously administered EVs. Driedonks et al.,[126] noted a robust uptake of intravenously-administered EVs by

circulating immune cells in Macaques. Thus, it is possible that under homeostatic conditions these cells largely accumulate in the spleen, but under chronic inflammation they may infiltrate the inflamed tissues in the periphery. Future work is needed to validate this potential mechanism, as the current study did not address the mechanism of biodistribution. Alternatively, blood vessel dysfunction in DMD may be another factor affecting the biodistribution of EVs in the mdx mouse. In DMD, it is thought that blood vessels may undergo degeneration and therefore have increased permeability. This could theoretically allow larger-sized particles such as EVs to access the musculature more easily. However, the mdx mice used in this study were relatively young (6-11 weeks), therefore, blood vessel degeneration was most likely not a significant factor. Thus, the inflammatory state of the peripheral tissues and immune cell migration may provide a better explanation of the results observed herein. Regardless, this study did not address the underlying mechanism of the biodistribution and future studies are warranted to investigate this more thoroughly.

In the second set of experiments, EVs were stained with the amine-reactive dye CellTracker Red CMTPX. To our surprise, the signal from these EVs could not be reliably detected above the background autofluorescence in any tissue. To ensure the labeling method worked as expected, the EVs were incubated with HEK293 cells in vitro and uptake of the fluorescent cargo was confirmed. Thus, these data suggest a number of possible limitations when using an amine-reactive probe and tracking EV biodistribution by examining the labeled protein delivered to each tissue. Firstly, it is becoming apparent that EVs are rather deplete of proteins. Many of the earlier estimates of EV protein content were derived using serum-containing media which is highly enriched in proteinaceous biomolecules (albumin, lipoproteins, etc.) in

combination with purification methods that co-precipitate with EVs, such as UC.[159] Although we utilized UC to purify the EVs, we used serum-free OptiMEM for the EV production medium followed by two rounds of UC to further dilute out contaminant biomolecules. Our resulting protein/particle ratio was thus exceedingly low (1.1 fg/p for HEK-EVs and 1.2 fg/p for MYMK-EVs). This alone may impair the ability of accurately tracking EV-derived protein as opposed to lipids which are more enriched in EVs.[109] Thus, a higher dosage of EVs is likely needed to accurately track the distribution of EV-derived protein. Further, the turnover of proteins within the recipient cells is likely greater than that of lipids given that proteins may rapidly become ubiquitinated and degraded by the ubiquitin proteasome or transported to lysosomes for degradation.[160] Finally, Driedonks et al.,[126] recently demonstrated the half-life of EVs in the circulation to be ~ 20-40 min. Similar to the first set of experiments using the DiD-labeled EVs, we harvested the organs from the mice 24 h after injection. Given these new data pertaining to EV half-life, this may have been too long of an incubation period and allowed too much time for the administered EV-derived protein to be degraded once delivered into recipient cells. Thus, future studies investigating the biodistribution of intravenously administered EV-derived protein will likely need to shorten this duration.

Another important finding from these experiments was a discrepancy noted in the particle concentration yielded from NTA when staining the EV samples with DiD as compared to CT-Red. The DiD-labeled EV samples exhibited a 2.36-fold increase in particle concentration relative to the CT-Red samples. As these samples originated from the same batches of producer cells, this brings the NTA data of the labeled EVs into question. There have been reports of the carbocyanine dyes, such as DiD, forming

micelles in aqueous solutions which could be registered as particles during NTA.[161] However, we used an additional round of UC to remove free dye and micelles, which we confirmed to be sufficient in preliminary experiments. Given these discrepancies in particle count, we used a fluorescent plate reader to dose the EVs, which ensures that equal amounts of labeled material are administered. Given these findings and the variability associated with NTA, measuring the fluorescent signal in each sample to choose a dosage appears to be essential for attaining consistent results. Thus, although the protein-derived signal was not detectable in any of the tissues, these experiments have provided a wealth of practical insights into the dyes, dosing and methods of detection utilized in EV biodistribution studies.

2.5 Conclusions

Overall, the MYMK-EV formulation showed promise in its ability to enhance delivery of protein into C2C12 myotubes in vitro but did not significantly alter the biodistribution toward skeletal or cardiac muscle in vivo. Unexpectedly, we observed a significant difference in the biodistribution of EVs administered in mdx mice relative to C57 mice. Most notably, there was a significant decline in signal in the spleen of the mdx mice relative to the C57 mice which occurred simultaneously with a redistribution of the signal to the peripheral tissues of the mdx mouse. We hypothesize that the immune system and the inflammatory state of the tissues may be involved in this redistribution given that the spleen is a reservoir for various immune cells which may feasibly uptake EVs in the circulation and migrate to tissues in a chronic state of inflammation. We failed to measure a signal consistently above background from the tissues harvested following administration of the CT-Red EVs. This is likely due to a

number of factors involving the exceedingly low quantity of protein in each EV, the potential for the EV-derived protein to be degraded following administration and the short EV half-life relative to the commonly used 24 h incubation period following administration of the EVs. Finally, when comparing the particle concentration between the DiD-EVs and CT-Red EVs, the DiD-EVs exhibited a drastically elevated particle concentration. This is likely due to some sort of artifact and should be taken into account when choosing doses of EVs to administer *in vivo*. Choosing an EV dose based on fluorescence intensity may be a more accurate and precise method relative to particle count. Overall, this study provides a potentially interesting mechanism of how EV cargoes are distributed following intravenous delivery in a diseased state as compared to a non-diseased state, with circulating immune cells potentially playing a critical role. In addition, our experiments attempting to use an amine-reactive dye to track the biodistribution of EVs provide a number of practical insights into staining and dosing EV samples for in vivo biodistribution studies. Future research is needed to fully elucidate the efficacy of using EVs as drug delivery vectors for skeletal and cardiac muscle.

Chapter 3

SPECIFIC AIM 2: EXAMINATION OF CHIMERIC MYOTROPIC EXTRACELLULAR VESICLE CANDIDATES

3.1 Introduction

A number of therapeutics have been investigated for the treatment of muscular pathologies, such as the muscular dystrophies.[22,26] Glucocorticoids remain the standard of care to ameliorate symptoms associated with the disease, which has reduced mortality and improved the quality of life in patients.[26] Adeno-associated virus (AAV)-mediated gene therapies aim to restore the expression of a wildtype gene, which has shown promising results in clinical trials.[22] Although these therapeutics have largely been successful, adverse events in patients remain a substantial problem for both treatment modalities.[24,36] Current therapeutics are non-specific to the musculature, leading to adverse effects in off-target tissue types. Thus, a myotropic (muscle-targeted) delivery vector is needed to improve the efficacy and limit the off-target effects of current therapeutics for these conditions.[24,36]

Extracellular vesicles (EVs) are cell-derived nanoparticles generally ranging in size from 30-1000 nm and have been proposed as a next-generation delivery vector for therapeutics.[130] EVs are suggested to be highly biocompatible due to their cellular origin and have the ability to be engineered to express various targeting moieties.[162] Displaying targeting moieties at the surface of EVs has been shown to enable enhanced tropism of the EVs for specific cell/tissue-types.[163] To generate EVs displaying targeting moieties, EV-enriched membrane proteins, such as the tetraspanin proteins or lysosome-associated membrane glycoprotein 2 isoform B (Lamp2b), are often utilized as scaffolds to which a targeting moiety of interest can be fused.[113]

Common methods used for this engineering process include transfecting the EV producer cells with plasmids encoding a hybrid protein or using a post-isolation conjugation method to attach the targeting moiety.[104] To date, Lamp2b is the most commonly used EV-enriched scaffolding protein as the tetraspanin proteins have a highly heterogenous expression pattern in EVs.[104] Specifically, Lamp2b has been used to generate EVs displaying the neuron-targeted rabies virus glycoprotein (RVG) for targeted delivery of a silencing ribonucleic acid (siRNA) to neurons in mice.[113] In another study, researchers used a similar approach to fuse the αv integrin-specific iRGD peptide (CRGDKGPDC) to Lamp-2b, which they showed to increase doxorubicin delivery to tumor cells in nude mice.[133]

Although the results of early studies using these scaffolding proteins appeared promising, recent research has brought into question the degree to which the hybrid constructs utilizing these scaffolding proteins are actually integrated into the EV membrane.[109] Newer and potentially more efficient scaffolding protein candidates, such as PTGFRN or the N-terminus of the EV-enriched protein, syntenin, have been identified.[109,114] Recent studies suggest that using these proteins as scaffolds for targeting moieties results in the generation of EV formulations with enhanced incorporation of the fusion proteins expressed in the producer cells.[109, 114]

Although EVs have the potential to be highly engineerable and biocompatible drug delivery vectors, no successful myotropic EV formulation has been generated to date. A previous formulation utilizing the myotropic peptide, ASSLNIA, fused to Lamp2b showed promising results in vitro, but failed to demonstrate myotropic biodistribution in vivo.[113] Other studies have reported enhanced myotropism of AAV and ASO drugs conjugated to myotropic peptides in vivo.[39,43] However, the pool of

myotropic EV formulations is lacking. Thus far, the strategies for muscle-targeted delivery of therapeutics have largely focused on engineering synthetic MPs, ASSLNIA and RRQPPRSISSHP, either directly to the therapeutic (ASO) or the vector used for delivery (AAV2 or EV).[39,43]

Thus, given the dearth of myotropic EV candidates and the recent discoveries of potentially improved scaffolding proteins, we investigated the myotropic properties of EVs displaying one of two myotropic peptides conjugated to the EV-enriched scaffolding protein, PTGFRN. We chose the previously identified myotropic peptides ASSLINA (MP1) and RRQPPRSISSHP (MP2) as they displayed promising myotropic properties when conjugated to other delivery vectors. We hypothesized that EVs displaying these myotropic peptides conjugated to PTGFRN would have an enhanced ability to deliver protein cargo into muscle cell-types relative to non-muscle cell-types in vitro.

3.2 Materials/Methods

3.2.1 Design and Production of Plasmids

The plasmid constructs were designed by modifying plasmids encoding a PTGFRN transgene with a GFP tag and CMV promoter to incorporate the genetic sequence encoding either MP1 or MP2 upstream of the PTGFRN transgene sequence. Once transcribed and translated in cells, this produces a chimeric protein construct with MP1 or 2 fused to the extracellular C-terminus of PTGFRN. The gene encoding the antibiotic resistance protein for neomycin was included in the plasmid design to allow for selection of cells exhibiting stable expression of the chimeric MPs using the

antibiotic geneticin. The plasmids were produced by the University of Michigan Vector Core Laboratory according to these specifications.

3.2.2 Optimization of Plasmid Transfection

To achieve the highest level of protein expression for each construct, transfection parameters were optimized for the plasmids encoding PTGFRN, MP1 and MP2 in HEK293 cells using varying quantities of the DNA and reagent. The cells were seeded at 1.0e4 cells/well and allowed to grow overnight to 60-80% confluency. The following day, the cells were incubated with 0.025-0.1 ug of plasmid DNA. The transfection reagent was used in 1ul:1ug DNA ratio in each group. The groups were then incubated for 4 hours at which time the media was switched back to normal growth medium (GM) containing 10% FBS and 1% p/s in High Glucose DMEM. The transfected cells were analyzed using the ImageExpress Pico (Molecular Devices, San Jose, CA) at 48 hours post-transfection to analyze transgene expression efficiency. A protein expression analysis program was utilized to analyze the expression of each protein construct based on the GFP signal associated with each protein.

3.2.3 Transfection and Positive Clone Selection

HEK293 cells were seeded at 5.0e5 cells per well of a 6-well plate (VWR, Radnor, PA). The cells were allowed to expand for 24 hours prior to transfection resulting in a confluency of 60-80% at the time of transfection the following day. Using the optimized DNA:reagent ratio found in the optimization experiments, the cells in each well were transfected with 3 ug of pDNA and 3 ul of transfection reagent. The cells were incubated in the DNA/reagent-containing media for 4 hours after which

the media was changed to fresh GM and the cells were expanded back to 90-95% confluency. The cells were then continuously passaged and expanded until they were in T175 flasks. At this point the media was switched to GM containing 1 mg/mL of geneticin to select cells stably expressing the plasmid constructs and removing those in which the plasmid was not integrated into the genome of the producer cells. A group of non-transfected HEK293 cells was also treated with the geneticin to ensure it was adequately removing all non-transfected cells over subsequent passages. Following this initial selection, fluorescence-assisted cell sorting (FACS) was then performed on a FACS Aria Fusion (BD BioSciences, Woburn, MA) to select for GFP-positive cells with a mean fluorescence intensity of 10e4-10e5 to ensure similar production of the GFP-tagged constructs in each of the cell lines generated. The selected cells were then expanded and passaged in GM until utilization in downstream experiments.

3.2.4 Chimeric Myotropic EV Production

Following the establishment of stable cell lines, cells were expanded into 875 cm^2 flasks (Falcon, Corning, NY). Once the cells reached 90-95% confluency in the 875 cm^2 flasks, they were washed twice with 10% OptiMEM or DMEM in 1X PBS and then switched to 75 ml of Opti-MEM for 24 h.

3.2.5 EV Purification

Following the 24 h incubation period, the conditioned OptiMEM was harvested and clarified by centrifugation at 500 x g for 10 min and 2,000 x g for 40

min. The EVs were then initially purified using UC at 100,000 x g for 60 min at 4℃ followed by an additional round of UC at 150,000 x g for 90 min for improved purity.

3.2.6 Nanoparticle Tracking Analysis (NTA)

A 532-nm green laser and NS300 FCTP Gasket (Malvern, PA) were utilized for characterizing the number and size of the EVs in each sample on a Nanosight NS300 (Malvern, PA). The EVs were analyzed at a camera level of 12 with a detection threshold of 10. Three 30 second videos were recorded for each sample. EVs were diluted to a concentration of ~1e9/mL for analysis and were administered into the gasket using a sterile BD Plastipak syringe (Becton Dickinson S.A., Madrid, Spain).

3.2.7 BCA Protein Assay

Protein assay was conducted following the manufacturer's instructions. EV samples were lysed using a vortex on the highest setting for three rounds of 10 seconds. The EVs were in a solution comprising 5X RIPA buffer diluted to a final concentration of 1X and 100X protease and phosphatase inhibitor cocktail diluted to a final concentration of 1X. The protein concentration was determined using a BioTek Synergy 2 plate reader (Agilent, Santa Clara, CA). The protein concentration derived herein was compared to the particle count obtained from NTA to determine the protein/particle ratio as a measure of sample purity.

3.2.8 Capillary Western Blot

Capillary western blotting was conducted on a Jess, Simple Western immunoblotting system (ProteinSimple, Bio-Techne, Minneapolis, MN) following the manufacturer's standard immunoassay instructions using the 12-230 kDa separation module. Due to sample restrictions, each EV formulation was only probed for the EV-enriched protein marker, ALIX. The HEK293 and M2 EV samples had lower concentrations than that recommended for the immunoassay (1 mg/mL) and were thus concentrated down as far as possible prior to the assay. All other samples were run at the recommended 1 mg/mL final protein concentration. HEK293 cell lysate was used as a positive control and the supernatant from UC was used as a negative control. The biotinylated protein ladder, 5X fluorescent master mix and dithiothreitol were prepared per the manufacturer's instructions and added accordingly to each sample prior to denaturation at 95℃ for 5 minutes. Anti-Alix Antibody was diluted 1:25 in antibody diluent 2 solution. Luminol and hydrogen peroxide were mixed at a 1:1 ratio. All reagents were loaded into the provided plate according to the instructions for the standard chemiluminescent immunoassay protocol and the samples were analyzed using the standard immunoassay procedure in the Compass Simple Western software using the following specifications: chemiluminescence, 12-230 kDa size range, 25 lane cartridge.

3.2.9 Transmission Electron Microscopy (TEM)

The EV samples were concentrated to ~ 1.0e11-2.0e11 particles/mL. 400 mesh carbon-coated copper grids were floated onto each EV sample. The grids were washed using four drops of water. They were then negatively stained with 2% uranyl acetate

(aq). The grids were then glow discharged with a Pelco easiGlow glow discharge unit (Ted Pella Inc, Redding, CA), making the carbon film hydrophilic. This was done just prior to application of the sample. EV samples were then imaged using a Zeiss Libra 120 transmission electron microscope (Oberkochen, Germany) operating at 120 kV. Images were obtained using a Gatan Ultrascan 1000 CCD camera (Warrendale, PA).

3.2.10 Cell Culture

HEK293 cells and C2C12 myoblasts were expanded in GM comprised of high glucose DMEM supplemented with 10% FBS and 1 % p/s. Both cell-types were periodically passaged as they reached a confluency of 80-90%. For the myotube experimental group, once the myoblasts reached 90-100% confluence, they were switched to high-glucose DMEM containing 2% horse serum and 1% penicillin/streptomycin to initiate differentiation of myoblasts into myotubes. Six days after the media transition, myoblasts had fully undergone fusion into mature myotubes and were utilized for downstream experiments. Primary human cardiomyocytes were cultured in myocyte growth medium supplemented with the provided supplement kit following the manufacturer's instructions. Human primary Kupffer cells were thawed and plated following the manufacturer's instructions for Kupffer cell monoculture. Briefly, cells were thawed at 37℃ for 1-2 minutes and then transferred to a conical tube containing 9 mL of ice-cold Kupffer cell monoculture medium consisting of RPMI 1640 base media with GlutaMAX-I and HEPES containing 10% FBS and 1% p/s. The cells were then plated at a density of 30,000 cells/well into 96-well plates coated with collagen-I. 4-6 hours after initial plating medium was exchanged for fresh

Kupffer cell monoculture medium. After 24 hours, the medium was changed once more and the cells were utilized for downstream experiments.

3.2.11 In Vitro Uptake Assays

Purified MT-EVs and control EVs produced in 2x 875 cm^2 culture flasks per experimental group were stained with 5 uM CellTracker Red CMTPX Dye for 45 minutes at 37℃ followed by washing with 25 mL of 1X PBS and UC at 150,000 x g for 60 min @ 4℃ to remove unbound dye. The pellet was re-suspended in 1 ml of 1X PBS and a BioTek fluorescent plate reader (Agilent, Santa Clara, CA) was then used to measure the fluorescence intensity of the labeled EVs diluted 1:10 in 1X PBS using excitation and emission wavelengths of 577/602 nm. Based on the fluorescence signal, the labeled HEK-EVs were administered to each cell line at a 1:10 dilution. The PTGFRN-, M1- and M2-expressing EV constructs were then administered at a concentration normalized to the HEK-EV group based on the fluorescence intensity obtained on the fluorescent plate reader. All cell lines previously mentioned, besides the Kupffer cells, were passaged into half surface area 96-well plates. The cells were allowed to expand overnight to achieve 60-80% confluency by the following day at which time the cells were administered one of four EV constructs. For the Kupffer cells, the cells remained in the 96-well plates that they were initially seeded into as these cells are not to be subcultured. EV doses were adjusted based on the surface area of the wells. The cells were incubated with the EVs for 24 hours at which time the media was switched to each cell line's respective growth medium containing 5uM DiO membrane dye for 15 minutes at 37℃. The dye was removed by washing three times with fresh media and replaced once more with media containing Live-Cell

Nucblue stain at a final concentration of two drops/mL of media. The cells were incubated an additional 20 minutes to allow for nuclear staining prior to imaging. Following this incubation period, the cells were imaged on the ImageExpress Pico at 37℃. The FITC (488 nm) channel was used to image the cell membranes labeled with DiO to obtain representative images confirming intracellular delivery. The EV-derived CT-Red-labeled protein was imaged using the Texas Red-568 channel. Following acquisition, the images were analyzed using a two-channel cell scoring assay in which the Image Express software quantifies the EV-derived CT-Red signal in the Texas Red-568 channel relative to the nuclear stain. The average cell intensity quantified by this assay was used to compare the EV-derived protein delivered into each cell-type.

3.2.12 Statistical Analysis

A two-way ANOVA with a Tukey post hoc test for multiple comparisons was utilized to test for statistical significance. For all in vitro experiments, three independent experiments were utilized. The data are presented as the average of the means +/- standard error. A p value < 0.05 was considered significant. All statistical analyses were conducted in GraphPad Prism 9.4.1.

3.2.13 Key Resources

Transfections

Reagent/Resource	Vendor	Catalog Number
PTGFRN (GFP-tagged) - Human prostaglandin	OriGene	RG222956

F2 receptor negative regulator		
ASSLNIA-PTGFRN-GFP (MP1)	University of Michigan Vector Core	
RRQPPRSISSHP-PTGFRN-GFP	University of Michigan Vector Core	
jetOPTIMUS DNA Transfection Reagent	Polyplus Transfection	117-07
Geneticin™ Selective Antibiotic (G418 Sulfate) (50 mg/mL)	Gibco, ThermoFisher Scientific	10131035

Cell Lines/Culture

Reagent/Resource	Vendor	Catalog Number
293 [HEK293]	American Type Culture Collective	CRL-1573
PTGFRN-HEK293	Stably transfected HEK293 cells (above)	
MP-1-HEK293	Stably transfected HEK293 cells (above)	
MP-2-HEK293	Stably transfected HEK293 cells (above)	
C2C12 Myoblasts	American Type Culture Collective	CRL-1772
Primary Human Cardiomyocytes	PromoCell	C-12810

Primary Human Kupffer Cells	Invitrogen, ThermoFisher	HUKCCS
Dulbecco's Modified Eagle Medium (DMEM), High Glucose	Gibco, ThermoFisher Scientific	11965092
Opti-MEM, Reduced Serum Medium	Gibco, ThermoFisher Scientific	31985062
Fetal Bovine Serum, Premium Plus (FBS)	Gibco, ThermoFisher Scientific	A4766801
Horse Serum (HS)	Gibco, ThermoFisher Scientific	16050122
RPMI 1640 Medium, GlutaMAX™ Supplement, HEPES	Gibco, ThermoFisher Scientific	72400047
Myocyte Growth Medium (Ready-to-use)	PromoCell	C-22070
Human Collagen-I	Sigma-Aldrich	32160405

Molecular Staining/Imaging

Reagent/Resource	Vendor	Catalog Number
NucBlue™ Live ReadyProbes™ Reagent (Hoechst 33342)	Invitrogen, ThermoFisher	R37605
Vybrant™ DiO Cell-Labeling Solution	Invitrogen, ThermoFisher Scientific	V22886
CellTracker™ Red CMTPX dye	Invitrogen, ThermoFisher Scientific	C34552

Protein Assay/Capillary Western Blot

Reagent/Resource	Vendor	Catalog Number
RIPA buffer (5X)	Thermo Scientific	J62524.AE
Halt™ Protease Inhibitor Cocktail, EDTA-Free (100X)	Thermo Scientific	87785
BCA Protein Assay Kit	Thermo Scientific	J63283.QA
12-230 kDa Separation Module, 8 x 25 capillary cartridges	ProteinSimple, BioTechne	SM-W004
EZ Standard Pack 1	ProteinSimple, BioTechne	PS-ST01EZ-8
Anti-Alix Monoclonal Antibody	Invitrogen, ThermoFisher Scientific	MA1-83977
Anti-Body Diluent 2	ProteinSimple, BioTechne	042-203
Streptavidin-Horse Radish Peroxidase (HRP) Conjugate	ProteinSimple, BioTechne	042-414
Anti-Mouse Secondary Antibody-HRP Conjugate	ProteinSimple, BioTechne	042-205
Chemiluminescent Substrate	ProteinSimple, BioTechne	PS-CS01
Wash Buffer	ProteinSimple, BioTechne	042-202
Sample Buffer	ProteinSimple, BioTechne	042-195

3.3 Results

3.3.1 Optimization of Plasmid Transfection

Transfection optimization experiments were initially conducted to find the optimal ratio for maximal expression of each construct by testing various DNA:transfection reagent ratios. These cells were imaged on an ImageExpress Pico using the 488 nm channel to detect the GFP tag associated with N-terminus of each protein construct. For all three of the recombinant protein constructs that were overexpressed, a ratio of 1 ug:1 ul of transfection reagent was found to produce the greatest amount of GFP signal when transiently transfected into HEK293 (Figure 3.1C). This ratio was chosen for the production of the cell lines used to generate the chimeric myotropic EV candidates.

3.3.2 Characterization of Stable Producer Cell Lines

Following transfection and antibiotic selection with Geneticin, each producer cell line underwent further selection using FACS. This experiment provided not only a method to select the cells producing the greatest quantities of each recombinant protein, but also characterize the proportion of the cell population expressing the constructs following antibiotic selection. For the PTGFRN-expressing cell line, 58.4% of cells were GFP-positive following antibiotic selection (Figure 3.1E). For the M1-expressing cell line, 69.1% of cells were GFP-positive following antibiotic selection (Figure 3.1F). For the M2-expressing cell line, 2.1% of cells were GFP-positive following antibiotic selection (Figure 3.1G). A GFP control transfection was conducted to examine the efficiency of each construct and set gating parameters for the FACS experiment (Figure A.3). 75.5% of the GFP-transfected cells were GFP-

positive during the run, indicating that the MP1 line showed the highest degree of transfection efficiency while the MP2 line showed the least efficiency. Thus, the MP2 line required further subsequent passaging to achieve the quantity of cells needed for downstream EV production. These data highlight the variability in the efficiency with which various plasmid constructs undergo homologous recombination following transient transfection and feasibility of generating stable producer cell lines thereafter. Regardless of the initial efficiency of incorporation, FACS confirmed the selection of cell populations 100% positive for GFP for each of the cell lines with a mean fluorescence intensity between 10e4 and 10e5 AU in order to promote similar protein expression profiles in each of the lines. This was then confirmed by obtaining representative images of each producer cell line (Figure 3.1 E-G).

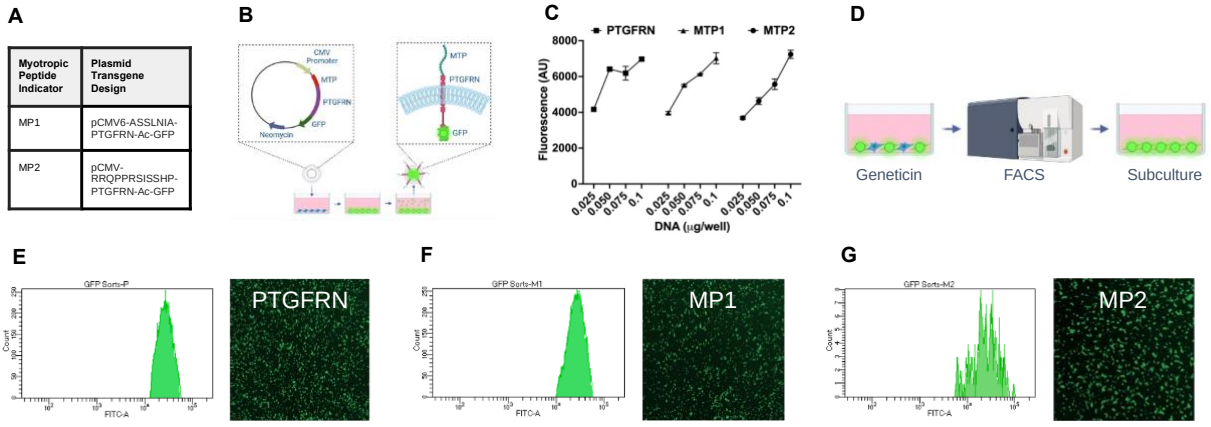

Figure 3.1 Production and characterization of the chimeric myotropic EV producer cell lines. **A)** Design of plasmids encoding myotropic protein 1 (MP1, ASSLNIA) and 2 (MP2, RRQPPRSISSHP). **B)** Workflow for transfecting plasmids into HEK293 cells to result in cells producing chimeric myotropic proteins of interest. **C)** Transfection efficiency at various DNA and transfection reagent concentrations (N = 3 independent experiments). **D)** Workflow for selecting stable-expressing cells via antibiotics and fluorescence-assisted cell sorting (FACS). **E)** Cell count and fluorescence intensity of selected cells in PTGFRN transfection group. **F)** Cell count and fluorescence intensity

of selected cells in MP1 transfection group. **G)** Cell count and fluorescence intensity of selected cells in MP2 transfection group. Representative images taken at 10X.

3.3.3 Characterization of EV Candidates

Each M-EV candidate was analyzed via NTA, TEM, BCA and capillary western blot. The PTGFRN and MP1-EV formulations had a higher particle concentration than the other two groups with the PTGFRN-EVs displaying a ~ 29-fold increase and the M1-EVs displaying a ~ 39-fold increase in particle concentration relative to the HEK-EV group (Figure 3.2A). TEM revealed that each sample contained particles with the typical size and morphology of EVs, although the EVs from the transfected cell lines generally appeared to be larger in size (Figure 3.2B-E), as was indicated on NTA (Figure 3.2A). This may suggest a shift away from smaller EV production, such as small ectosomes and exosomes, and toward larger EV populations, such as large ectosomes/microvesicles and apoptotic bodies. Western blot analysis was also conducted on these samples using a capillary western blotting system (Figure A.4). However, due to the low particle and protein yields in the HEK and MP2-EV samples, data was only generated for the PTGFRN and MP1-EV samples, which confirmed the presence of the EV protein marker, ALIX. ALIX was also found in the cell lysate of HEK cells and in smaller amounts in the supernatant from UC, suggesting either not all of the EVs were pelleted by the UC protocol or ALIX was also released by the cells to some extent in a soluble form.

A

EV Candidate	Particle Concentration (p/mL)	Mean Size (nm)	Modal Size (nm)	Protein (fg)/Particle
HEK	9.1e9	179	126	2.0
PTGFRN	2.75e11	195	139	0.3
MP1	3.6e11	200	156	0.4
MP2	5.8e9	192	134	2.9

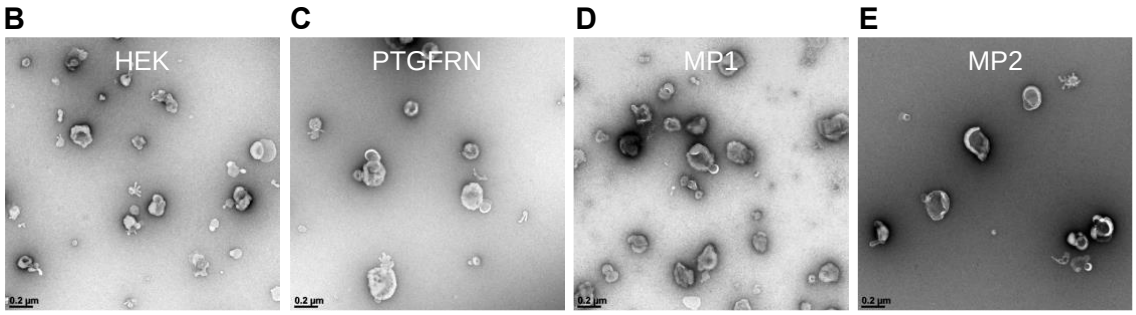

Figure 3.2 Characterization of chimeric myotropic EV formulations. **A**) Nanoparticle tracking analysis data pertaining to the concentration and size of the particles produced from each cell line in addition to the protein content of each EV formulation. **B**) Representative TEM images of each EV formulation, displaying the size and morphology of the EVs in each group. HEK = human embryonic kidney cell. PTGFRN = Prostaglandin F2 Receptor Inhibitor, MP1 = myotropic protein 1, MP2 = myotropic protein 2. N = 3 independent experiments.

3.3.4. In Vitro Uptake Assays

Each EV formulation was labeled with CT-Red and administered to various recipient cell-types in vitro at equal fluorescence intensities as determined using a fluorescent plate reader (Figure A.5). EVs were administered to HEK293, human primary cardiomyocytes, C2C12 myotubes, and human primary Kupffer cells for 24 hours. Interestingly, the PTGFRN-EV formulation showed significant increases in delivery to each cell-type relative to the non-engineered HEK-EVs except for the Kupffer cells: HEK293 cells (7.9-fold), CM (2.2-fold), C2C12 (4.5-fold) with the

highest differential from the non-engineered HEK-EVs found in the HEK293 line and the highest overall signal in the CM line (Figure 3.3B). Similar to the PTGFRN EVs, the MP1 EVs showed significant increases in delivery to each cell-type relative to the non-engineered HEK EVs except for the Kupffer cells: HEK293 cells (6.5-fold), CM (2.4-fold), C2C12 (2.4-fold) with slightly higher delivery to the CM line and slightly lower delivery to the HEK293 and C2C12 lines (Figure 3.3B). The MP2 EVs did not achieve significantly greater protein delivery in any of the tested cell lines relative to the non-engineered HEK EVs, except for the Kupffer Cells, with a 0.5-fold increase in delivery into HEK293 cells and CM, a 1.1-fold increase in C2C12 and a 2.0-fold increase in delivery to the Kupffer cells (Figure 3.3B). The PTGFRN EVs showed significantly greater protein delivery in each cell line than the MP2 EVs except for in the Kupffer cells (Figure 3.3B). The MP1 EVs displayed significantly greater delivery than the MP2 EVs in the HEK293 and CM lines but not the C2C12 myotubes or Kupffer cells (Figure 3.3B). Overall, the PTGFRN and MP1 EVs showed the highest delivery of protein cargo into the HEK293, CM and C2C12 cells, whereas the MP2 EVs showed the highest delivery in the Kupffer cells.

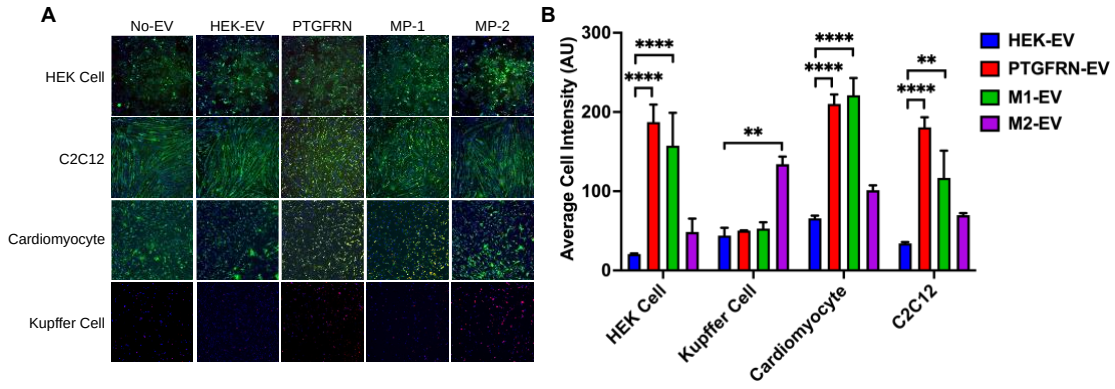

Figure 3.3 Uptake assays of chimeric myotropic EV candidates in muscle and non-muscle cell-types. **A**) Representative 10X images of EV protein (red/yellow) delivered into various cell-types in vitro. Green = cell membrane. Blue = nuclei. **B**) Quantitative analysis of fluorescently-labeled EV protein delivered into each cell-type. PTGFRN = Prostaglandin F2 Receptor Inhibitor, MP1 = myotropic protein 1, MP2 = myotropic protein 2. N = 3 independent experiments. ** $p < 0.01$, **** $p < 0.0001$.

3.4 Discussion

In the current study, we examined the myotropic properties of novel chimeric myotropic EV candidates in muscle and non-muscle cell-types in vitro. Surprisingly, the PTGFRN EVs, not expressing either of the two myotropic peptide candidates, appeared to show the highest degree of myotropism. The MP1 EV candidate displayed similar tropism to that of the PTGFRN EVs, but with slightly less delivery to the C2C12 myotubes. The MP2 EV candidate performing the worst in regard to myotropism.

Interestingly, PTGFRN has a predicted function involved in the myoblast fusion and is also highly expressed in the heart.[164] Although further research is needed to reveal the mechanism of PTGFRN in muscle and heart function, this is a potentially interesting explanation of how this protein may promote enhanced affinity to myotubes and cardiomyocytes. Although it showed the greatest affinity for myotubes

and cardiomyocytes, the PTGFRN-EVs also displayed a robust increase in delivery to HEK293 cells, which was utilized here as a non-muscle cell type. However, it is important to note that although the HEK293 cell line is an embryonic kidney cell line, HEK293 cells express numerous proteins often attributed to neural and muscle cell types, such as neurofilament protein subunits and muscarinic acetylcholine receptors as well as the Dp71 isoform of the protein dystrophin.[165,166] Thus, HEK293 cells may not be an optimal selection as a "non-muscle" cell-type. Further, the PTGFRN EVs did not show increased affinity for the Kupffer cells, the resident macrophage of the liver responsible for removal of drug products from the circulation,[154] suggesting their uptake may actually be somewhat selective to muscle and related cell-types.

The MP1 EVs showed a similar trend in delivery to the various cell types with the highest uptake in the cardiomyocytes, followed by the HEK293 cells and C2C12 myotubes and no significant change from HEK293 EVs in delivery to Kupffer Cells. Although this was a similar trend, it is worth noting that the MP1 EVs were less efficient at delivering cargo into the C2C12 myotubes than the EVs expressing PTGFRN alone. Of the three experimental EV formulations tested, the MP2 EV formulation showed the least affinity for the HEK293 cells, cardiomyocytes, and C2C12 myotubes and showed the greatest affinity for the Kupffer cells. Given the previous literature, it was expected that the EVs displaying the myotropic peptides would show the greatest affinity for the C2C12 myotubes and possibly the cardiomyocytes. In previous studies however, these peptides were incorporated into the AAV capsid, directly conjugated to an ASO, or in the case of the attempted myotropic EV formulation, expressed as a hybrid protein with Lamp2b as the scaffold.[39,43,113] Thus, there was no previous literature predicting how these peptides

would function as a hybrid protein with PTGFRN as the scaffold. Additionally, given the predicted function of PTGFRN based on its sequence and structure, it is feasible that this protein has its own myotropic properties and fusing additional peptides to the extramembranous domain dampens this effect.[164]

MP1 (ASSLNIA) was identified in a study that used a high-throughput phage display assay to present various short peptides on the surface of bacteriophages that were then incubated with C2C12 myotubes.[167] This assay identified ASSLNIA as the peptide that enabled the greatest infectivity of the bacteriophage into the myotubes; however, this experiment did not include other cell types. The researchers followed up their initial phage display assay with an in vivo experiment where the ASSLNIA-expressing phage or a control phage were administered to mice via tail vein injection.[167] Although they showed enhanced delivery to skeletal and cardiac muscle, the phage was still largely delivered to the liver, with a notable amount of phage ending up in the kidneys as well. Thus, a fully differentiated kidney or hepatocyte cell line would have been a useful cell line in the current study to examine how closely the MP1 EV performed to the initial phage experiment. It is notable that the MP1 EVs did not show enhanced affinity to the Kupffer cells, suggesting the formulation may be somewhat selective to cells of a myogenic lineage. Biodistribution studies are needed to follow up the findings herein to fully validate any potential myotropic properties in vivo.

MP2 (RRQPPRSISSHP) was identified via phage display assay in 2014 by Gao et al.[43] In this study the researchers conjugated MP-2 to a phosphorodiamidate morpholino oligomer (PMO) and compared the in vivo biodistribution and ability to restore dystrophin expression in mdx mice to that of an MP1-PMO conjugate. In these

experiments, they found MP2 to be a superior myotropic candidate compared to MP1, with robust delivery to the skeletal and cardiac muscle along with improved dystrophin restoration.[43] These findings are in conflict with the findings of the current study in which the MP2 EV formulation performed the worst in regards to myotropism as compared to MP1 and PTGFRN EV formulations. This was a surprising finding given the promise of this peptide in the previous literature; however, a 12-mer peptide conjugated to a 25 base pair nucleotide is a far different construct than that same peptide expressed as a part of a larger hybrid protein displayed on the surface of a 100-200 nm biological nanoparticle. Thus, it cannot be assumed that the EV formulation will behave the same as a peptide-PMO conjugate. To our surprise, in the current study the MP2 EV formulation showed the highest affinity for the Kupffer cells. The authors that identified this peptide did not investigate the delivery specifically to Kupffer cells, but did note a decreased delivery of the MP2-PMO to the liver.[43] However, these were in vivo studies, whereas the current study was in vitro. It has been demonstrated that in vivo, smaller molecules tend to stay in the circulation longer, increasing the distribution to the peripheral tissues relative to the liver and spleen where larger molecules/particles are largely taken up.[154] This could feasibly lead to different results, as compared to the current study, which utilized in vitro experiments in which each cell-type was directly exposed to each EV candidate. Thus, biodistribution studies are needed to further investigate the tropism of the MP2 EVs in vivo.

It is also important to note that in the current study, we did not analyze the degree of incorporation of each recombinant protein into the EVs. Flow cytometry experiments using a ubiquitous EV counterstain in combination with the endogenous

GFP tag associated with each recombinant protein would provide context to the results of the uptake assay. Specifically, incorporation of one protein construct relative to another may influence the degree to which the proteins facilitate uptake into the recipient cells. We did however use FACS to select stable producer cells in a similar range of fluorescence intensity to ensure the expression of each protein construct was similar in the EV-producing cells. Further analysis of the final EV products is needed to fully optimize the production of these formulations and parse out whether the observed effects were due to the functionality of the recombinant protein or due to differences of incorporation into the EV membrane.

Interestingly, NTA revealed a notable difference in the number of particles produced by the PTGFRN (~ 29-fold increase) and MP1 EV (~ 39-fold increase) groups relative to the non-engineered EV group, whereas the MP2 EV group largely yielded a similar particle count. Additionally, all of the EVs from the transfected groups displayed larger particle diameters than the non-engineered HEK EVs. Transfections can expose the cells to harsh conditions due to the cationic reagent utilized and the over-expression of foreign proteins that may have cytotoxic effects on the transfected cells.[168] Although all cells used for EV generation were maintained at a viability $\geq$ 90%, slight variances between cell lines could feasibly change the composition of the secretome.[169] Thus, we utilized TEM to assess the morphology of the EVs produced. To our surprise, the EVs in the PTGFRN and MP1 looked morphologically similar to those in the HEK293 and M2 groups, despite the drastic elevation in particle count. As our FACS data suggests, the cells transfected with the PTGFRN and MP1 plasmids showed much higher transfection efficiency than those transfected with MP2, thus it is possible that the abundance of proteins produced by

these transfections resulted in the cells releasing the proteins via enhanced EV production. It is also important to note the increase in particle size observed via NTA and TEM as this suggests a shift away from the production of smaller EV populations, such as small ectosomes and exosomes, and toward larger EV populations, such as large ectosomes/microvesicles and apoptotic bodies.[73,169,] This is critical when considering EVs as drug delivery vectors because alterations in the size of the carrier may alter which cell-types are able to be accessed by the EVs in vivo.[154] Although the current study was limited to in vitro analyses, this is an important consideration for future in vivo studies.

3.5 Conclusions

Overall, this study elucidates the feasibility of producing various chimeric myotropic EV formulations using PTGFRN as the scaffold for the myotropic peptide candidates. Surprisingly, we found that PTGFRN itself imparted the greatest degree of myotropism relative to control HEK293 EVs and the two chimeric myotropic EV candidates. This presents new potential therapeutic targets for the PTGFRN-EVs which are already being utilized in clinical trials for the delivery of anti-tumor therapies. However, it should be noted that the current study used a limited number of "off-target" cell-types and skeletal muscle presents a difficult drug target containing capillaries with continuous endothelium. Thus, extensive in vivo biodistribution studies are needed to validate any potential myotropic properties of the EV formulations presented herein.

Chapter 4

CONCLUSION

4.1 Summary

Muscular pathologies comprise a devastating group of diseases and disorders that are often debilitating and may be fatal. The most prevalent and severe genetic muscle disease is Duchenne Muscular Dystrophy, in which a mutation in the dystrophin gene results in the lack of dystrophin protein expression.[11] This results in progressive muscle degeneration and fibrosis, which eventually results in heart failure.[170] The most promising class of therapeutics for the treatment of these types of diseases are gene therapies delivered via the adeno-associated viral (AAV) vector.[22] Although this technology has revolutionized the way we treat genetic disorders, many limitations involving immunogenicity, specificity and capacity of the vector still remain.[35] In recent years interest has spiked in using biological lipid nanoparticles, extracellular vesicles (EVs), as a next-generation drug delivery platform with low immunogenicity, targeting capabilities and enhanced storage relative to AAV vectors.[130]

In our first study, we examined the in vivo biodistribution and in vitro cell-type affinity of various novel myotropic EV candidates. In the in vivo biodistribution study, we examined the biodistribution of EVs expressing the myogenic fusion protein, TMEM8C (MyoMaker, MYMK) as compared to non-engineered HEK293 following systemic administration. This route was utilized as to provide the EVs access to all of the skeletal muscles, as opposed to a more localized approach such as intramuscular injection. Although the MYMK-EVs showed promising myotropic properties when incubated with C2C12 myotubes in vitro, they failed to significantly alter biodistribution in vivo. However, we did find a significant alteration in the

biodistribution of both EV formulations when comparing that of the mdx mouse model with the wildtype C57 mouse model. Specifically, both EV formulations showed a significant decrease in signal in the spleen and non-significant increases in the peripheral tissues, except for the brain. This suggests that circulating immune cells could play a role in the distribution of intravenous drug products and this varies with disease state. Further experiments, such as directly labeling PBMCs or administering labeled-EVs to PBMCs ex vivo and then administering the cells to mice, are needed to validate this mechanism. Another route may be to utilize immune cells capable of transcytosis, such as leukocytes, as the EV producer line which could then be engineered to express the myotropic EV candidates. Endothelial and muscle cells may also present interesting candidates as producer cell lines. In any case, the scalability of the cell line chosen for EV production is always a major concern, as large quantities of EVs are needed for biodistribution experiments. Additionally, we observed a marked change in particle count depending on the type of stain (lipophilic vs. amine-reactive) that was utilized. This could mean that the lipophilic dye is generating some sort of artifactual signal during nanoparticle tracking analysis and calls into question the validity of using NTA as a means of dosing EVs for downstream experiments. For this reason, we cannot definitively report the number of actual EVs in the samples as opposed to dye-derived artifacts. For this reason, the dose in the amine-reactive dye labeled EV experiments was normalized to the lipophilic dye experiments based on the number of producer cells rather than particle count. Using the fluorescent plate reader to dose the EVs also provides data on the incorporation of the dye into the EVs in each sample. NTA does not calculate this and thus although particle count may be the same, samples may vary in composition and thus have differing levels of dye

incorporation. Given that the final measurement of biodistribution is reliant on the fluorescent signal in each tissue, having differing amounts of dye incorporation in different samples may lead to error in the signal derived from the tissues. Additionally, characterization data reporting the density of the MYMK protein at the surface of the EVs would provide further context to these findings as ligand density may reasonably affect the ability of the EVs to bind to the recipient muscle cells. Future studies should look to measure this to determine the effect of MYMK protein density on MYMK-EV biodistribution. Overall, although it appears that we can achieve enhanced myotropism of EVs in vitro, it remains to be seen whether this tissue type can be successfully targeted in vivo.

In the second study we examined the myotropic properties of chimeric myotropic EV candidates in vitro by displaying two different myotropic peptides on the EV membrane protein PTGFRN and incubating the EVs with muscle and non-muscle cell types. Surprisingly, the EVs expressing the PTGFRN protein alone demonstrated the highest degree of myotropism relative to non-engineered EVs and those expressing the myotropic peptides. Analysis of the PTGFRN amino acid sequence revealed that it has predicted functions in myoblast fusion and in lieu of the current data this functionality may impart myotropic properties to this protein.[164] In addition, we did see roughly fourfold greater protein/particle in the HEK and MP2-EV groups as compared to the PTGFRN and MP1-EV groups, likely due to the increased EV production noted in the latter two groups. This is unlikely to have affected the results, as the dose of EVs administered to each cell-type was normalized to the quantity of fluorescently labeled protein in each sample. These data are interesting; however, we did not collect data on the degree to which each protein is incorporated

into the EVs produced, in which variances could change the tropism of the EVs. Further, as was observed in the previous study, in vitro results are not always able to be recapitulated in vivo and thus biodistribution studies are needed to validate any potential myotropic properties of these EVs.

4.2 Perspectives

The data herein question the ability of engineered EVs to deliver molecular cargoes to skeletal muscle in a targeted manner. In each group, the skeletal muscle displayed the second lowest signal next to the brain. Both of these organs contain capillaries with continuous endothelium that appears to efficiently block particles in the size range of EVs from transcytosing across the barrier.[148] However, we did observe a marked decrease in EV-derived signal in the spleen of mdx mice relative to C57 mice along with a non-significant increase in all of the peripheral tissues. This suggests a role of circulating immune cells in the redistribution of intravenously administered drug products that varies with disease state. We also examined the myotropic properties of novel chimeric myotropic EV candidates, identifying the EV-enriched protein, PTGFRN, as having potential myotropic properties in vitro. These findings will need further validation in vivo. EVs are touted as a biocompatible, engineerable drug delivery platform; however, numerous considerations, such as the accessibility of the target cell-type, the scaffolding protein utilized and the probe used to trace the EVs may impact the measured tropism/affinity of the EVs. Extensive research is still needed to fully assess the validity of EVs as a drug delivery vector for skeletal muscle.

REFERENCES

1. Lovering, R.M., Porter, N.C., Bloch R.J. The muscular dystrophies: From genes to therapies. *Phys ther*. **85**(12), 1372-1388 (2005).

2. Morley, J.E., Thomas, D.R., Wilson M.G. Cachexia: Pathophysiology and clinical relevance. *Am j clin nutr*. **83**(4), 735-743 (2005).

3. Crisafulli, S, Sultana, J, Fontana, A, Salvo, F, Messina, S, Trifirò, G. Global epidemiology of duchenne muscular dystrophy: An updated systematic review and meta-analysis. *Orphanet j rare dis*. **15**(1), 1-141 (2020).

4. Gao, Q.Q., McNally, EM. The dystrophin complex: Structure, function, and implications for therapy. *Compr Physiol*. **5**(3), 1223-1239 (2011).

5. Sander, M., Chavoshan, B., Harris, S.A., et al. Functional muscle ischemia in neuronal nitric oxide synthase-deficient skeletal muscle of children with duchenne muscular dystrophy. *PNAS*. **97**(25), 13818-13823 (2000).

6. Rando, T.A. Role of nitric oxide in the pathogenesis of muscular dystrophies: A two hit hypothesis of the cause of muscle necrosis. *Mic res tech*. **55**(4), 223-235 (2001).

7. Meghna, P., Danesh, H., Sopariwala, N., et al. Metabolic dysfunction and altered mitochondrial dynamics in the utrophin-dystrophin deficient mouse model of duchenne muscular dystrophy. *PLoS One*. **10**(4), 1-19 (2015).

8. Chang, N.C., Chevalier, F.P., Rudnicki, M.A. Satellite cells in muscular dystrophy: lost in polarity. *Trends Mol Med*. **22**(6):479-496 (2016).

9. Bello, L., Pegoraro, E. The "Usual suspects": Genes for inflammation, fibrosis, regeneration, and muscle strength modify duchenne muscular dystrophy. *JCM*. **8**(5), 649 (2019).

10. De Palma, C., Morisi, F., Cheli, S., et al. Autophagy as a new therapeutic target in duchenne muscular dystrophy. *Cell death dis*. **3**(11), e418 (2012).

11. Dongsheng, D., Nathalie, G., Shin'ichi, T., Eugenio M., Annemieke A. Duchenne muscular dystrophy. *Nat Rev Dis Primers*. **7**(13) (2021).

12. Schram, G., Fournier A., Leduc H., et al. All-cause mortality and cardiovascular outcomes with prophylactic steroid therapy in duchenne muscular dystrophy. *J Am College Cardiol*. **61**(9), 948-954 (2013).

13. Thada, P.K., Bhandari, J., Umapathi, K.K. Becker muscular dystrophy. *Stat Pearls*. 1-11 (2022).

14. Neri, M., Rossi, R., Trabanelli, C., et al. The genetic landscape of dystrophin mutations in italy: A nationwide study. *Front Genet*. **11**, 131 (2020).

15. Bauer, J., Morley, J.E., Schols, A.M., et al. Sarcopenia: A time for action. an SCWD position paper. *J Cachexia Sarcopenia Muscle*. **10**(5), 956-961 (2019).

16. Porporato, P.E. Understanding cachexia as a cancer metabolism syndrome. *Oncogenesis*. **5**(2), e200 (2016).

17. Peixoto, D.S.D., Santos, J.M.O., Costa, E.S.M.P., Gil Da Costa, R.M., Medeiros, R. Cancer cachexia and its pathophysiology: Links with sarcopenia, anorexia and asthenia. *J Cachexia Sarcopenia Muscle*. **11**(3), 619 (2020).

18. Argilés, J., Busquets, S., Toledo, M., López-Soriano, F. The role of cytokines in cancer cachexia. *Curr opin supp pall care*. **3**(4), 263-268 (2009).

19. Patel, H.J., Patel, B.M. TNF-α and cancer cachexia: Molecular insights and clinical implications. *Life sci*. **170**, 56-63 (2017).

20. Londhe, P., Guttridge, D.C. Inflammation induced loss of skeletal muscle. *Bone*. **80**, 131-142 (2015).

21. Yao, S., Chen Z., Yu, Y., et al. Current pharmacological strategies for duchenne muscular dystrophy. *Fron cell dev biol*. **9**, 689533 (2021).

22. Papanikolaou, E., Bosio, A. The promise and the hope of gene therapy. *Front gen ed*. **3**, 1-14 (2021).

23. Dai, A., Baspinar, O., Yesilyurt, A., et al. Efficacy of stem cell therapy in ambulatory and nonambulatory children with duchenne muscular dystrophy – phase I–II. *DNND*. **8**(63), 63-77 (2018).

24. McDonald, C.M., Henricson, E.K., Abresch, R.T., et al. Long-term effects of glucocorticoids on function, quality of life, and survival in patients with duchenne muscular dystrophy: A prospective cohort study. *Lancet*. **319**, 451-461 (2017).

25. Vandamme, C., Adjali, O., Mingozzi, F. Unraveling the complex story of immune responses to AAV vectors trial after trial. *Hum Gene Ther*. **28**(11), 1061 (2017).

26. Kourakis, S., Timpani, C.A., Campelj, D.G., et al. Standard of care versus new-wave corticosteroids in the treatment of duchenne muscular dystrophy: Can we do better? *Orphanet J Rare Dis*. **16**(1), 117 (2017).

27. Quattrocelli, M., Salamone, I.M., Page, P.G., et al. Intermittent glucocorticoid dosing improves muscle repair and function in mice with limb-girdle muscular dystrophy. *Am J Pathol*. **187**(11), 2520–2535 (2017).

28. Quattrocelli, M., Barefield, D.Y., Warner, J.L., et al. Intermittent glucocorticoid steroid dosing enhances muscle repair without eliciting muscle atrophy. *J clin invest.* 1**27**(6), 2418-2432 (2017).

29. U.S. Food and Drug Administration. What is gene therapy? https://www.fda.gov. Updated 2018.

30. Crudele, J.M., Chamberlain, J.S. AAV-based gene therapies for the muscular dystrophies. *Hum mol gen*. **28**, R102-R107 (2019).

31. Rinaldi, C., Wood, M.J.A. Antisense oligonucleotides: The next frontier for treatment of neurological disorders. *Nat Rev Neur*. **14**, 9-21 (2018).

32. Gaj, T., Sirk, S.J., Shui, S., Liu, J. Genome-editing technologies: Principles and applications. *Cold Spring Harbor perspectives in biology*. **8**(12), a023754 (2016).

33. Naso, M.F., Tomkowicz, B., Perry, W.L., Strohl, W.R. Adeno-associated virus (AAV) as a vector for gene therapy. *BioDrugs*. **31**(4), 317 (2017).

34. Deyle, D.R., Russell, D.W. Adeno-associated virus vector integration. *Curr Opin Mol Ther.* **11**(4), 442–447 (2019).

35. Colella, P., Ronzitti, G., Mingozzi, F. Emerging issues in AAV-mediated in vivo gene therapy. *Mol Ther Methods Clin Dev*. **8**(87), 87-104 (2018).

36. Ronzitti, G., Gross, D., Mingozzi, F. Human immune responses to adeno-associated virus (AAV) vectors. *Front immune*. **11**(670), 1-13 (2020).

37. Calcedo, R., Vandenberghe, L.H., Gao, G., et al. Worldwide epidemiology of neutralizing antibodies to adeno-associated viruses. *J Inf Dis*. **199**(3), 381-390 (2009).

38. Srivastava, A. In vivo tissue-tropism of adeno-associated viral vectors. *Curr opin virol*. **21**, 75-80 (2016).

39. Yu, C., Yuan, Z., Cao, Z., et al. A muscle-targeting peptide displayed on AAV2 improves muscle tropism on systemic delivery. *Gene therapy*. **16**(8), 953-962 (2009).

40. Li, C., Samulski, R.J. Engineering adeno-associated virus vectors for gene therapy. *Nat Rev Genet*. **21**, 255–272 (2020).

41. Chen, S., Sanmiguel, J., Lock, M., et al. Biodistribution of AAV8 vectors expressing human low-density lipoprotein receptor in a mouse model of homozygous familial hypercholesterolemia. *Hum Gene Ther Clin Dev*. **24**(4), 154-160 (2013).

42. Halbert, C.L., Allen, J.M., Chamberlain, J.S. AAV6 vector production and purification for muscle gene therapy. *Methods Mol Biol*. **1687**, 257-266 (2018).

43. Gao, X., Zhao, J., Han, G., et al. Effective dystrophin restoration by a novel muscle-homing Peptide–Morpholino conjugate in dystrophin-deficient mdx mice. *Mol ther*. **22**(7), 1333-1341 (2014).

44. Skopenkova, V.V., Egorova, T.V., Bardina, M.V. Muscle-specific promoters for gene therapy. *Acta Nat.* **13**(1), 47 (2021).

45. Kim, I. A brief overview of cell therapy and its product. *J Kor As Oral Max Sur*. **39**(5), 201-202 (2013).

46. El-Kadiry, A.E., Rafei, M., Shammaa, R. Cell therapy: Types, regulation, and clinical benefits. *Front med*. **8**, 756029 (2021).

47. Chang, E., Jin, S., Nam, M., Kim, S. Human induced pluripotent stem cells : Clinical significance and applications in neurologic diseases. *J of Kor Neuro Soc*. **62**(5), 493-501 (2019).

48. Berry, S.E. Concise review: Mesoangioblast and mesenchymal stem cell therapy for muscular dystrophy: Progress, challenges, and future directions. *Stem cells trans med*. **4**(1), 91-98 (2015).

49. Xu, X., Wilschut, K., Kouklis, G., et al. Human satellite cell transplantation and regeneration from diverse skeletal muscles. *Stem cell reports*. **5**(3), 419-434 (2015).

50. Shi, Y., Inoue, H., Wu, J.C., Yamanaka, S. Induced pluripotent stem cell technology: A decade of progress. *Nat Rev Drug Discov*. **16**(2), 115 (2016).

51. Takahashi, K., Yamanaka, S. Induction of pluripotent stem cells from mouse embryonic and adult fibroblast cultures by defined factors. *Cell*. **126**(4), 663-676 (2006).

52. Hallett, P., Deleidi, M., Astradsson, A., et al. Successful function of autologous iPSC-derived dopamine neurons following transplantation in a non-human primate model of parkinson's disease. *Cell stem cell*. **16**(3), 269-274 (2015).

53. McTague, A., Rossignoli, G., Ferrini, A., et al. Genome editing in iPSC-based neural systems: From disease models to future therapeutic strategies. *Front gen edit*. **3**, 630600 (2021).

54. Darabi, R., Pan, W., Bosnakovski, D., et al. Functional myogenic engraftment from mouse iPS cells. *Stem Cell Rev and Rep*. **7**(4), 948-957 (2012).

55. Zhu, Y., Yang, Y., Zhang, Y., et al. Placental mesenchymal stem cells of fetal and maternal origins demonstrate different therapeutic potentials. *Stem cell res ther*. **5**(2), 48 (2014).

56. Grove, J.E., Bruscia, E., Krause, D.S. Plasticity of bone Marrow–Derived stem cells. *Stem cells*. **22**(4), 487-500 (2004).

57. Tsuji, W., Rubin, J.P., Marra, K.G. Adipose-derived stem cells: Implications in tissue regeneration. *World j stem cells*. **6**(3), 312-321 (2014).

58. Pittenger, M.F., Discher, D.E., Péault, B.M., et al. Mesenchymal stem cell perspective: Cell biology to clinical progress. *npj Regen Med*. 4(1) (2019).

59. Karantalis, V., DiFede, D., Gerstenblith, G., et al. Autologous mesenchymal stem cells produce concordant improvements in regional function, tissue perfusion, and fibrotic burden when administered to patients undergoing coronary artery bypass grafting: The prospective randomized study of mesenchymal stem cell therapy in patients undergoing cardiac surgery (PROMETHEUS) trial. *Circ res*. **114**(8), 1302-1310 (2014).

60. Behfar, A., Yamada, S., Crespo-Diaz R., et al. Guided cardiopoiesis enhances therapeutic benefit of bone marrow human mesenchymal stem cells in chronic myocardial infarction. *J Am College Cardiol*. **56**(9), 721-734 (2010).

61. Hocking, A.M., Gibran, N.S. Mesenchymal stem cells: Paracrine signaling and differentiation during cutaneous wound repair. *Exp cell res*. **316**(14), 2213-2219 (2010).

62. Pankajakshan, D., Agrawal, D.K. Mesenchymal stem cell paracrine factors in vascular repair and regeneration. *J Biomed Tech Res*. 1(1), 10 (2014).

63. Feng, S., Chen, F., Cao, J., et al. Restoration of muscle fibers and satellite cells after isogenic MSC transplantation with microdystrophin gene delivery. *Biochem biophys res comm*. **419**(1), 1-6 (2012).

64. Vieira, N.M., Bueno, C.R., Brandalise, V., et al. SJL dystrophic mice express a significant amount of human muscle proteins following systemic delivery of human Adipose-Derived stromal cells without immunosuppression. *Stem cells.* **26**(9), 2391-2398 (2008).

65. Zammit, P.S., Golding, J.P., Nagata, Y., et al. Muscle satellite cells adopt divergent fates. *J cell biol.* **166**(3), 347-357 (2004).

66. Goel, A.J., Rieder, M., Arnold, H., et al. Niche cadherins control the quiescence-to-activation transition in muscle stem cells. *Cell reports.* **21**(8), 2236-2250 (2017).

67. Chen, B. The regulatory role of myomaker and myomixer-myomerger-minion in muscle development and regeneration. *Cell mol life sci.* **77**(8), 1551-1569 (2020).

68. Bi, P., Ramirez-Martinez, A., Li, H., et al. Control of muscle formation by the fusogenic micropeptide myomixer. *Science*. **356**(6335), 323 (2017).

69. Bareja, A., Billin, A.N. Satellite cell therapy – from mice to men. *Skel musc.* **3**(1), 2 (2013).

70. Laumonier, T., Bermont, F., Hoffmeyer, P., et al. Human myogenic reserve cells are quiescent stem cells that contribute to muscle regeneration after intramuscular transplantation in immunodeficient mice. *Sci rep*. **7**(1), 3462-12 (2017).

71. Syverud, B.C., Lee, J.D., VanDusen, K.W., Larkin, L.M. Isolation and purification of satellite cells for skeletal muscle tissue engineering. *J regen med*. **3**(2), 117 (2014).

72. Puymirat, J., Campbell, C. Transplantation of myoblasts to duchenne muscular dystrophy (DMD) patients. https://www.clinicaltrials.gov/ct2/show/NCT02196467. Updated 2021.

73. Théry, C., Witwer, K.W., Aikawa, E., et al. Minimal information for studies of extracellular vesicles 2018 (MISEV2018): A position statement of the international society for extracellular vesicles and update of the MISEV2014 guidelines. *J Extracell Vesicles*. **7**(1), 1535750 (2018).

74. Teng, F., Fussenegger, M. Shedding light on extracellular vesicle biogenesis and bioengineering. *Adv Sci*. **8**(1), 2003505 (2020).

75. Van Niel, G., Carter, D.R.F., Clayton, A., et al. Challenges and directions in studying cell–cell communication by extracellular vesicles. *Nat Rev Mol Cell Biol*. **23**(5), 369-382 (2022).

76. Sun, M., Xue, X., Li, L., et al. Ectosome biogenesis and release processes observed by using live-cell dynamic imaging in mammalian glial cells. *Quant Imaging Med Surg*. **11**(11), 4604-4616 (2021). https://search.proquest.com/docview/2594292624. doi: 10.21037/qims-20-1015.

77. Mulcahy, L.A., Pink, R.C., Carter, D.R.F. Routes and mechanisms of extracellular vesicle uptake. *J extracell vesicles*. **3**(1), 24641 (2014).

78. Tian, T., Zhu, Y., Zhou, Y., et al. Exosome uptake through clathrin-mediated endocytosis and macropinocytosis and mediating miR-21 delivery. *J biol chem*. **289**(32), 22258-22267 (2014).

79. Walravens, A., Smolgovsky, S., Li, L., et al. Mechanistic and therapeutic distinctions between cardiosphere-derived cell and mesenchymal stem cell extracellular vesicle non-coding RNA. *Sci Rep*. **11**(1), 8666 (2021).

80. Bian, S., Zhang, L., Duan, L., et al. Extracellular vesicles derived from human bone marrow mesenchymal stem cells promote angiogenesis in a rat myocardial infarction model. *J Mol Med*. **92**(4), 387-397 (2013).

81. Shuler, K.T., Wilson, B.E., Muñoz, E.R., Mitchell, A.D., Selsby, J.T., Hudson, M.B. Muscle stem cell-derived extracellular vesicles reverse hydrogen peroxide-induced mitochondrial dysfunction in mouse myotubes. *Cells*. **9**(12), 2544 (2020).

82. Aminzadeh, M.A., Rogers, R.G., Fournier, M., et al. Exosome-mediated benefits of cell therapy in mouse and human models of duchenne muscular dystrophy. *Stem cell reports*. **10**(3), 942-955 (2018).

83. Hansen, L., Liu, W., Joseph, G., Weiss, D. The paracrine effects of satellite cells on collateral vessel formation. *The FASEB Journal*. (2018)

84. Baraniak, P.R., McDevitt, T.C. Stem cell paracrine actions and tissue regeneration. *Regen med*. **5**(1), 121-143 (2010).

85. Gowen, A., Shahjin, F., Chand, S., et al. Mesenchymal stem cell-derived extracellular vesicles: Challenges in clinical applications. *Front cell dev biol*. **8**, 149 (2020).

86. Arslan, F., Lai, R.C., Smeets, M.B., et al. Mesenchymal stem cell-derived exosomes increase ATP levels, decrease oxidative stress and activate PI3K/akt pathway to enhance myocardial viability and prevent adverse remodeling after myocardial ischemia/reperfusion injury. *Stem cell research*. **10**(3), 301-312 (2013).

87. Nakamura, Y., Miyaki, S., Ishitobi, H., et al. Mesenchymal-stem-cell-derived exosomes accelerate skeletal muscle regeneration. *FEBS letters*. **589**(11):1257-1265 (2015).

88. Alcaraz, M.J., Compañ, A., Guillén, M.I. Extracellular vesicles from mesenchymal stem cells as novel treatments for musculoskeletal diseases. *Cells*. **9**(1), 98 (2019).

89. Bian, X., Ma, K., Zhang, C., Fu, X. Therapeutic angiogenesis using stem cell-derived extracellular vesicles: An emerging approach for treatment of ischemic diseases. *Stem Cell Res Ther*. **10**(1), 158 (2019).

90. Burrello, J., Monticone, S., Gai, C., et al. Stem cell-derived extracellular vesicles and immune-modulation. *Front cell dev biol*. **4**, 83 (2016).

91. Sandonà, M., Di Pietro, L., Esposito, F., et al. Mesenchymal stromal cells and their secretome: New therapeutic perspectives for skeletal muscle regeneration. *Front bioeng biotech*. **9**, 652970 (2021).

92. Reis, M., Mavin, E., Nicholson, L., et al. Mesenchymal stromal cell-derived extracellular vesicles attenuate dendritic cell maturation and function. *Front immunol*. **9**, 2538 (2018).

93. Henao Agudelo, J.S., Braga, T.T., Amano, M.T., et al. Mesenchymal stromal cell-derived microvesicles regulate an internal pro-inflammatory program in activated macrophages. *Front Immunol*. **8**, 881 (2017).

94. Leng, L., Dong, X., Gao, X., et al. Exosome-mediated improvement in membrane integrity and muscle function in dystrophic mice. *Mol ther.* **29**(4), 1459-1470 (2021).

95. Mitchell, R., Mellows, B., Sheard, J., et al. Secretome of adipose-derived mesenchymal stem cells promotes skeletal muscle regeneration through synergistic action of extracellular vesicle cargo and soluble proteins. *Stem Cell Res Ther*. 10(1), 116 (2019).

96. Whittaker, T.E., Nagelkerke, A., Nele, V., et al. Experimental artefacts can lead to misattribution of bioactivity from soluble mesenchymal stem cell paracrine factors to extracellular vesicles. *J Extracell Vesicles*. **9**(1), 1807674 (2020).

97. Fang, J., Zhang, S., Liu, Z., et al. Skeletal muscle stem cells confer maturing macrophages anti-inflammatory properties through insulin-like growth factor-2. *Stem Cells Trans Med*. **9**(7), 773 (2020).

98. Fry, C.S., Kirby, T.J., Kosmac, K., et al. Myogenic progenitor cells control extracellular matrix production by fibroblasts during skeletal muscle hypertrophy. *Cell stem cell*. **20**(1), 56-69 (2017).

99. Murach, K.A., Vechetti, I.J., Van, Pelt, D.W., et al. Fusion-independent satellite cell communication to muscle fibers during load-induced hypertrophy. *Function*. **1**(1), zqaa009 (2020).

100. Ibrahim, A.G., Cheng, K., Marbán, E. Exosomes as critical agents of cardiac regeneration triggered by cell therapy. *Stem cell reports*. **2**(5), 606-619 (2014).

101. Xu, Y., Patnaik, S., Guo, X., et al. Cardiac differentiation of cardiosphere-derived cells in scaffolds mimicking morphology of the cardiac extracellular matrix. *Acta biomat.* **10**(8), 3449-3462 (2014).

102. Grigorian-Shamagian, L., Liu, W., Fereydooni, S., et al. Cardiac and systemic rejuvenation after cardiosphere-derived cell therapy in senescent rats. *Euro heart j*. **38**(39), 2957-2967 (2017).

103. Mentkowski, K.I., Mursleen, A., Snitzer, J.D., et al. CDC-derived extracellular vesicles reprogram inflammatory macrophages to an arginase 1-dependent proangiogenic phenotype. *Am J Phys Heart Circ Phys*. **318**(6), 1447-1460 (2020).

104. Jia, X., Tang, J., Yao, C., Yang, D. Recent progress of extracellular vesicle engineering. *ACS biomat sci eng*. **7**(9), 4430-4438 (2021).

105. Gupta, V., Sengupta, M., Prakash, J., Tripathy, B.C.. Production of recombinant pharmaceutical proteins. *Basic and applied aspects of biotechnology*. 77-101 (2016).

106. Nishikawa, M., Takakura, Y. Exosome-based tumor antigens–adjuvant co-delivery utilizing genetically engineered tumor cell-derived exosomes with immunostimulatory CpG DNA. *Biomat*. **111**, 55-65 (2016).

107. Li, Z., Zhou, X., Wei, M., et al. In vitro and in vivo RNA inhibition by CD9-HuR functionalized exosomes encapsulated with miRNA or CRISPR/dCas9. *Nano Lett*. **19**(1), 19 (2018).

108. Cheng, Q., Shi, X., Han, M., et al. Reprogramming exosomes as nanoscale controllers of cellular immunity. *J Am Chem Soc*. **140**(48),16413 (2018).

109. Dooley, K., McConnell, R.E., Xu, K., et al. A versatile platform for generating engineered extracellular vesicles with defined therapeutic properties. *Mol ther*. **29**(5), 1729-1743 (2021).

110. Jang, S.C., Economides, K.D., Moniz, R.J., et al. ExoSTING, an extracellular vesicle loaded with STING agonists, promotes tumor immune surveillance. *Comm biol*. **4**(1), 497 (2021).

111. Cohen, R. A first-in-human study of CDK-002 (exoSTING) in subjects with advanced/metastatic, recurrent, injectable solid tumors. clinicaltrials.gov Web site. https://clinicaltrials.gov/ct2/show/NCT04592484. Updated 2022.

112. Kamerkar, S., Leng, C., et al. Exosome-mediated genetic reprogramming of tumor-associated macrophages by exoASO-STAT6 leads to potent monotherapy antitumor activity. *Sci. Adv*. **8**, eabj7002 (2022).

113. Wood, M.J.A., Alvarez-Erviti, L., Seow, Y., et al. Delivery of siRNA to the mouse brain by systemic injection of targeted exosomes. *Nat biotech*. **29**(4), 341-345 (2011).

114. Gupta, D., Wiklander, O.P.B., Görgens, A., et al. Amelioration of systemic inflammation via the display of two different decoy protein receptors on extracellular vesicles. *Nat biomed eng*. **5**(9), 1084-1098 (2021).

115. Pi, F., Binzel, D.W., Lee, T.J., et al. Nanoparticle orientation to control RNA loading and ligand display on extracellular vesicles for cancer regression. *Nat Nanotech*. **13**(1), 82 (2018).

116. Yang, Z., Shi, J., Xie, J., et al. Large-scale generation of functional mRNA-encapsulating exosomes via cellular nanoporation. *Nat Biomed Eng*. **4**(1), 69 (2019).

117. Pomatto, M.A.C., Bussolati, B., D'Antico, S., et al. Improved loading of plasma-derived extracellular vesicles to encapsulate antitumor miRNAs. *Mol ther. Methods clin dev.* **13**, 133-144 (2019).

118. Auber, M., Fröhlich, D., Drechsel, O., et al. Serum-free media supplements carry miRNAs that co-purify with extracellular vesicles. *J extracell vesicles*. **8**(1), 1656042 (2019).

119. Kooijmans, S.A., Schiffelers, R.M., Zarovni, N., et al. Modulation of tissue tropism and biological activity of exosomes and other extracellular vesicles : New nanotools for cancer treatment. *Pharmacol Res*. **111**, 487-500 (2016).

120. Garofalo, M., Villa, A., Crescenti, D., et al. Heterologous and cross-species tropism of cancer-derived extracellular vesicles. *Theranostics*. **9**(19), 5681 (2019).

121. Hoshino, A., Costa-Silva, B., Shen, TL. et al. Tumour exosome integrins determine organotropic metastasis. *Nature*. **527**, 329–335 (2015).

122. Ji, Q., Zhou, L., Sui, H., et al. Primary tumors release ITGBL1-rich extracellular vesicles to promote distal metastatic tumor growth through fibroblast-niche formation. *Nat Commun*. **11**(1), 1211 (2020).

123. Kang, M., Jordan, V., Blenkiron, C., Chamley, L.W. Biodistribution of extracellular vesicles following administration into animals: A systematic review. *J Extracell Vesicles*. **10**(8), e12085 (2021).

124. Wiklander, O.P.B., Nordin, J.Z., O'Loughlin A, et al. Extracellular vesicle in vivo biodistribution is determined by cell source, route of administration and targeting. *J Extracell Vesicles*. **4**(1), 26316 (2015).

125. Wen, S., Dooner, M., Papa, E., et al. Biodistribution of mesenchymal stem cell-derived extracellular vesicles in a radiation injury bone marrow murine model. *Int j mol sci*. **20**(21), 5468 (2019).

126. Driedonks, T., Jiang, L., Carlson, B., et al. Pharmacokinetics and biodistribution of extracellular vesicles administered intravenously and intranasally to macaca nemestrina. *J Extracell Biol.* **1**(10), e59 (2021).

127. Ciullo, A., Li, C., Li, L., et al. Biodistribution of unmodified cardiosphere-derived cell extracellular vesicles using single RNA tracing. *J extracell vesicles*. **11**(1), e12178 (2022).

128. Grange, C., Tapparo, M., Bruno, S., et al. Biodistribution of mesenchymal stem cell-derived extracellular vesicles in a model of acute kidney injury monitored by optical imaging. *Int j mol med*. **33**(5), 1055-1063 (2014).

129. Kim, M.S., Haney, M.J., Zhao, Y., et al. Engineering macrophage-derived exosomes for targeted paclitaxel delivery to pulmonary metastases: *In vitro and in vivo evaluations.* **14**(1):195-204 (2018).

130. Herrmann, I.K., Wood, M.J.A., Fuhrmann, G. Extracellular vesicles as a next-generation drug delivery platform. *Nat nanotech*. **16**(7), 748-759 (2021).

131. Yang, J., Zhang, X., Chen, X., et al. Exosome mediated delivery of miR-124 promotes neurogenesis after ischemia. *Mol ther Nuc acids*. **7**, 278-287 (2017).

132. Altei, W.F., Pachane, B.C., Dos Santos, P.K., et al. Inhibition of αvβ3 integrin impairs adhesion and uptake of tumor-derived small extracellular vesicles. *Cell Commun Signal*. **18**(1), 158 (2020).

133. Tian, Y., Li, S., Song, J., et al. A doxorubicin delivery platform using engineered natural membrane vesicle exosomes for targeted tumor therapy. *Biomaterials*. **35**(7), 2383-2390 (2013).

134. Zhou, Y., Yuan, Y., Liu, M., et al. Tumor-specific delivery of KRAS siRNA with iRGD-exosomes efficiently inhibits tumor growth. *ExRNA*. **1**(28), 1-7 (2019).

135. Bai, J., Duan, J., Liu, R., et al. Engineered targeting tLyp-1 exosomes as gene therapy vectors for efficient delivery of siRNA into lung cancer cells. *Asian j pharm sci*. **15**(4), 461-471 (2020).

136. Liang, Y., Xu, X., Li, X., et al. Chondrocyte-targeted MicroRNA delivery by engineered exosomes toward a cell-free osteoarthritis therapy. *ACS Appl Mater Interfaces*. **12**(33), 36938 (2020).

137. Xu, X., Liang, Y., Ouyang, K., et al. Exosome-mediated delivery of kartogenin for chondrogenesis of synovial fluid-derived mesenchymal stem cells and cartilage regeneration. *Biomaterials*. **269**, 120539 (2021).

138. Ohno, S., Takanashi, M., Sudo, K., et al. Systemically injected exosomes targeted to EGFR deliver antitumor MicroRNA to breast cancer cells. *Mol ther*. **21**(1), 185-191 (2013).

139. Haraszti, R.A., Miller, R., Didiot, M., et al. Optimized cholesterol-siRNA chemistry improves productive loading onto extracellular vesicles. *Mol ther*. **26**(8),1973-1982 (2018).

140. Wang, Y., Chen, X., Tian, B., et al. Nucleolin-targeted extracellular vesicles as a versatile platform for biologics delivery to breast cancer. *Theranostics*. **7**(5), 1360-1372 (2017).

141. Smyth, T., Petrova, K., Payton, N.M., et al. Surface functionalization of exosomes using click chemistry. *Bioconj chem*. **25**(10), 1777-1784 (2014).

142. Jia, G., Han, Y., An, Y., et al. NRP-1 targeted and cargo-loaded exosomes facilitate simultaneous imaging and therapy of glioma in vitro and in vivo. . *Biomaterials*. **178**, 302-316 (2018).

143. Koh, E., Lee, E.J., Nam, G.H., et al. Exosome-SIRPα, a CD47 blockade increases cancer cell phagocytosis. . *Biomaterials*. **121**, 121-129 (2017).

144. Cui, G., Guo, H., Li, H., et al. RVG-modified exosomes derived from mesenchymal stem cells rescue memory deficits by regulating inflammatory responses in a mouse model of alzheimer's disease. *Immunity & ageing*. **16**(1), 10 (2019).

145. Liang, Y., Duan, L., Lu, J., Xia, J. Engineering exosomes for targeted drug delivery. *Theranostics*. **11**(7), 3183 (2021).

146. Nozoe, K.T., Akamine, R.T., Mazzotti, D.R., et al. Phenotypic contrasts of duchenne muscular dystrophy in women: Two case reports. *Sleep science.* **9**(3), 129-133 (2016).

147. Geeurickx, E., Tulkens, J., Dhondt, B., et al. The generation and use of recombinant extracellular vesicles as biological reference material. **10**(1), 3288 (2019).

148. Aird, W.C. Phenotypic heterogeneity of the endothelium: I. structure, function, and mechanisms. *Circ Res.* **100**(2), 158-173 (2007).

149. Latroche, C., Gitiaux, C., Chrétien, F. Skeletal muscle microvasculature: A highly dynamic lifeline. *Physiology.* **30**(6), 417-427 (2015).

150. Kutchy, N.A., Ma, R., Liu, Y., et al. Extracellular vesicle-mediated delivery of ultrasmall superparamagnetic iron oxide nanoparticles to mice brain. *Front Pharmacol.* **13**, 819516 (2022).

151. Khalin, I., Adarsh, N., Schifferer, M., et al. Size-Selective transfer of lipid Nanoparticle-Based drug carriers across the blood brain barrier via vascular occlusions following traumatic brain injury. *Small.* **18**(18), e2200302 (2022).

152. Wu, J. The enhanced permeability and retention (EPR) effect: The significance of the concept and methods to enhance its application. *J pers med*. **11**(8), 771 (2021).

153. Wilhelm, S., Tavares, A.J., Dai, Q., et al. Analysis of nanoparticle delivery to tumours. *Nat rev mat*. **1**(5), 16014 (2016).

154. Skotland, T., Iversen, T.G., Llorente, A., Sandvig, K. Biodistribution, pharmacokinetics and excretion studies of intravenously injected nanoparticles and extracellular vesicles: Possibilities and challenges. *Adv drug deliv rev*. **186**, 114326 (2022).

155. Sharma, P., Basu, S., Mitchell, R.W, et al. Role of dystrophin in airway smooth muscle phenotype, contraction and lung function. *PLoS ONE*. **9**(7), e102737 (2014).

156. Caudal, D., François, V., Lafoux, A., et al. Characterization of brain dystrophins absence and impact in dystrophin-deficient dmd mdx rat model. *PLoS ONE*. **15**(3), e0230083 (2020).

157. Wada, E., Hamano, T., Matsui, I., et al. Renal involvement in the pathogenesis of mineral and bone disorder in dystrophin-deficient mdx mouse. *J Physiol Sci*. **69**(4), 661 (2019).

158. Luster, A.D., Alon, R., Von Andrian, U.H. Immune cell migration in inflammation: Present and future therapeutic targets. *Nat Immunol*. **6**(12), 1182-1190 (2005).

159. Brennan, K., Martin, K., FitzGerald, S.P., et al. A comparison of methods for the isolation and separation of extracellular vesicles from protein and lipid particles in human serum. *Sci rep*. **10**(1),1039 (2020).

160. Vanderschuren, K., Arranz-Gibert, P., Khang, M., et al. Tuning protein half-life in mouse using sequence-defined biopolymers functionalized with lipids. *PNAS*. **119**(4), e2103099119 (2022).

161. Tertel, T., Schoppet, M., Stambouli, O., et al. Imaging flow cytometry challenges the usefulness of classically used extracellular vesicle labeling dyes and qualifies the novel dye exoria for the labeling of mesenchymal stromal cell–extracellular vesicle preparations. *Cytotherapy*. **24**(6), 619 (2022).

162. Zhu, X., Badawi, M., Pomeroy, S., et al. Comprehensive toxicity and immunogenicity studies reveal minimal effects in mice following sustained dosing of extracellular vesicles derived from HEK293T cells. *J extracell vesicles*. **6**(1), 1324730 (2017).

163. Sutaria, D.S., Badawi, M., Phelps, M.A., Schmittgen, T.D.. Achieving the promise of therapeutic extracellular vesicles: The devil is in details of therapeutic loading. *Pharm Res*. **34**(5), 1053-1066 (2017).

164. PTGFRN prostaglandin F2 receptor inhibitor [homo sapiens (human)]. National Center for Biotechnology Information: Gene Web site. https://www.ncbi.nlm.nih.gov/gene/5738#gene-expression. Updated 6-Nov-22.

165. Nishida, A., Yasuno, S., Takeuchi, A., et al. HEK293 cells express dystrophin Dp71 with nucleus-specific localization of Dp71ab . *Histochem Cell Biol*. **146**(3), 301-9 (2016).

166. Shaw, G., Morse, S., Ararat, M., et al. Preferential transformation of human neuronal cells by human adenoviruses and the origin of HEK 293 cells. *FASEB J*. **16**(8), 869-71 (2002).

167. Samoylova, T.I., Smith, B.F. Elucidation of muscle-binding peptides by phage display screening. *Muscle Nerve*. **22**(4), 460 (1999).

168. Kim, T.K., Eberwine, J.H. Mammalian cell transfection: The present and the future. *Anal Bioanal Chem*. **397**(8), 3173-3178 (2010).

169. Li, M., Liao, L., Tian, W. Extracellular vesicles derived from apoptotic cells: An essential link between death and regeneration. *Front cell dev biol*. **8**, 573511 (2020).

170. Adorisio, R., Mencarelli, E., Cantarutti, N., et al. Duchenne dilated cardiomyopathy: Cardiac management from prevention to advanced cardiovascular therapies. *JCM*. **9**(10), 3186 (2020).

Appendix A

SUPPLEMENTARY FIGURES

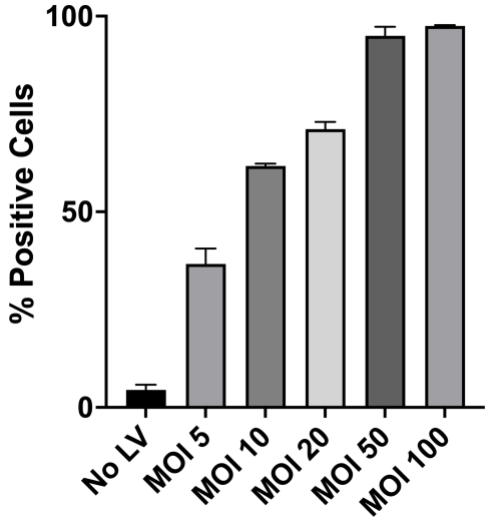

Figure A.1 Determination of sufficient multiplicity of infection (MOI) for lentivirus (LV) transfection. MOI 10 was determined to be sufficient for transfection followed by FACS to select positive cells.

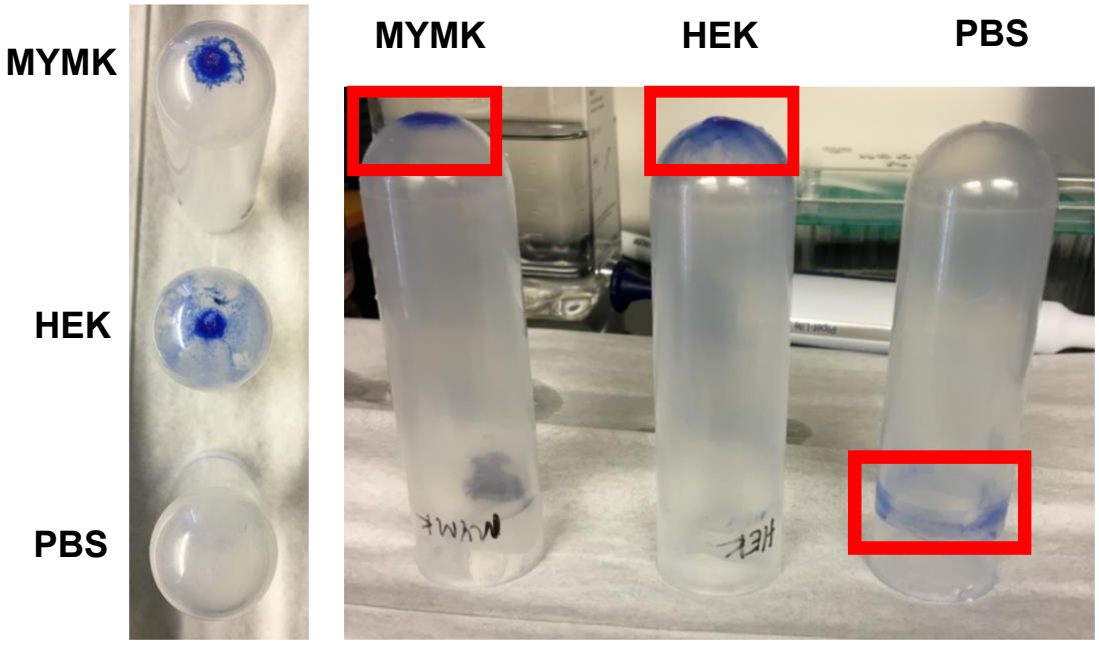

Supplementary Figure A.2 Removal of unbound DiD via UC at 150,000 x g for 1 hour. Left: top view of MYMK and HEK EV pellets, stained with 5 uM DiD at the bottom of their respective tubes and no visible pellet in the UC tube with equivalent DiD mixed with PBS. Right: Lateral view of MYMK and HEK-EV pellets labeled with 5 uM DiD at the bottom of their respective UC tubes and a visible stained region at the top of the UC tube with equivalent DiD mixed with PBS.

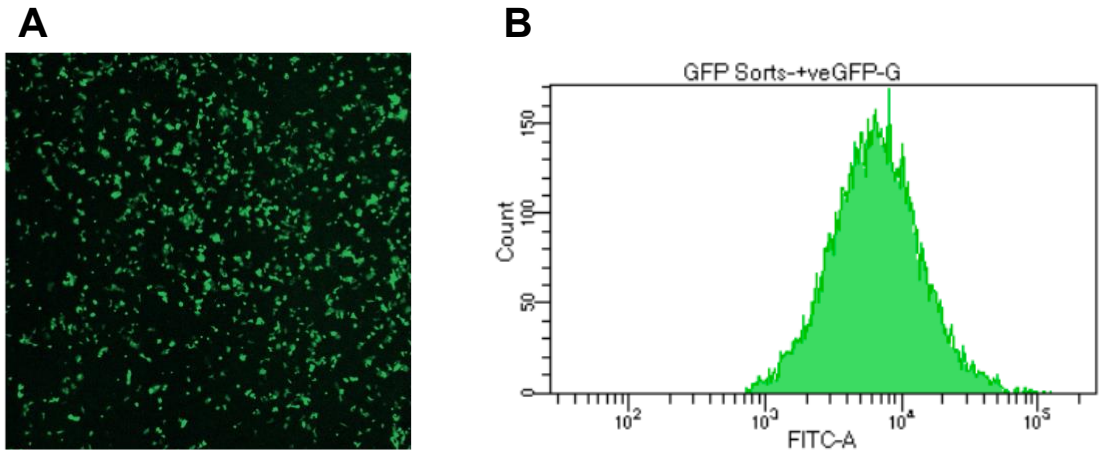

Figure A.3 GFP-transfected cells selected with Geneticin and FACS. A) Representative image of stable GFP-expressing HEK293 cells. B) FACS data demonstrating the fluorescence intensity of the GFP-expressing HEK293 cells following selection with Geneticin.

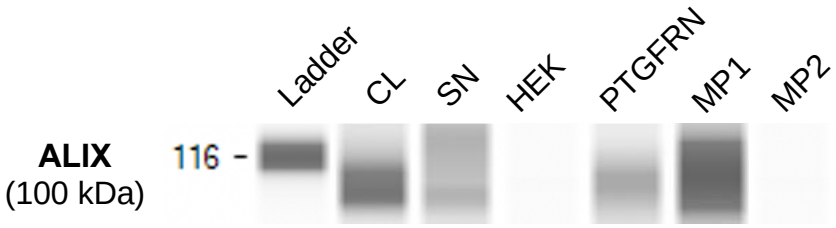

Figure A.4 Capillary western blot analyzing HEK293 cell lysate (CL), UC supernatant (SN), HEK293 EVs, PTGFRN EVs, MP1 EVs and MP2 EVs confirming signal for ALIX (100 kDa) in the CL, SN, PTGFRN and MP1 samples but not the HEK and MP2 due to low particle/protein concentrations in those samples.

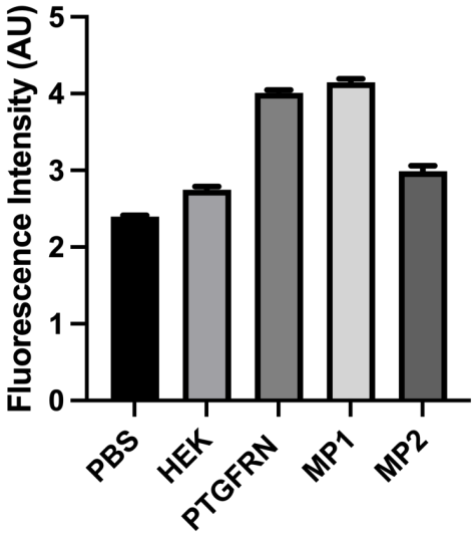

Figure A.5 Fluorescence intensity of Cell Tracker Red-labeled chimeric myotropic EV candidates at 1:10 dilution. Data were used to calculate doses of EVs for in vitro uptake experiments.

Appendix B

IACUC APPROVAL FORM

University of Delaware
Institutional Animal Care and Use Committee
Application to Use Animals in Research
(New and 3-Yr submission)

Title of Protocol: Pharmacokinetics of Human Embryonic Kidney Cell-Derived Extracellular Vesicles with Modified Membrane Proteins	
AUP Number: 1387-2021-0	**(4 digits only — if new, leave blank)**
Principal Investigator: Matthew Hudson	
Common Name (Strain/Breed if Appropriate): C57, mdx **Genus Species:** mus musculus	
Date of Submission: 10/18/21	

Official Use Only

IACUC Approval Signature: [signature], DVM

Date of Approval: 11/4/22